

**DEVELOPMENT AND ANALYSIS OF GRASSHOPPER-LIKE
JUMPING MECHANISM IN BIOMIMETIC APPROACH**

**A THESIS SUBMITTED TO
THE GRADUATE SCHOOL OF NATURAL AND APPLIED
SCIENCES
OF
MIDDLE EAST TECHNICAL UNIVERSITY**

BY

AYLİN KONEZ EROĞLU

**IN PARTIAL FULFILLMENT OF THE REQUIREMENTS
FOR
THE DEGREE OF MASTER OF SCIENCE
IN
MECHANICAL ENGINEERING**

SEPTEMBER 2007

DEVELOPMENT AND ANALYSIS OF GRASSHOPPER-LIKE JUMPING
MECHANISM IN BIOMIMETIC APPROACH

submitted by **AYLİN KONEZ EROĞLU** in partial fulfillment of the requirements
for the degree of **Master of Science in Mechanical Engineering, Middle East
Technical University** by,

Prof. Dr. Canan ÖZGEN
Dean, Graduate School of Natural and Applied Sciences

Prof. Dr. S. Kemal İDER
Head of Department, Mechanical Engineering

Prof. Dr. Metin Akkök
Supervisor, Mechanical Engineering Dept., METU

Examining Committee Members:

Prof. Dr. Suat Kadiođlu
Mechanical Engineering Dept., METU

Prof. Dr. Metin Akkök
Mechanical Engineering Dept., METU

Prof. Dr. Abdulkadir Erden
Mechatronics Engineering Dept., Atılım University

Assoc. Prof. Dr. İlhan Konukseven
Mechanical Engineering Dept., METU

Prof. Dr. Müfit Gülgeç
Mechanical Engineering Dept., Gazi University

Date:

05.09.2007

I hereby declare that all information in this document has been obtained and presented in accordance with academic rules and ethical conduct. I also declare that, as required by these rules and conduct, I have fully cited and referenced all material and results that are not original to this work.

Name, Last Name:

Signature:

ABSTRACT

DEVELOPMENT AND ANALYSIS OF GRASSHOPPER-LIKE JUMPING MECHANISM IN BIOMIMETIC APPROACH

Konez Erođlu, Aylin

M.S., Department of Mechanical Engineering

Supervisor: Prof. Dr. Metin Akkök

September 2007, 125 pages

Highly effective and power efficient biological mechanisms are common in nature. The use of biological design principles in engineering domain requires adequate training in both engineering and biological domains. This requires cooperation between biologists and engineers that leads to a new discipline of biomimetic science and engineering. Biomimetic is the abstraction of good design from nature. Because of the fact that biomimetic design has an important place in mechatronic applications, this study is directed towards biomimetic design of grasshopper-like jumping mechanism.

A biomimetic design procedure is developed and steps of the procedure have followed through all the study. A literature survey on jumping mechanisms of grasshoppers and jumping robots and bio-robots are done and specifically apteral types of grasshoppers are observed. After the inspections, 2D and 3D mathematical models are developed representing the kinematics and dynamics of the hind leg movements. Body-femur, femur-tibia and tibia-ground angles until take-off are obtained from the mathematical leg models. The force analysis of the leg models with artificial muscles and biological muscles are derived from the torque analysis. A

simulation program is used with a simple model for verification. The horizontal displacement of jumping is compared with the data obtained from the simulation program and equation of motion solutions with and without air resistance.

Actuators are the muscles of robots that lead robots to move and have an important place in robotics. In this scope, artificial muscles are studied as a fourth step of biomimetic design. A few ready-made artificial muscles were selected as an actuator of the grasshopper-like jumping mechanism at the beginning of the study. Because of their disadvantages, a new artificial muscle is designed and manufactured for mini bio-robot applications. An artificial muscle is designed to be driven by an explosion obtained due to the voltage applied in a piston and cylinder system filled with dielectric fluid. A 3.78-mm diameter Teflon piston is fitted with a clearance into a Teflon cylinder filled with a 25.7- mm fluid height and maximum 225 V is applied to the electrodes by using an electrical discharge machine (EDM) circuit. The force on the piston is measured by using a set-up of Kistler piezoelectric low level force sensor. The data obtained from the sensor is captured by using an oscilloscope, a charge meter, and a GPIB connecting card with software, Agilent. From the experiments, the new artificial muscle force is about 300 mN giving a 38:1 force to weight ratio and percentage elongation is expected to be higher than that of the natural muscles and the other artificial muscles. From the force analysis of the leg model, it is shown that the measured force is not enough alone for jumping of an about 500 mgr body. An additional artificial muscle or a single muscle designed with the same operating principle giving higher force to weight ratio is recommended as a future study.

Keywords: biomimetic design, jumping mechanism, grasshoppers, artificial muscles, bio-robots

ÖZ

ÇEKİRGE BENZERİ SIÇRAMA MEKANİZMASININ BİYOBENZETİM YAKLAŞIMLA GELİŞTİRİLMESİ VE ANALİZİ

Konez Erođlu, Aylin

Yüksek Lisans, Makina Mühendisliđi Bölümü

Tez Yöneticisi: Prof. Dr. Metin Akkök

Eylül 2007, 125 sayfa

Yüksek seviyede etkin ve güç kullanımında verimli biyolojik mekanizmalar doğada yer almaktadır. Biyolojik tasarım prensiplerinin mühendislik alanında kullanabilmesi biyoloji ve mühendislik alanlarında yetenek gerektirir. Biyologların ve mühendislerin bu ortaklaşa çalışma gereksinimi yeni bir disiplin olan biyobenzetim bilim ve mühendisliğinin gelişimine yol açmıştır. Biyobenzetim, doğada var olan iyi tasarımların taklit edilmesidir. Biyobenzetim mekatronik uygulamalarda önemli bir yere sahiptir, bu nedenle bu çalışma çekirge benzeri sıçrama mekanizmasının biyobenzetim tasarımını yönetmektedir.

Biyobenzetimle tasarım yöntemi geliştirilmiş ve bu yöntemin basamakları bütün çalışma boyunca takip edilmiştir. Çekirge sıçrama mekanizmalarının, sıçramalı robotların ve biyo-robotların kaynak araştırması yapılmış ve özellikle çekirgelerin kanatsız türleri gözlemlenmiştir. Bu çalışmadan sonra, arka bacak kinematik ve dinamik hareketlerini veren 2 boyutlu ve 3 boyutlu matematik modeller geliştirilmiştir. Sıçramaya kadar olan vücut-femur, femur-tibia ve tibia-yer açıları bu modellerden elde edilmiştir. Suni kaslı ve biyolojik kaslı bacak modellerinin kuvvet analizi tork analizinden çıkartılmıştır. Doğrulama için simülasyon programı basit bir

model ile kullanılmıştır. Sıçramanın yatay mesafesi bu simülasyon programı ile hava dirençli ve dirençsiz hareket denklemlerinin sonuçları ile karşılaştırılmıştır.

Robotikte önemli bir yere sahip olan eyleyiciler robotları hareket ettiren kaslardır. Bu nedenle, suni kaslar biyobenzetimle tasarımın dördüncü basamağı olarak çalışılmıştır. Bu çalışmanın başında, çekirgemi sıçrama mekanizmasının eyleyicisi olarak birkaç hazır suni kas seçilmiştir. Bu kasların dezavantajları nedeniyle mini biyo-robot uygulamaları için yeni bir kas tasarlanmış ve üretilmiştir. Dielektrik sıvı ile dolu piston-silindir sistemine uygulanan voltajdan kaynaklanan patlama ile sürülen bir suni kas tasarlanmıştır. 3.78 mm çaplı bir teflon pistonun boşluklu yerleştirildiği plastik silindirdeki 25.7 mm sıvı yüksekliğine elektrotlara elektroerozyon makina (EDM) devresinden maksimum 225 V uygulanmıştır. Kistler piezoelektrik düşük seviye kuvvet algılayıcısı ile pistondaki kuvvet ölçülmüştür. Algılayıcıdan gelen veriler, bir osiloskop, bir yük büyütücüsü ve GPIB iletişim kartı ile bir yazılım, Agilent, kullanılarak toplanmıştır. Deneyle göre, yeni suni kasın kuvveti yaklaşık 300 mN, kuvvetin ağırlığa oranı 38:1 ve boydaki uzama yüzdesinin biyolojik kaslara ve diğer suni kaslara göre daha yüksek olması beklenmektedir. Bacak modelindeki kuvvet analizine göre bu kuvvetin yaklaşık 500 mgr'lık bir gövdeyi sıçratmak için yeterli olmadığı görülmüştür. Daha sonra çalışılmak üzere ilave suni kaslı ya da kuvvetin ağırlığa olan oranı daha yüksek olan tek kaslı bir tasarım önerilmektedir.

Anahtar Kelimeler: Biyobenzetimle tasarım, sıçrama mekanizması, çekirgeler, suni kaslar, biyo-robotlar

To My Parents, My Dear Husband and M. Kemal ATATÜRK

ACKNOWLEDGEMENTS

The author would like to express her appreciation and thankfulness to Prof. Dr. Abdulkadir Erden for his encouragements, advice, guidance, and support that created this study. The author wishes to express her thanks to Prof. Dr. Metin Akkk for his supports and advice.

The author also wishes to thank Assoc. Prof. Dr. Atef Qasrawi, Assoc. Prof. Dr. Fuad Aliew, Asst. Prof. Dr. Blent İrfanođlu, and Instructor Kutluk Bilge Arıkan for their suggestions and comments. Also the author would like to thank Emrah Demirci, Alper Gner, Dilek zgr and Gzde Eminođlu for their support and friendship. The author wants to thanks Tahsin Tecelli pz for his great effort on my experimental studies.

The author would like to thank Hacettepe University, Department of Biology for their contributions to capturing a special genius of grasshoppers, Pholidoptera, an apteral type in Ankara. Special thanks to Atılım University, Department of Mechatronics Engineering for material and laboratory support. The technical assistance of Mehmet akmak is gratefully acknowledged.

Authors acknowledge the State Planning Organization of Turkey (DPT) for their funding via the research project entitled “Development and implementation of micro machining (especially Micro-EDM) methods to produce (design and manufacture) of mini/micro machines/robots”.

The author thanks to *Mustafa Kemal Atatrk* for his gift, Trkiye. We would be nothing without him. Finally many thanks to my parents and my husband, Barıř Erođlu, for their invaluable and endless support in all my life. This thesis is dedicated to my all family.

TABLE OF CONTENTS

ABSTRACT.....	iv
ÖZ.....	vi
DEDICATION.....	viii
ACKNOWLEDGEMENT.....	ix
TABLE OF CONTENTS.....	x
LIST OF TABLES.....	xiv
LIST OF FIGURES.....	xv
CHAPTER	
1. INTRODUCTION.....	1
1.1 Biomimetics and Biomimetic Design.....	2
1.2 Scope of the Thesis.....	5
2. LITERATURE SURVEY ON THE ANATOMY OF GRASSHOPPER.....	6
2.1 Anatomy of Grasshopper Legs.....	6
2.1.1 Anatomy of Grasshopper Muscles.....	9
2.1.2 Working Mechanism of Hind Leg Joints.....	11
2.2 Grasshopper Jumping Mechanism.....	13
3. JUMPING AND/OR HOPPING MECHANISMS AND INSECT-LIKE ROBOTS.....	17
3.1 Hopping Machine.....	17

3.2 Monopod Hopping Robots	17
3.3 Omni-Pede (Serpentine Robot)	18
3.4 A Small, Insect-Inspired Robot	19
3.5 Biomimetic Hexapod Robot.....	20
3.6 Cricket Micro-Robot	21
3.7 Quadraped Jumping Robot.....	23
3.8 Lobster Robot	24
4. MODELING AND ANALYSIS OF GRASSHOPPER-LIKE JUMPING	
MECHANISM	25
4.1 3D Leg Model.....	25
4.1.1 Mathematical Model Description for 3D Leg Model	25
4.1.2 Kinematic Analysis for 3D Leg Model.....	26
4.1.3 Kinematic and Dynamic Analyses According to Experimental	
Data	29
4.2 2D Leg Model.....	31
4.2.1 Mathematical Model for 2D Leg Model	31
4.2.2 Kinematic Analysis	32
4.2.3 Dynamic Analysis	33
4.3 Results of the 2D and 3D Leg Model	35
4.4 Results of the Torques of the 2D Leg Model	38
4.5 Kinematic Analysis of the 3D Leg Model with MSC. Adams	
Simulation	39
5. ARTIFICIAL MUSCLES AND DEVELOPMENT OF A NEW	
ARTIFICIAL MUSCLE	42
5.1 Literature Survey on Artificial Muscles	42
5.1.1 Braided Pneumatic Actuators (BPA); McKibben Artificial	
Muscles; Air Muscles.....	45
5.1.2 Shape Memory Alloys (SMA)	48
5.1.3 Electroactive Ceramics (EAC).....	50

5.1.4 Electromagnetic.....	51
5.1.5 Piezoelectric	51
5.1.6 Electroactive Polymer Artificial Muscle (EAP or EPAM).....	52
5.1.7 Antagonistically-Driven Linear Actuator (ANTLA)	60
5.1.8 Baughman and Colleagues’ Artificial Muscles.....	60
5.1.9 A Comparison of Artificial Muscles	61
5.2 Studies on Artificial Muscles	64
5.2.1 A New Artificial Muscle Design and Manufacture	67
5.2.2 Characteristics of Force Sensor Set-up Used in the New Artificial Muscle	72
 6. PRELIMINARY DESIGN OF JUMPING MECHANISM OF GRASSHOPPER-LIKE ROBOT	 79
6.1 Design of Jumping Mechanism of Grasshopper-like Robot Model.....	79
6.2 Discussion of the Artificial Muscle Force.....	82
 7. CONCLUSIONS AND FURTHER RECOMMENDATIONS	 84
7.1 Discussion and Conclusions	84
7.2 Suggestions for Future Work	86
 REFERENCES.....	 88
 APPENDICES	 98
 APPENDIX	
 A. ANALYTICAL SOLUTION OF BODY HEIGHT AND BODY-FEMUR	
ANGLE	99
A.1 Calculation of Body-Height	99
A.1.1 Polynomial Solution.....	100
A.1.2 Lagrange Interpolating Polynomials Solution	101
A.1.3 Least Square Regression, Polynomial Regression Solution	101

A.1.4 Result of the Body Height Analysis.....	103
A.2 Calculation of Femur-Tibia (Knee) Angle.....	104
A.2.1 Polynomial Solution.....	106
A.2.2 Lagrange Interpolating Polynomials Solution	106
A.2.3 Least Square Regression, Polynomial Regression Solution	106
A.2.4 Result of the Femur-Tibia Angle Analysis	108
B. CALCULATION OF BODY-FEMUR ANGLE	110
C. 2D LEG MODEL RESULTS	112
D. CALCULATION OF MASSES AND VOLUMES OF FEMUR-TIBIA.....	113
E. DYNAMIC MODEL OF THE GRASSHOPPER LEG	115
F. TORQUE RESULTS OF 2D LEG MODEL.....	123
G. ARTIFICIAL MUSCLES	124

LIST OF TABLES

Table 1.1	Characteristic similarities of biology and engineering system (Bar-Cohen, 2006)	2
Table 2.1	Degrees of freedom of the hind leg joint	8
Table 3.1	CWRU Hexapod Robots features	21
Table 4.1	Experimental data (Burrows and Morris, 2003) used for jumping simulation.....	27
Table 4.2	Body height and femur tibia angle parabolic curves according to a time interval.....	28
Table 4.3	Body form of Pholidoptera and a different genuise and their jumping performance (Burrows and Morris, 2003)	30
Table 4.4	Jumping performance data of Pholiptera motion.....	41
Table 5.1	Comparison of natural muscle and man-made actuator technologies (Arora, 2005; Pelrine, Kornbluh, et.al, 2002	45
Table 5.2	Some Artificial Muscles and a Natural Muscle Comparison.....	63
Table 5.3	Kistler, Type 9205 Low Force Sensor Technical Data (Kistler Data Sheet, 2005)	74
Table A.1	Time and body height values according to initial conditions	102
Table A.2	Time and the angle values according to initial conditions.....	107
Table C.1	2D Leg Model Angles Results	112
Table F.1	Torque Results.....	123
Table G.1	Illustration the advantages and disadvantages of electronic and ionic EAPs as outlined by Halloran and Malley, 2004 and Bar- Cohen, 2004	124
Table G.2	EAP infrastructure (Cohen, 2005).....	125

LIST OF FIGURES

Figure 1.1	The main topics of Biomimetic design procedure.....	3
Figure 1.2	Pictures of grasshoppers of <i>Isophya Nervosa</i> captured in Ankara	4
Figure 2.1	Anatomy of a Grasshopper (Konez, Erden and Akkök, 2006).....	7
Figure 2.2	Hind leg with segments identified (Fauske, 2002; Laksanacharoen, Pollack, et al., 2005; Laksanacharoen, Quinn and Ritzmann, 2003)	7
Figure 2.3	Hinge Joint Model	8
Figure 2.4	Extensor muscle (top of the femur) and flexor muscle (bottom of the femur) (Heitler, 2005)	9
Figure 2.5	The structure of the lump a. the lump from the outside looks like a pit, b. the lump sticks into the joint (Heitler, 2005)	9
Figure 2.6	Working strategy of the lump	10
Figure 2.7	Muscles working mechanism (Heitler, 2005).....	11
Figure 2.8	The joint region of a hind and middle legs a. hind leg knee joint, b. middle leg knee joint (Heitler, 2005)	12
Figure 2.9	Anatomy of the femur-tibia joint of a left hind leg of a mature locust (Burrows and Morris, 2001)	12
Figure 2.10	The scanning electron micrograph of the a. spring cuticle (semi- lunar process), b. normal cuticle (tibial cuticle, (Heitler, 2005)).....	13
Figure 2.11	The trajectory of a female Pholidoptera during a jump. The numbers give the time before and after take-off at 0 ms (Burrows and Morris, 2003).....	15
Figure 2.12	Selected frames from the same jump, a. Viewed from the side, b. Viewed head-on (Burrows and Morris, 2003).	15
Figure 2.13	A routine program of grasshopper jumping (Heitler, 2005).....	16
Figure 3.1	a. 5 cm Monopod Hopping Robot, b. The simulated 2-D robot has five degrees of freedom. Forces were modeled with springs and dampers (Wei, Nelson, Quinn, Verma and Garverick, 2005).....	18

Figure 3.2	A view of OmniPede prototype (Granosik and Borenstein, 2004).....	18
Figure 3.3	a. The jumping mechanism of Mini-Whegs in retracted (top) and released (bottom) positions, b. Composite of video frames showing Mini-Whegs jumping high over a 9 cm barrier (Lambrecht, Horchler, et.al, 2005).....	19
Figure 3.4	a. An American Cockroach, b. Biobot (Delcomyn and Nelson, 2000)	20
Figure 3.5	Working process of the pneumatic muscle (Delcomyn and Nelson, 2000)	20
Figure 3.6	Anatomy of the cricket micro-robot (Birch, Quinn, et al., 2005).....	21
Figure 3.7	A view of the Cricket Cart Robot (Birch, Quinn, Hahm, Phillips, et al., 2005).....	22
Figure 3.8	a. A Hybrid robot, b. One leg of the hybrid robot (Birch, Quinn, et.al, 2005).....	22
Figure 3.9	Locomotion Concept of Jumping Quadruped (Kikuchi, Ota and Hirose, 2003).....	23
Figure 3.10	A view of Quadruped Jumping Robot (Titech, 2006)	23
Figure 3.11	A view of Lobster robot (Safak and Adams, 2002).....	24
Figure 4.1	The grasshopper (Pholidoptera) leg model (CM: Centre of Mass) ...	26
Figure 4.2	The changes in the Femur-Tibia angle, body height and velocity of body movement during a jump by a Pholidoptera male (Burrows and Morris, 2003).....	27
Figure 4.3	a. Body height ($z(t)$), b. Femur-Tibia angle ($\alpha(t)$) of body movement of a Pholidoptera male before take-off for positive time definite	28
Figure 4.4	2D Leg Model.....	32
Figure 4.5	Position of a grasshopper leg until take-off.....	33
Figure 4.6	Mass distribution of the leg model	33
Figure 4.7	Variations of Femur-Tibia, Body-Femur, and Ground-Tibia angles until take-off.....	36

Figure 4.8	Variations of position of centre of mass coordinates until take-off.....	36
Figure 4.9	A plot of velocity until take-off.....	37
Figure 4.10	A body height variation along horizontal distance until take-off.....	37
Figure 4.11	A graph of time-torque results of 2D leg model where T is the total torque; T1 is the hip actuator torque; T2 is the knee actuator torque.....	38
Figure 4.12	Total torque of 2D leg model	38
Figure 4.13	A grasshopper is modeled by using MSC. Adams Simulation Program	39
Figure 4.14	Displacement analysis of grasshopper-Like by using MSC. Adams 2005	40
Figure 4.15	Like-grasshopper jumping analysis by using MSC. Adams 2005 R2 b. Velocity analysis, b. Kinetic energy analysis.....	40
Figure 5.1	A Swimming Robot Actuated by Living Muscle Tissue (Huge Herr, Robert, 2004)	43
Figure 5.2	The force-length relationship of Braided Pneumatic Actuator's compared to that of muscle (Kingsley, 2005; Colbrunn, 2000).....	46
Figure 5.3	A view of BPA a. A braided pneumatic actuator (Kingsley, 2005), b. An inflated (bottom) and uninflated (top) actuator (Colbrunn, 2000).....	46
Figure 5.4	Working Mechanism of a pneumatic muscle (Biorobotic, 2006).....	47
Figure 5.5	Case Western University Hybrid Robot with rear leg, its actuator is a McKibben Artificial muscle (Birch, et al., 2005).....	47
Figure 5.6	a. The hardware system of a leg design model, b. The leg model (Colbrunn, 2000).....	48
Figure 5.7	Basic Principles of SMA (Kapps, 2007).....	49
Figure 5.8	Polarization is a result of the alignment of piezoelectric domains a. disk after polarization, b. applied voltage same polarity as poling voltage: disk lengthens, c. applied voltage opposite	

	polarity as poling voltage: disk contracts (O'Halloran and O'Malley, 2004).....	51
Figure 5.9	A view of EAP, EPAM Roll Actuator from Artificial Muscle (Lowe, 2006	52
Figure 5.10	EAP actuators-energy density/frequency characteristics (Ducheon, 2005).....	52
Figure 5.11	Principle of operation EAP actuated devices (Bar-Cohen, 2000)	53
Figure 5.12	A view of Ionic EAPs, a. Ionic gel at reference state, b. activated state (O'Halloran and O'Malley, 2004; Bar-Cohen, 2004).....	54
Figure 5.13	a. An illustration of the IPMC gripper concept, b. A four-finger gripper (Shahinpoor and Kim, 2004).	54
Figure 5.14	Electronic EAPs a. Ferroelectric polymer in the reference state (left) and in its actuated state (right), b. circular strain test of a dielectric elastomer with carbon grease electrodes c. electrostrictive graft elastomer (O'Halloran and O'Malley, 2004)...	55
Figure 5.15	Working mechanism of Dielectric EAP (Ashley, 2003)	56
Figure 5.16	Comparison of artificial muscle properties (Ashley, 2003)	57
Figure 5.17	A variety of actuator configurations for dielectric elastomers, where the arrows the direction of actuation (O'Halloran and O'Malley, 2004).....	58
Figure 5.18	Spring Roll a. EAP roll actuator (Ducheon, 2005), b. Push-pull actuators, c. Bending rolls (Ashley, 2003).....	58
Figure 5.19	a. FLEX 2, b. Skitter (Peline, Kornbluh, Pei, Stanford, et.al, 2002)	59
Figure 5.20	An example of the Longitudinal EAP actuator (Bar-Cohen, 1997).....	59
Figure 5.21	Mechanical structure of ANTLA (Choi, Jung, Ryew, et.al, 2005)....	60
Figure 5.22	Chronological order of invention of a few actuators/artificial muscles	61
Figure 5.23	Max. Stress-Strain Graph for Actuator Materials (Bonser, Harwin, Hayes, et.al, 2004).....	62

Figure 5.24	Actuator Max. Strain-Power Density Graph (Kapps, 2007).....	62
Figure 5.25	Pneumatic artificial muscle model (Festo, 2006)	64
Figure 5.26	A view of set-up with Festo Pneumatic (McKibben) Artificial Muscle (Atılım University, Biomimetic Design Laboratory).....	65
Figure 5.27	A characteristic curve of Festo MAS 10 pneumatic muscles (Festo, 2006)	66
Figure 5.28	Working mechanism of grasshopper-like leg set-up of Festo pneumatic artificial muscle a. flexor artificial muscle is inflated, b. extensor muscle is inflated	66
Figure 5.29	A schematic view of the artificial muscle working mechanism	67
Figure 5.30	Piston and cylinder systems.....	68
Figure 5.31	A view of explosion due to electric discharge in piston-cylinder artificial muscle (Atılım University, Machine Shop).....	69
Figure 5.32	A view of a vertical piston position set-up whose circuit is detached from the EDM (Atılım University, Machine Shop).....	70
Figure 5.33	RC circuit set-ups a. with conventional micrometer and insulation for electrical wire, b. with digital micrometer and electrical isolation (Atılım University, Biomimetic Design Laboratory).....	71
Figure 5.34	A plastic cylinder- teflon piston system and its apparatus for using EDM (Atılım University, Machine Shop).....	71
Figure 5.35	The general construction of a. Kistler 9205 type force sensor, b. coupling element where SW 5.5 is a fork wrench (Kistler data sheet, 2005)	73
Figure 5.36	A view of Kistler force sensor set-up (Atılım University, Machine Shop)	73
Figure 5.37	The artificial muscle mechanism	75
Figure 5.38	The artificial muscle mechanism with a coupling element and a force sensor, Catia P3V5R10	76
Figure 5.39	The construct of artificial muscle mechanism, coupling element and force sensor and the force analysis set-up	76

Figure 5.40	A top view of the artificial muscle and the force sensor technical drawing with dimensions, Catia P3V5R10	77
Figure 5.41	An output screen showing force sensor and applied voltage using Agilent software for the experiments	77
Figure 6.1	A view of grasshopper-like bio-robot, Catia P3V5R10 drawing	80
Figure 6.2	a. A prototype of design of leg model, Catia P3V5R10, b. The working mechanism of new artificial muscle prototype in a jumping leg model (Atılım University, Biomimetic Design Laboratory).....	81
Figure 6.3	Position of centre of mass prototype in a jumping leg model until take-off (Atılım University, Biomimetic Design Laboratory)	81
Figure 6.4	A view of leg model with extensor and flexor biological muscles....	82
Figure 6.5	A view of leg model using single artificial muscle	83
Figure A.1	Body height ($z(t)$) of body movement of a Pholidoptera male before take-off for positive time definite	99
Figure A.2	Mathcad 2000 body height solutions, polynomial, Lagrange and least square methods solutions	104
Figure A.3	Femur-Tibia angle ($\alpha(t)$) of body movement of a Pholidoptera male before take-off for positive time definite	105
Figure A.4	Mathcad 2000 femur-tibia angle solutions, polynomial, Lagrange and least square methods solutions	109
Figure D.1	Mathematical models of the femur and tibia	113

CHAPTER 1

INTRODUCTION

Nature has highly effective and power efficient mechanisms. One of the recent challenges in Mechatronics Engineering is to mimic biological systems in robot design in engineering domain to make use of the efficient mechanisms in biological domain. This approach is known as biomimetic design and may have significant improvements in future engineering technology. The main aim of this work is to develop a typical case study for biomimetic design. “Grasshopper jumping” is selected as the topic of the case study. There is no particular reasoning in this selection.

Legged locomotion has been used by biological systems since the beginning of the biological life on earth. Although wheeled vehicles are so familiar and ubiquitous in our modern way of life, legged vehicles, especially jumping locomotion, are preference because of their better mobility in rough terrain (Savant, 2003) but they need extra effort to control their locomotion (Delcomyn and Nelson, 2000). Actually, surfaces for transportation like roadways and railways are not needed for the bio-robot transportation.

Insects in particular are well known not only for their speed and agility but also for their ability to traverse some of the most difficult terrains. Insects can be found navigating sparse or rocky ground, climbing vertical surfaces, or even walking upside down (Kingsley, 2005). In addition to walking, many insects jump to escape from predators, to increase their speed across land, or to launch into flight. Some insects, like bush crickets or grasshoppers, have long hind (rear) legs, so they can leap longer distances than insects of comparable mass with shorter legs (Lambrecht, Horchler and Quinn, 2005). Because of the challenge of these mechanisms jumping

mechanisms of the ensifera insects (e.g. crickets or grasshoppers) have been studied as a good source for bio-robotics by many researchers. A grasshopper-like jumping mechanism design is selected for biomimetic design in this thesis.

1.1 BIOMIMETICS AND BIOMIMETIC DESIGN

“The term biomimetics, which was coined by Otto H. Schmitt, represents the studies and imitation of nature’s methods, mechanisms and processes”, Bar-Cohen, 2006. *Biomimetics* (Biologically Inspired Technologies) is the abstraction of good design from nature (University of Reading, 1992) and its aim is to mimic biological life or systems (Leeuwen and Vreeken, 2004).

Biomimetic robots borrow their structure, senses and behavior from animals, such as humans or insects, (Stanford, 2005) and plants. *Biomimetic design* is design of a machine, a robot or a system in engineering domain that mimics operational and/or behavioral model of a biological system in nature. One can take biologically identified characteristics and seek an analogy in terms of engineering as shown in the Table 1.1.

Table 1.1 Characteristic similarities of biology and engineering system (Bar-Cohen, 2006)

Biology	Engineering	BIO- engineering/ mimetics/ nics/ mechanics
Body	System	System with multifunctional materials and structures are developed emulating the capability of biological systems.
Skeleton and bones	Structure and support struts	Support structures are part of every man-made system
Brain	Computer	Advances in computers are being made emulating the operation of the human brain
Intelligence	Artificial intelligence	There are numerous aspects of artificial intelligence that have been inspired by biology including augmented reality, autonomous systems, computational intelligence, expert systems, fuzzy logic, etc
Senses	Sensors	Computer vision, artificial vision, radar, and other proximity detectors all have direct biological analogies.
Muscles	Actuators	Artificial muscles
Electrochemical power generation	Rechargeable batteries	The use of biological materials to produce power will offer mechanical systems enormous advantages.

In this thesis the procedure given in Figure 1.1 is followed. The titles include a few subtitles but they cannot be described clearly step by step. All of them are mentioned in the related parts.

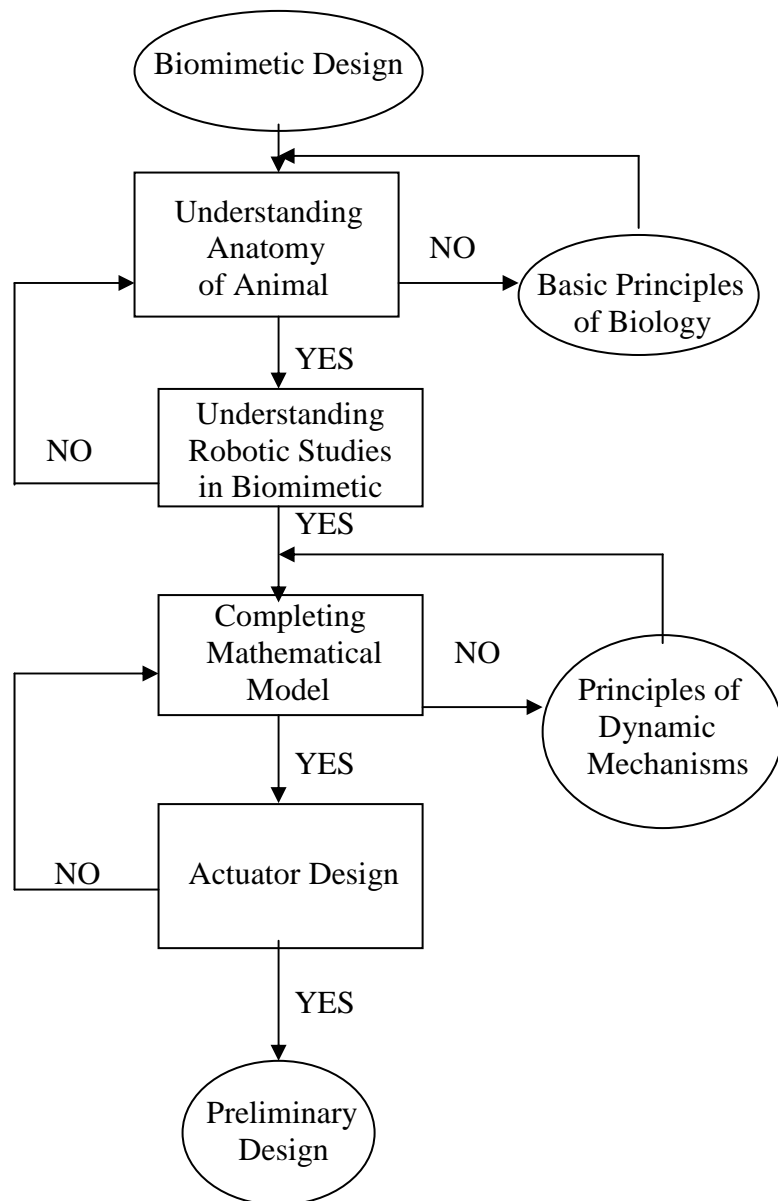


Figure 1.1 The main topics of Biomimetic design procedure

Before starting any biomimetic design, an extensive survey and analysis of jumping mechanism of the grasshopper in biology domain is necessary. There are many geniuses of grasshoppers in and around the Ankara region. Apterale types are selected to observe their behavior of the jumping locomotion. The species of the *Isophya nervosa* are seen frequently in this region. Many of these are observed in their natural environment and many others are captured and their bodies are studied (e.g. bodies' weight, length of their real legs). A picture of the captured grasshoppers is given in the Figure 1.2. Some useful data are collected, sorted, and analyzed for *Isophya nervosa*. However, mechanical structure of the insect-like robot is modeled from the Pholidoptera. This insect is selected as a model because its structure and physiology are reasonably well known. A mathematical model is developed for the genius of Pholidoptera. The data from the experimental results of the Pholidoptera is used to evaluate the mathematical model. A new artificial muscle is developed to be used in the mechanism.



Figure 1.2 Pictures of grasshoppers of *Isophya Nervosa* captured in Ankara

1.2 SCOPE OF THE THESIS

This work is intended to develop a jumping mechanism for a “grasshopper-like” robot. Biomimetic design of an animal for robot technology can be classified by lots of titles and subtitles. Organization of this thesis can be summarized according to this classification. In Chapter 2, literature survey about grasshoppers is presented. Anatomy of grasshoppers jumping mechanism, a biological force system of grasshoppers, and jumping strategy of them are summarized in this chapter.

Jumping and hopping robots are discussed in Chapter 3. Biomimetic studies on robot technology are examined briefly in this part. In Chapter 4, a mathematical model is developed and its analysis is completed for the jumping mechanism. 2 DOF and 3 DOF models are studied and the position of a grasshopper’s hind legs is determined from these models. Moreover, joints torque is analyzed.

In addition to these chapters, in Chapter 5, artificial muscles are considered as actuators of biomimetic design. The technical features of some important artificial muscles are tabulated. A challenge point of this thesis is the artificial muscle study. An artificial muscle is not only developed but also added in the literature as a new technological actuator. Force analysis of the actuator is completed with Kistler, Low Level Force Piezoelectric Sensor. After design of the actuator, preliminary design of grasshopper-like jumping mechanism is mentioned briefly in Chapter 6. All of chapters are concluded and further recommendations are given in Chapter 7.

CHAPTER 2

LITERATURE SURVEY ON THE ANATOMY OF GRASSHOPPER

As mentioned in the previous chapter, Biomimetic term comes from mimicking nature. If nature systems are to be mimicked in engineering, anatomy of them should be studied as a first step of biomimetic design. In this study, not only walking mechanism of grasshoppers jumping system is presented but also two jumping styles of grasshoppers are summarized briefly.

2.1 ANATOMY OF GRASSHOPPER LEGS

Grasshoppers have six legs, like most of the other insects, match in pairs across their thorax. Anatomy of a grasshopper is illustrated in Figure 2.1 which was generated by Enchanted Learning (1999) and Konez, Erden and Akkök (2006) to show the details of the legs on the body. Figure 2.2 shows all of the six legs inherited from the same animal- a locust of the species *Schistocerca gregaria*. Bigger rear (hind or metathoracic, (Fauske, 2002)) leg is advantageous for jumping (Pfadt, 2002), because it increases the length over which the jumper can exert a pushing force on the ground.

Each of three pairs of legs, though very different in size and function, has five distinct segments; coxa, trochanter, femur, tibia and tarsus as shown in Figure 2.2. These segmental constructions are highly efficient for actuation, so grasshoppers optimize their specialized locomotors' behaviors (Birch, Quinn, et al., 2005). The hind tibia has two rows of spines and enlarged movable spurs (*calcaria* or calcar, (Fauske, 2002)) at its apex. The number of spines and the length of calcars vary

among species. There are two *claws* at the end of the tarsus, which give the grasshopper a good gripping ability and prevent sliding when it pushes on the ground as it jumps (Heitler, 2005). A pad between these claws is called *arolium* (Pfadt, 2002) and it has an important function to create friction with the ground surface.

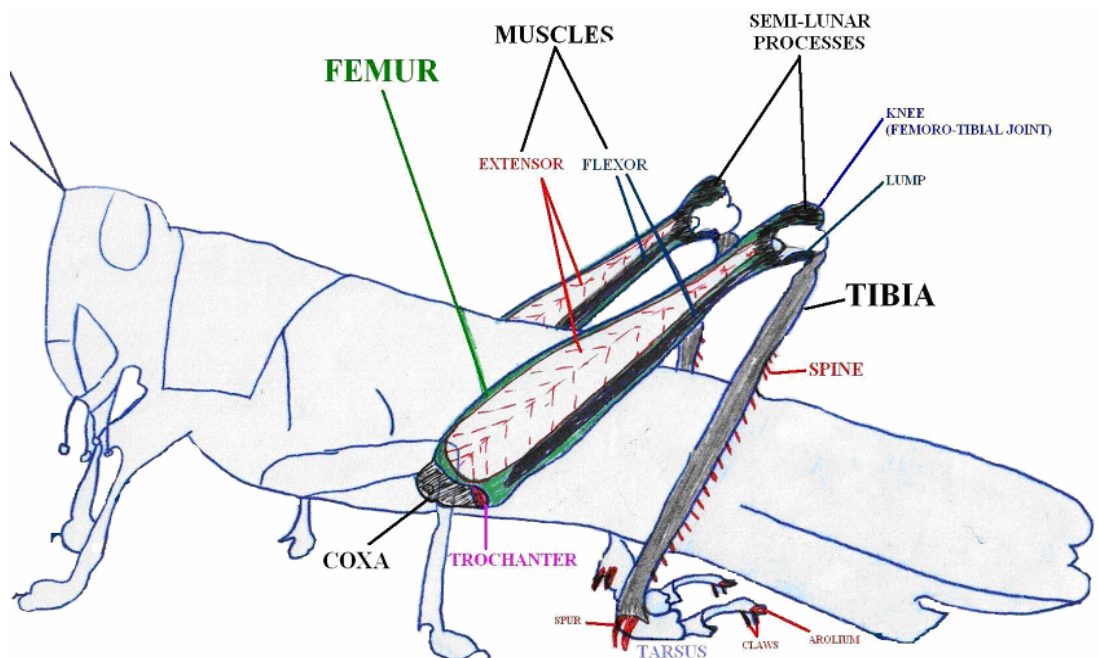


Figure 2.1 Anatomy of a Grasshopper (Konez, Erden and Akkk, 2006)

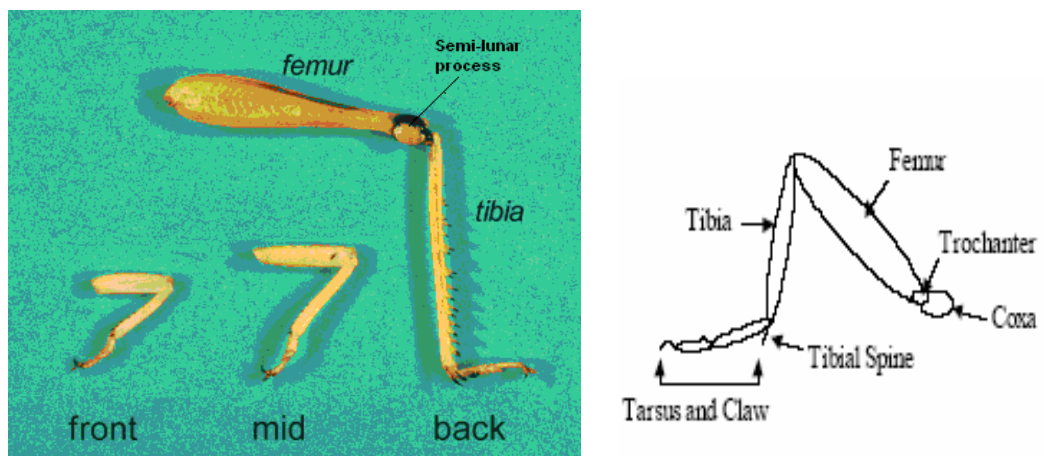


Figure 2.2 Hind leg with segments identified (Fauske, 2002; Laksanacharoen, Pollack, et al., 2005; Laksanacharoen, Quinn and Ritzmann, 2003).

Segment joints can have a single or multiple degrees of freedom (DOF) for a hind leg. Those are given in Table 2.1. The significant feature of the coxa is the existence of a soft tissue, 3 DOF joint that connects it to the body of the animal, enabling complex positioning of the entire leg. Since the coxa segment is very small in all legs of the grasshopper, it is ignored in robotics.

The trochanter is an even smaller segment, connecting the coxa and femur through two 1 DOF joints (Laksanacharoen, Pollack, et.al, 2005). The joint between the trochanter and femur has very little movement; trochanter is considered to be negligible in the biomimetic robot design approach, so reducing high level DOF is secured. Insect legs also have a foot-like tarsus, but in order to keep the legs relatively simple, it is modeled as a flexible plate. The femur-tibia (FT) and tibia-tarsus (TT) joints are also 1 DOF. With the exception of the mostly immobile trochanter-femur joint, all of the 1 DOF joints (a simple hinge joint, Figure 2.3) act in the same plane (Laksanacharoen, Pollack, et.al, 2005).

Table.2.1 Degrees of freedom of the hind leg joint

Joint	Degrees of Freedom (DOF)	Total DOF	
Body-Coxa	3 DOF		Body-Femur joint is 3DOF
Coxa-Femur	1 DOF	Coxa-Trochanter-Femur (CTF) joint is 1DOF	
Coxa-Trochanter	1 DOF		
Trochanter-Femur	Very small movement		
Femur-Tibia (FT)	1 DOF		
Tibia-Tarsus (TT)	1 DOF		



Figure 2.3 Hinge Joint Model

2.1.1 Anatomy of Grasshopper Muscles

The hind femur is the enlarged jumping spring of the hind legs; it includes flexor and extensor muscles inside the exoskeleton (hard shell). These muscles can be seen in Figure 2.4. Because of its size and pennate anatomy, the extensor muscle is stronger than the flexor. In a pennate muscle, the fascicles form a common angle with the tendon. Because the muscle cells pull at an angle, contracting pennate muscles do not move their tendons.

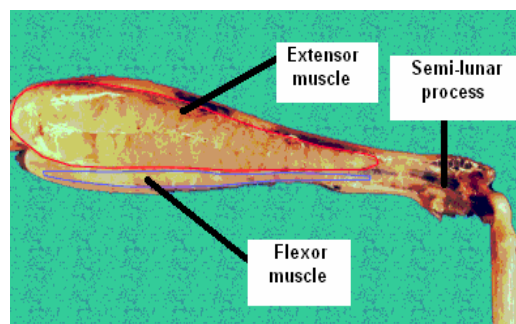


Figure 2.4 Extensor muscle (top of the femur) and flexor muscle (bottom of the femur) (Heitler, 2005)

Although the flexor muscle's size is smaller than extensor muscle's, it can work as nearly stronger as extensor muscle due to *lump* structure. In the knee of the hind leg there is a structure which looks like a small black pit. This pit is in fact a *lump* that sticks into the cavity of the femur (Figure 2.5).

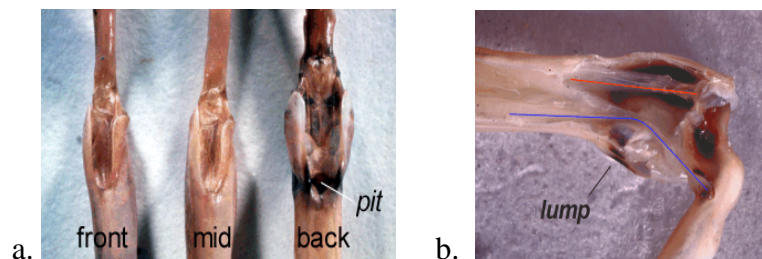


Figure 2.5 The structure of the lump a. the lump from the outside looks like a pit, b. the lump sticks into the joint (Heitler, 2005)

“The lump is absolutely crucial for the jump, because it enables the weak flexor muscle to hold the tibia flexed against the strong extensor muscle during the energy build-up”, Heitler, 2005. Working mechanism’s animation is given Figure 2.6. Two features account for this:

- **The lever system**

The lump changes the angle with which the flexor tendon pulls on the tibia. When the tibia is fully flexed, the flexor muscle has a very direct line of pull on the tibia, while the extensor has a very indirect line of pull. The flexor thus has a large mechanical advantage over the extensor muscle.

- **The tendon pocket**

An additional feature comes into play in the fully flexed position. There is a small pocket in the middle of the flexor tendon, close to where it joins onto the tibia. As the tibia comes into the fully flexed position, this pocket arrives over the lump, and slides down onto it. This further increase the ability of the flexor muscle to hold the tibia flexed against the strong extensor muscle.

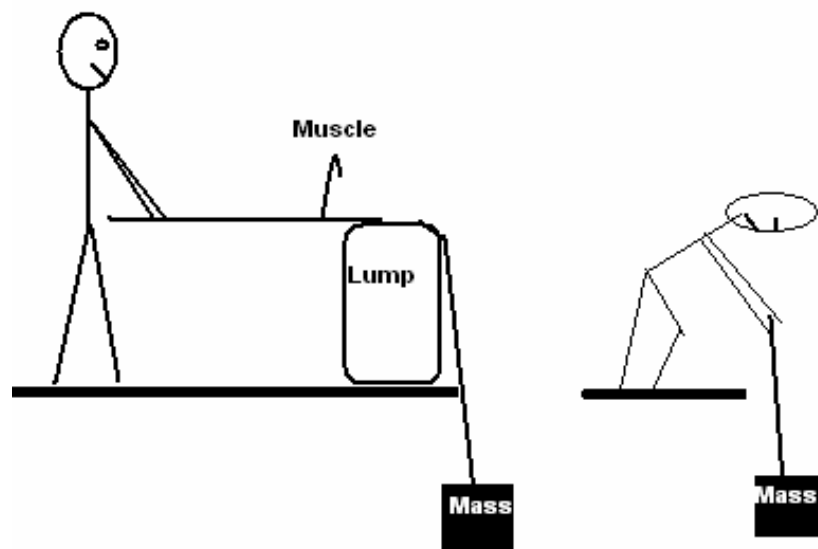


Figure 2.6 Working strategy of the lump

2.1.2 Working Mechanism of Hind Leg Joints

Muscles working mechanism is given in Figure 2.7. When one of the muscle contracts, it pulls on its tendon and moves the tibia one way, when the other muscle contracts, it moves the tibia the other way (Heitler, 2005).

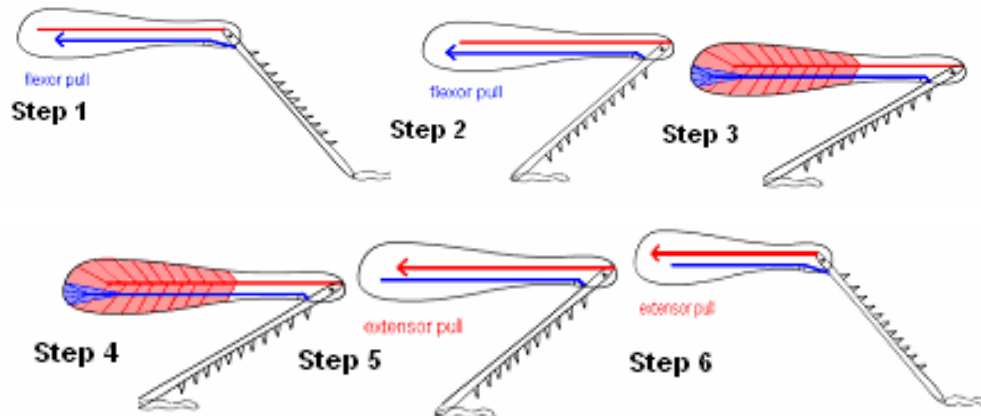


Figure 2.7 Muscles working mechanism (Heitler, 2005)

Grasshoppers have a like-catapult (*semi-lunar process*), the black half-moon shaped region, in the hind legs made from special cuticle (Figure 2.4). This process is only found on the hind legs—it is completely missing from the front and middle legs (Figure 2.8). This structure has a similar function of a torsion spring and store energy (Burrows and Morris, 2002; Heitler, 2005). About half of the jumping energy is stored in these processes (Bennet-Clark, 1975; Burrows and Morris, 2002; Heitler, 2005) at femur-tibia joint (Figure 2.9) while the remainder is stored in extensor tendon and cuticle of the femur (Bennet and Clark, 1975).

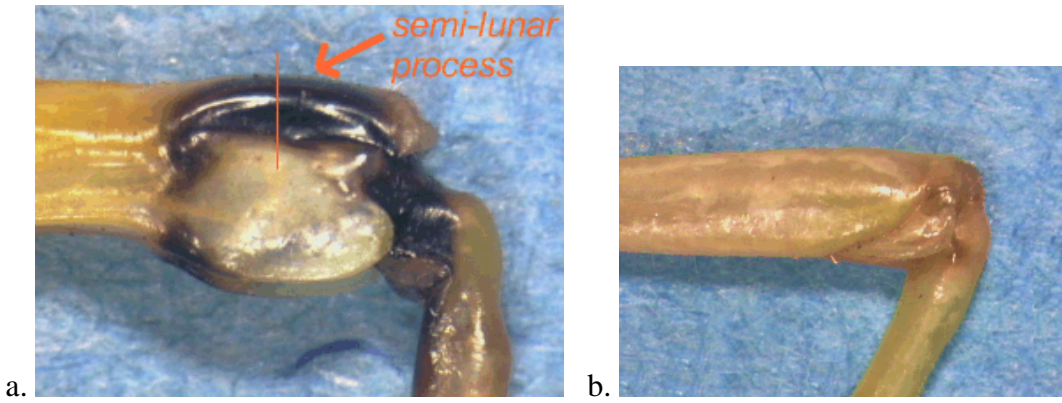


Figure 2.8 The joint region of a hind and middle legs a. hind leg knee joint, b. middle leg knee joint (Heitler, 2005)

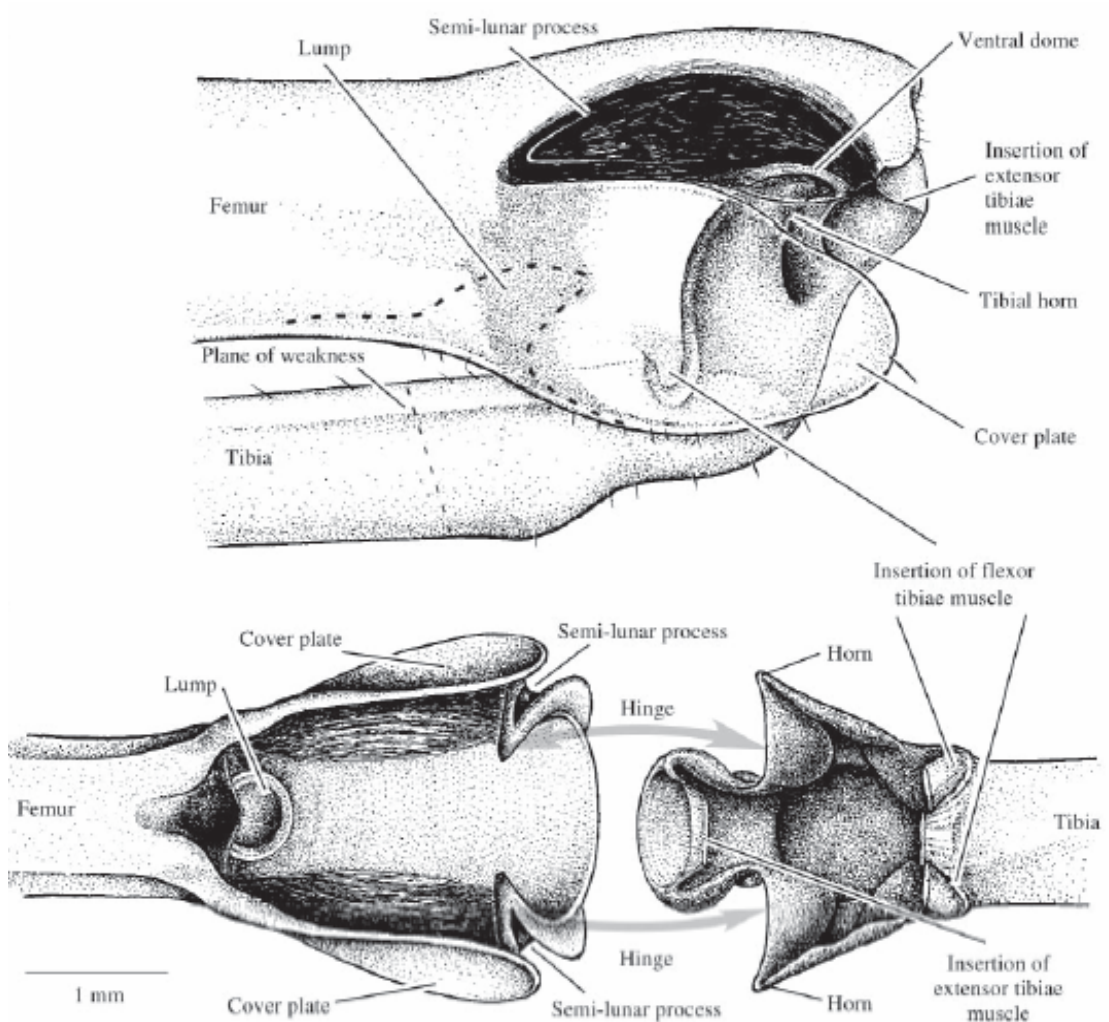


Figure 2.9 Anatomy of the femur-tibia joint of a left hind leg of a mature locust (Burrows and Morris, 2001)

The spring cuticle is extremely uniform in consistency, almost glass-like (Figure 2.10). It is very stiff, and thus it is able to store significant amount of energy for a relatively small amount of bending (like strong elastic in a catapult). Although normal cuticle is quite strong in the sense, not easily break, because of its nonuniform structure it is very bendy and flexible, and cannot be use for storing energy (Heitler, 2005).

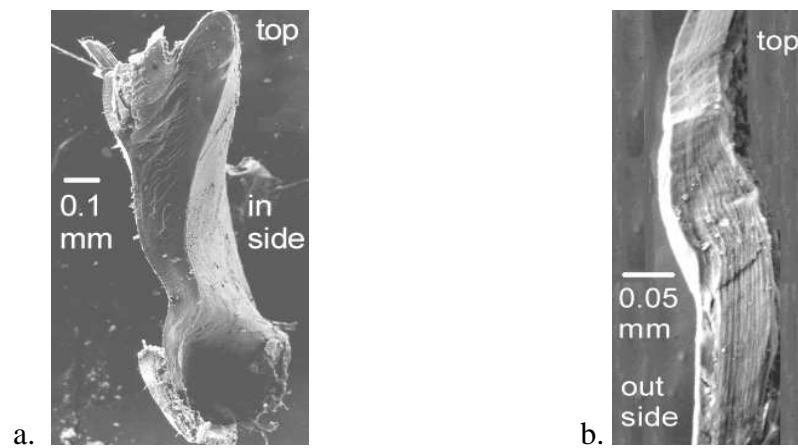


Figure 2.10 The scanning electron micrograph of the a. spring cuticle (semi-lunar process), b. normal cuticle (tibial cuticle, (Heitler, 2005)).

2.2 GRASSHOPPER JUMPING MECHANISM

If a proportion between body mass and muscles, used in jumping, is the same, jumping height is almost the same for small and large animals (Burrows and Morris, 2003). A good jump depends on two conditions (Emporia State University, 2005; Heitler, 2005);

- The legs on the ground should create thrust with a high force. If the thrust is too low, the animal may not have high initial velocity and it cannot land very far.
- The legs have to develop this force in a short time. If the thrust builds up too slowly, the legs extend standing on tip-toe before the thrust reaches its maximum.

Two different jumping styles are proposed;

I. According to Burrows and Morris (2003), similar as Pholidoptera's jumping (Figure 2.11 and 2.12);

1. A jump begins with a forward rotation of the hind legs at their body-coxa joints and a flexion of the tibia about the femur as shown in Figure 2.11. The flexion of the tibia is not always complete so that one or both hind legs could begin their rapid extension movement from the partially extended position.
2. As the hind tibiae are extended, the body is raised from the ground and the forwardly directed antennae are swung backwards to point over the body as shown in Figure 2.12.a.
3. When viewed from the front side, the hind legs can be seen to rotate outwards at their joints with the coxa, and both the middle and front legs depress at their coxa joints and extend at their femur-tibia joints as illustrated in Figure 2.12.b.
4. The continuing elevation of the body eventually leads to the front and middle legs losing contact with the ground before the hind legs, so that it is the hind legs that provide the thrust for the final 10-12 ms before the insect becomes airborne as it is shown in Figure 2.11.

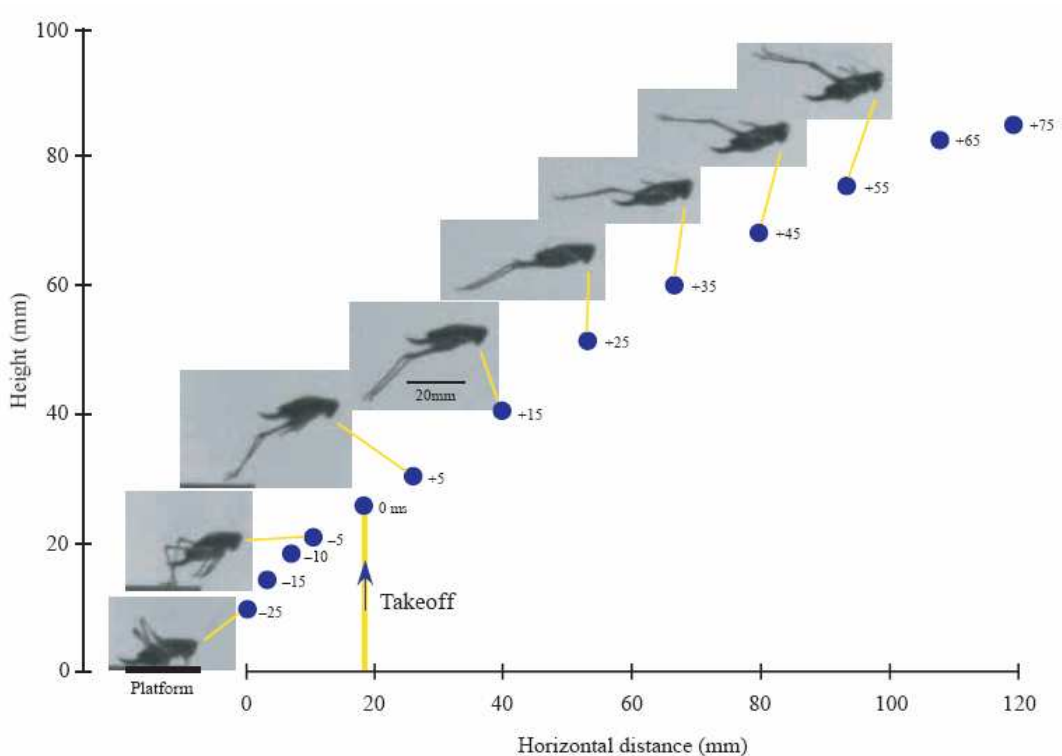


Figure 2.11 The trajectory of a female Pholidoptera during a jump. The numbers give the time before and after take-off at 0 ms (Burrows and Morris, 2003).

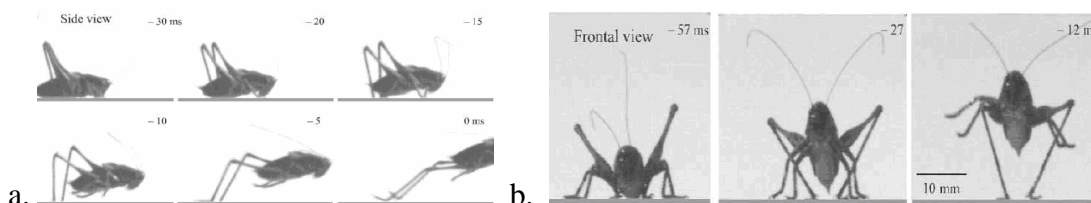


Figure 2.12 Selected frames from the same jump a. Viewed from the side, b. Viewed head-on (Burrows and Morris, 2003).

II. According to Heitler (2005), grasshopper jumping goes through a set of routine activity (a motor program) before it actually takes off as shown in Figure 2.7 and 2.13. The main difference between these two jumping styles is that Heitler's motor program has a co-activation in which flexor and extensor muscles contract together which is fit with Hill's muscle model. The contraction of the flexor muscle keeps the tibia in the fully flexed position, so that the simultaneous contraction of the extensor

muscle bends the springs in the joint, rather than extending the leg. The extensor muscle contraction is quite slow (about half a second), and this means that the muscle can contract with maximum force. The energy of the contraction is stored in the semi-lunar shaped region. The other difference is that knee (femur-tibia joint) is closer to the surface when starting to the jumping instead of maintaining the initial position, i.e. knee is movable.

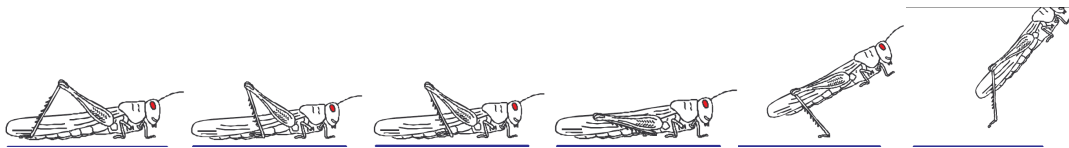


Figure 2.13 A routine program of grasshopper jumping (Heitler, 2005)

In this chapter the anatomy of grasshoppers' hind leg is summarized and compared with mid and front legs. Extensor and flexor muscles and semi-lunar process of grasshoppers are described briefly and working mechanism of legs and muscles' significance are emphasized. Since the Pholidoptera structure and physiology are reasonably well-known, and empirical data of this type are observed in the literature, the studies of Burrows and Morris (2003) will be considered in proceeding chapters.

CHAPTER 3

JUMPING AND/OR HOPPING MECHANISMS AND INSECT-LIKE ROBOTS

After the survey on the grasshoppers jumping mechanism in the literature, some hopping and jumping machines and robots that utilizes of jumping mechanisms are investigated as a second step of the biomimetic design.

3.1 HOPPING MACHINE

In 1983, a hopping machine, with only one leg, was built by Raibert at Carnegie-Mellon University (Wei, Nelson, et al., 2005). The leg has three degrees of freedom. The vertical motion was provided by a pneumatic cylinder, which is mounted on the body frame via a gimbal joint.

3.2 MONOPOD HOPPING ROBOTS

Raibert (1986; 1993) developed several monopod robots that hop. Although they were not statically stable, their controllers achieved active dynamic stabilization. He showed that the control theory that governs the performance of monopod robots could be used to control multi-legged ones. In contrast, Ringrose (1997) developed several monopod robots that are not only statically stable, but are also passively dynamically stable. The special shape of its foot creates this stability. The foot's curvature causes a restoring torque to be imparted to the robot if it begins to tip over. Kingsley (1999) also developed a monopod hopping robot (Figure 3.1, (Wei, Nelson, et al., 2005)). The robot, Figure 3.1, fits into a 5 cm³. This robot is autonomous, and is

designed to be statically and passively dynamically stable. Hopping is achieved through the excitation of a spring-mass system at its resonant frequency.

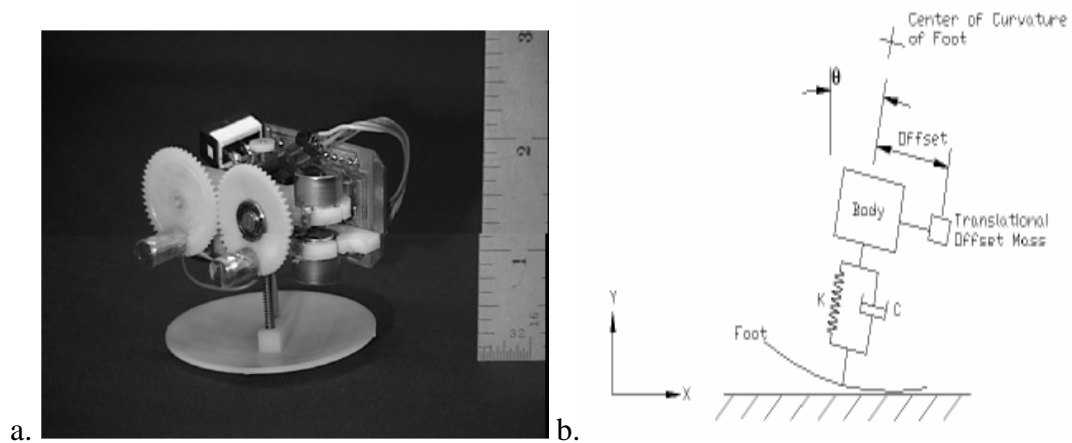


Figure 3.1 a. 5 cm Monopod Hopping Robot, b. The simulated 2-D robot has five degrees of freedom. Forces were modeled with springs and dampers (Wei, Nelson, Quinn, Verma and Garverick, 2005).

3.3 OMNIPEDA (SERPENTINE ROBOT)

OmniPede was developed at the University of Michigan's Mobile Robotics Lab for the study of serpentine robot actuation (Figure 3.2). Pneumatic cylinders are used to actuate the 2 DOF articulate joints that connect the segments.



Figure 3.2 A view of OmniPede prototype (Granosik and Borenstein, 2004)

3.4 A SMALL, INSECT-INSPIRED ROBOT

Mini-Whegs weights less than 90 g, but can run at over three body-lengths per second and surmount 3.8 cm high obstacles. It incorporates fully independent running and jumping modes of locomotion using mechanic power (Morrey, et.al, 2003). The controllable jumping mechanism allows it to leap as high as 18 cm (Figure 3.3, (Lambrecht, Horchler, and Quinn, 2005)).

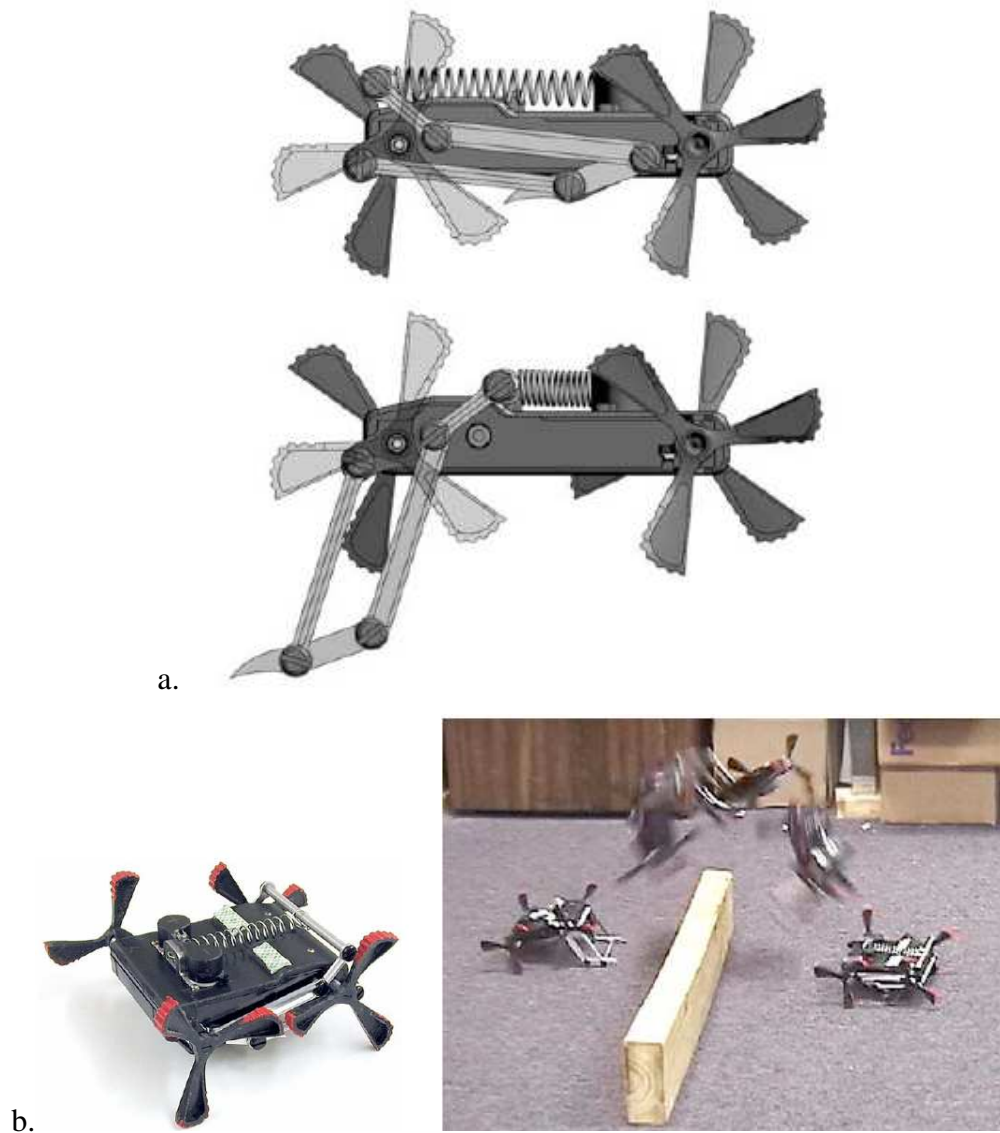


Figure 3.3 a. The jumping mechanism of Mini-Whegs in retracted (top) and released (bottom) positions, b. Composite of video frames showing Mini-Whegs jumping high over a 9 cm barrier (Lambrecht, Horchler, and Quinn, 2005).

3.5 BIOMIMETIC HEXAPOD ROBOT

Based on the features of an agile insect, the American cockroach is worked on a six legged robot with 58 cm length, 14 cm width, and 23 cm height (Figure 3.4). The legs of the robot were designed with three segments; coxa, femur and tibia. Tarsus and trochanter were ignored in this design. Each of joints between body-coxa, coxa-femur and femur tibia is a simple hinge joint. The robot, biobot, is powered by pneumatic actuators. Functional use of a single dual action cylinder provides movement in two directions as shown in Figure 3.5. The cylinder generates either flexion or extension of the next limb segment depending on which chamber is filled with pressurized air. The robot is considerably heavy, 11 kg, in relation to its size due to the weight of the valve (Delcomyn and Nelson, 2000).

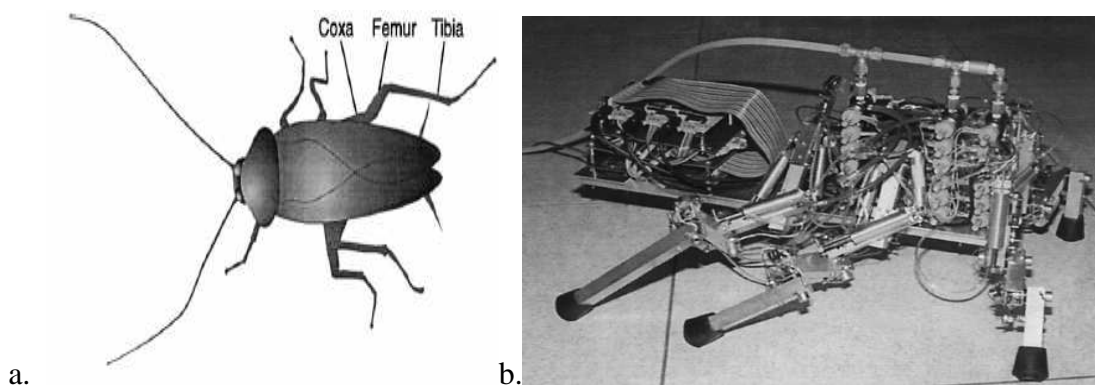


Figure 3.4 a. An American Cockroach, b. Biobot (Delcomyn and Nelson, 2000)

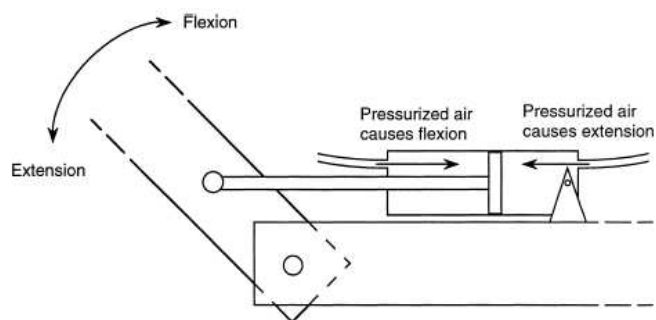


Figure 3.5 Working process of the pneumatic muscle (Delcomyn and Nelson, 2000)

3.6 CRICKET MICRO-ROBOTS

CWR University Cricket Micro-robot: Researchers at Case Western Reserve University (CWRU) have developed three hexapod robots based on insects (Figure 3.6, (Birch, Quinn, Hahm, et al., 2005; Birch, Quinn, Hahm, et al., 2000; Espenscheid, Quinn, Beer and Chiel, 1993; Webb and Harrison, 2005)). Important features of these robots are tabulated in Table 3.1 (Espenscheid, Quinn, Beer and Chiel, 1993).

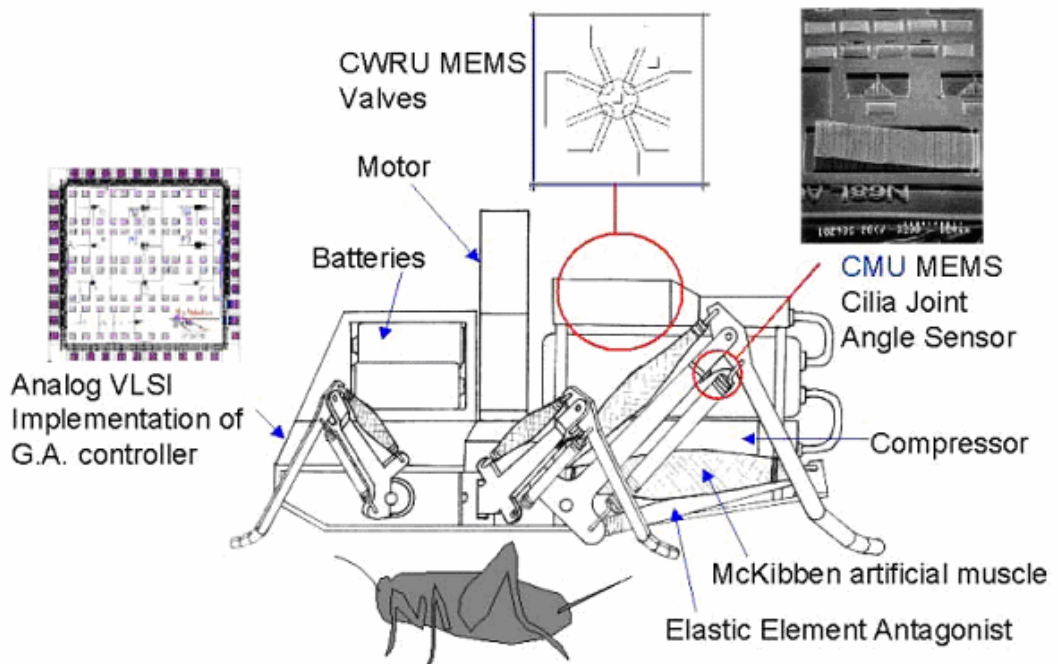


Figure 3.6 Anatomy of the cricket micro-robot (Birch, Quinn, et al., 2005)

Table 3.1 CWRU Hexapod Robots features

Robots	Based on	DOF	Controllers	Size
RI	Stick insects	2 DOF in each leg	Neural Network Controller	Much larger than their animal models
RII	Stick insects	3 DOF in each leg	Controllers were developed to enable insect-like gait movement	
RIII	Cockroach (Blaberus Discoidalis)	Hind legs; 3 DOF Middle legs; 4 DOF Front legs; 5 DOF	Complex Postural Controller	Much larger than their animal models

Cricket Cart Robot: Actuators, sensors and controllers were tested on this simple legged platform, “Cricket Cart Robot”. It was constructed by mounting a pair of the cricket robot’s rear legs on a wheeled cart as shown in Figure 3.7.

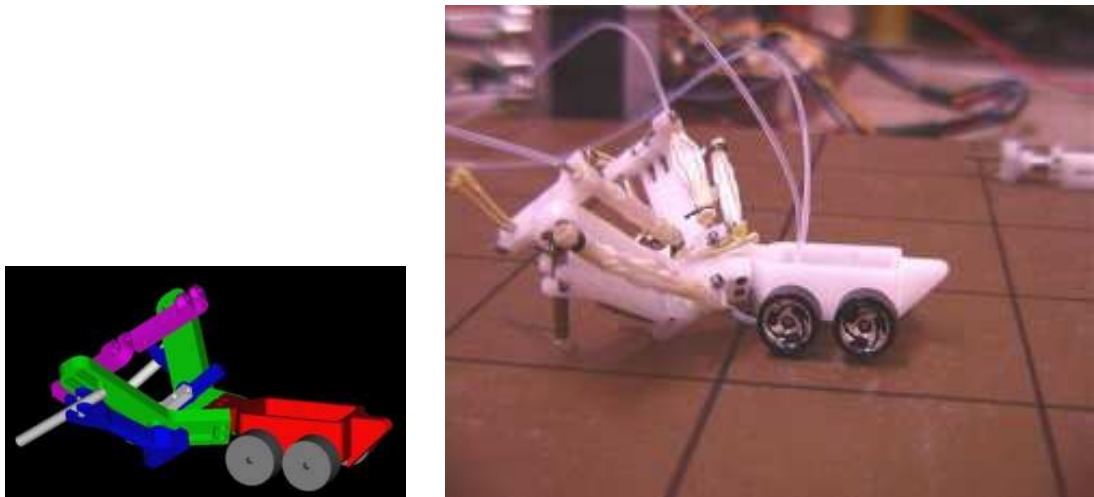


Figure 3.7 A view of the Cricket Cart Robot (Birch, Quinn, Hahm, Phillips, et al., 2005).

A Miniature Hybrid Robot Propelled by Legs: The autonomous hybrid micro-robot uses its rear legs for propulsion and its front wheel help to support the body weight (Figure 3.8). As a result, hybrid means that it uses both wheels and legs.

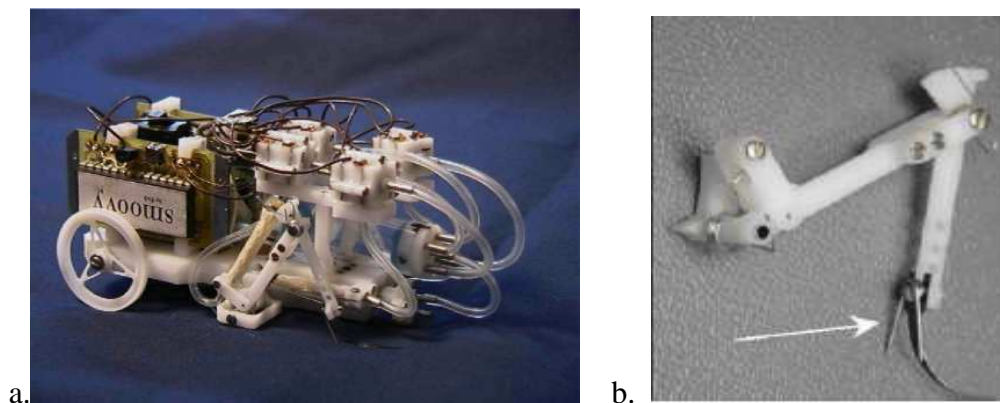


Figure 3.8 a. A Hybrid robot, b. One leg of the hybrid robot (Birch, Quinn, et.al, 2005)

3.7 QUADRUPED JUMPING ROBOT

The robot was designed by legs which widely spread like spiders (Figure 3.9). The legs are consisted of 4-bar linkages (Kikuchi, Ota et.al, 2003). Legs are controlled by a pair of pneumatic cylinders as shown in Figure 3.10. It can jump only at the same position; it protects its lateral position which is different from the first idea of concept (Titech, 2006).

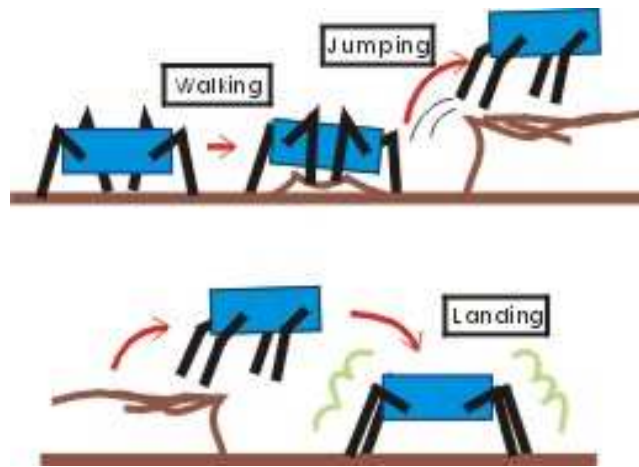


Figure 3.9 Locomotion Concept of Jumping Quadruped (Kikuchi, Ota et.al, 2003)



Figure 3.10 A view of Quadruped Jumping Robot (Titech, 2006)

3.8 LOBSTER ROBOT

A biomimetic robot based on the American lobster was developed and built at Northeastern University. Safak and Adams, 2002, emphasize that “The robot is intended for autonomous remote-sensing operations in rivers and/or the littoral zone ocean bottom with robust adaptations to irregular bottom contours, current and surge”.

The robot is an 8-legged ambulatory vehicle, as shown in Figure 3.11, with 3-degrees-of-freedom per leg. A pair of Nitinol artificial muscle modules, shows the shape memory effect, is used for all leg joints. The Nitinol muscle modules are activated by an electrical current. The generated heat brings about a phase transformation and provides recovery of the strain. The Nitinol muscle modules are attached to a mechanical system of levers, which produce the rotator motion of the robot joints (Safak and Adams, 2002).

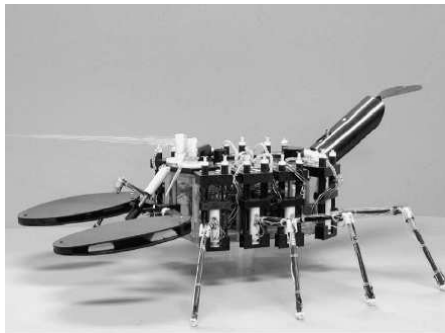


Figure 3.11 A view of Lobster robot (Safak and Adams, 2002)

Jumping and/or hopping mechanisms and insect-like robots are introduced briefly in this chapter. Most of them can only walk and are controlled with pneumatic actuators. Nowadays bio-robotic scientists are focused on jumping mechanisms of insects. One of the well-known of these studies is the Cricket-like, hexapod, robot. This robot is able to not only jump but also walk with pneumatic artificial muscles. However, jumping features of the cricket-like robot are weaker compared to the real model and they have to be improved.

CHAPTER 4

MODELING AND ANALYSIS OF GRASSHOPPER-LIKE JUMPING MECHANISM

Developing a biomimetic design requires careful focusing and modeling on the biological domain to mimic the biological functions in engineering domain. Third step of the biomimetic design is to develop a mathematical model and analyzing it on the way of the biomimetic design tree. Equations of the leg models are developed by the following steps;

- a. A mathematical model description for the leg,
- b. Kinematic analysis of the leg,
- c. Dynamic analysis of the leg.

Two leg models, 2D and 3D, are developed in this chapter. Three structures, coxa, trochanter, and tarsus, are ignored to reduce complexity of the models.

4.1 3D LEG MODEL

4.1.1 Mathematical Model Description for 3D Leg Model

Insects usually have many degrees of freedom. If bio-robots have degrees of freedom as many as the real one has, they would be complicated mechanisms to analyze and control. Although a robot may have many moving parts, these are all connected together and execute a fixed cycle, which can be specified by a few parameters. Consequently, reducing the number of degrees of freedom to a manageable level is necessary to analyze leg structures easily.

Ways of managing complexity may be summarized as follows;

1. Reducing the number of DOF; analytically, by finding approximations, constraints and by designing machines with the minimum number of joints.
2. Splitting a complex problem into several simpler ones by, for example, separating the control of quantities which do not interact significantly.

A leg model is developed with 2 segments instead of 5 segments in the actual model and the model has 3 degrees of freedom (DOF). Trochanter, coxa and tarsus structures are ignored for not only 2D of leg model but also 3D of leg model.

4.1.2 Kinematic Analysis for 3D Leg Model

There are two joints in the 3D model; body-femur and femur-tibia, and there are also three angles; femur- tibia angle, $\alpha(t)$, and body-femur angles, $\beta(t)$ and $\gamma(t)$ as shown in Figure 4.1. The position of centre of mass is represented as x, y, and z and can be expressed in terms of the femur length, L_1 , and the tibia length, L_2 , as;

$$x(t) = L_1 \cdot \cos(\gamma(t)) \cdot \sin(\beta(t)) - L_2 \cdot \cos(\gamma(t)) \cdot \sin(\beta(t) - \alpha(t)) + 0.27 \quad (4.1)$$

$$y(t) = L_1 \cdot \cos(\beta(t)) \cdot \sin(\gamma(t)) - L_2 \cdot \cos(\beta(t) - \alpha(t)) \cdot \sin(\gamma(t)) + 2.42 \quad (4.2)$$

$$z(t) = -L_1 \cdot \cos(\gamma(t)) \cdot \cos(\beta(t)) + L_2 \cdot \cos(\gamma(t)) \cdot \cos(\beta(t) - \alpha(t)) \quad (4.3)$$

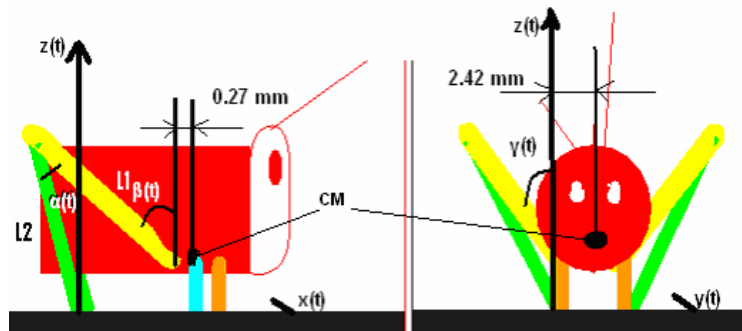


Figure 4.1 The grasshopper (Pholidoptera) leg model (CM: Centre of Mass)

According to the published experimental data $L_1=17.1$ mm, $L_2= 15.6$ mm (Table 4.1, (Burrows and Morris, 2003)). To prevent complexity of the robot and reducing the number of degrees of freedom to a manageable level the rear legs also froze the active $\gamma(t)$ joint at 30° . $\alpha(t)$ and $z(t)$ are taken from the experimental data of Burrow and Morris, given in Figure 4.2.

Table 4.1 Experimental data (Burrows and Morris, 2003) used for jumping simulation

Body Structure	Total body mass (M)	415 mg
	Hind leg tibia length (L_{tibia})	15.6 mm
	Hind leg femur length (L_{femur})	17.1 mm
	Hind leg femur max.-min. diameter ($D_1- D_2$)	3.2-0.8 mm
	Tibia tubular construction diameter (D_3)	0.6 mm
	Extensor muscle occupying a cross-sectional area	4.4 mm^2
	Flexor muscle occupying a cross-sectional area	1.08 mm^2
	Angle of rotation of tibia	165°
	Lump Thickness	130 μm
Jumping Performance	Horizontal distance (d)	302 mm
	Take-off angle (α)	33.8 deg
	Potential Energy (E_p)	$20\mu\text{J}$
	Co-contraction time (ms)	50-250
	Density coefficient of leg material (ρ)	1.025 kg/m^3

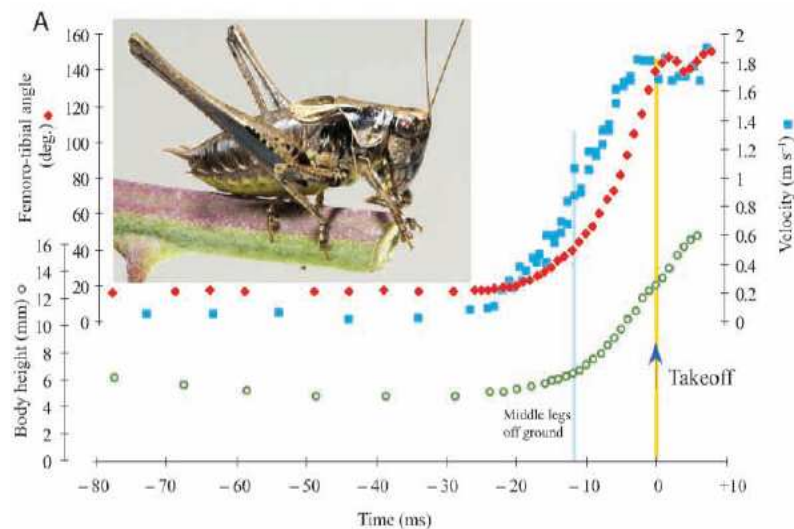


Figure 4.2 The changes in the Femur-Tibia angle, body height and velocity of body movement during a jump by a Pholidoptera male (Burrows and Morris, 2003).

Body height and femur-tibia angle changes are assumed to be zero in the interval between -80 ms to -20 ms, so the changes can be ignored. Hence, the body height ($z(t)$) and Femur-Tibia angle ($\alpha(t)$) can be represented analytically by using the empirical data obtained from the Figure 4.3 where -20 ms are shifted to origin for using positive time in equations. The formulae are tabulated in the Table 4.2 for a positive time interval to be used in the kinematical analysis.

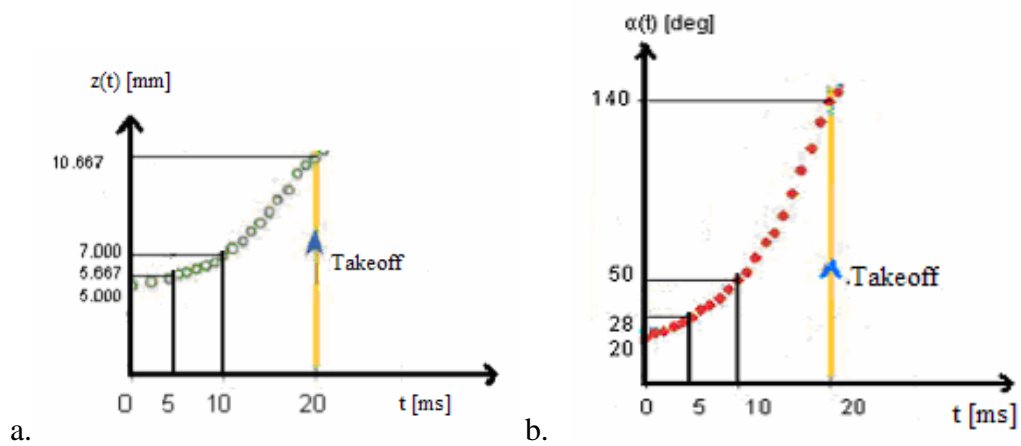


Figure 4.3 a. Body height ($z(t)$), b. Femur-Tibia angle ($\alpha(t)$) of real body movement of a Pholidoptera male before take-off for positive time definite.

Table 4.2 Body height and femur tibia angle parabolic curves according to a time interval.

Time (t (ms))	$0 \leq t \leq 20$
body height ($z(t)$ (mm))	$-0.00332333t^3 + 0.018305t^2 + 0.0501833t + 5$
femur-tibia angle(α (deg))	$0.00133333t^3 + 0.026t^2 + 0.26666675t + 20$

$\beta(t)$ can be determined from the equations (4.1), (4.2) and (4.3), the way of solution is given in Appendix B.

$$\beta(t) = \delta(t) + a \cos\left(\frac{z(t)}{E(t)}\right) \quad (4.4)$$

where $E(t) = \sqrt{(C + D \cdot \cos(\alpha(t)))^2 + (D \cdot \sin(\alpha(t)))^2}$;

$$\delta(t) = a \tan\left(\frac{D \cdot \sin(\alpha(t))}{C + D \cdot \cos(\alpha(t))}\right);$$

$$C = -L1 \cdot \cos(\gamma(t))$$

and

$$D = L2 \cdot \cos(\gamma(t))$$

The body velocity during taking-off is determined;

$$V(t) = \left(\left(\frac{dx(t)}{dt} \right)^2 + \left(\frac{dz(t)}{dt} \right)^2 \right)^{1/2} \quad (4.5)$$

4.1.3 Kinematic and Dynamic Analyses According to Experimental Data

Some biologists have already developed mathematical models for understanding jumping mechanisms of locust and grasshopper species. A summary of these studies about Pholidoptera and a different genus which cannot jump are given in Table 4.3. The generally accepted approach is that the motion of a jumping animal after it leaves the ground is similar to a *ballistic* movement (Heitler, 2005).

Table 4.3 Body form of Pholidoptera and a different genius and their jumping performance (Burrows and Morris, 2003)

Insect	Body		Leg length		Jumping				
	mass (mg)	Length (mm)	Tibia (mm)	Femur (mm)	Distance (mm)	Extension time (ms)	Takeoff		Energy (μ J)
							Velocity (m.s^{-1})	Angle (deg)	
Pholidoptera ♀	602 ± 42	23.2 ± 0.8	17.8 ± 0.3	18.7 ± 0.4	296 ± 14.7	32.6 ± 0.95	2.12 ± 0.33		1380
Pholidoptera ♂	415 ± 20	21.6 ± 0.6	15.6 ± 0.2	17.1 ± 0.2	302 ± 11.5	30.6 ± 2.7	1.51 ± 0.2	33.8 ± 2.1	490
Carausius morosus ♀ (cannot jump)	1100 ± 4	78 ± 0.15	17	17	-	-	-	-	-

A mathematical model, used by Elliot, Zumstein, Forman, Nongthomba and Sparrow (2004) and Burrows and Morris, (2002), is borrowed to develop equations of motion with two separate assumptions;

i. Air resistance is ignored: If the air resistance is neglected, the horizontal distance, d , jumped by a fly is determined solely by its velocity on take-off, V_0 , and the angle of take-off, α :

$$d = \frac{V_0^2}{g} \cdot \sin(2\alpha) \Rightarrow V_0 = \sqrt{\frac{g \cdot d}{\sin(2\alpha)}} \quad (4.6)$$

where g is the acceleration due to gravity. When the grasshopper jumps, it accelerates its body to the take-off velocity by extending the hind legs rapidly. The average acceleration required to achieve a particular velocity depends on the rear leg length, $L = L_{\text{femur}} + L_{\text{tibia}}$ over which acceleration, a , takes place:

$$a = \frac{V_0^2}{2 \cdot L} \quad (4.7)$$

Potential energy is $E_p = M_b \cdot g \cdot h$ where M_b is the mass of body (not including the legs since these are still in contact with the ground) and h is the centre of mass height gained until take-off (Burrows and Morris, 2002, Burrows and Morris, 2003). Experimental

data of Burrows and Morris, 2002, given in Table 4.1, are considered in the computation. Thus, the height gained until take-off can be calculated after determining the mass of the body without legs. The mass of the femur can be calculated as two cylinders with diameters 3.2 mm and 0.8 mm and lengths 10.26 mm and 6.84 mm, respectively. Tibia is also taken as a cylinder with 0.6 mm in diameter. Therefore, the mass of the body and initial height of body can be found easily by using these assumptions.

ii. Air resistance is not ignored: Air resistance is an important energy loss for small insects so that the actual kinetic energy at take-off is larger than the kinetic energy without air resistance. In order to estimate the actual kinetic energy at take-off, Elliott, et al, (2004) observed *Drosophila* (from which the wings had been removed) moving vertically upwards in air and in vacuum. 20% of the energy was reported to be lost to air resistance for flies projected upwards 100 mm. If the assumption is that the same loss occurs in the experiments, the kinetic energy at take-off, allowing for air resistance ($E_{k,air}$), will be 1.25 times higher than the energy required without air resistance. This would require the take-off velocity to be increased by $\sqrt{1.25}$ (Elliott, et al, 2004).

4.2 2D LEG MODEL

4.2.1 Mathematical Model for 2D Leg Model

A two-actuator model having 2 DOF is considered in the analysis. Model consists of three links and two actuators, one at hip joint and another at knee joint as seen in the Figure 4.4. Although the model is a very simplified one, it will help in determining optimum parameters for a higher degree of freedom system.

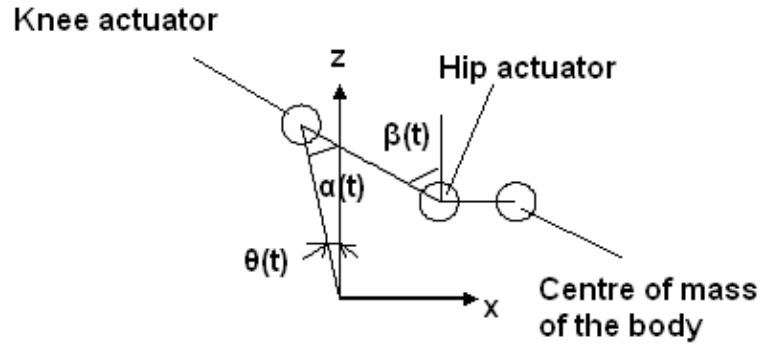


Figure 4.4 2D Leg Model

4.2.2 Kinematic Analysis

The position of centre of mass is given for hip-knee joint actuators model;

$$x(t) = 0.866.L_1.\sin(\beta(t)) - 0.866.L_2.\sin(\theta(t)) + 0.27 \quad (4.8)$$

$$z(t) = -0.866.L_1.\cos(\beta(t)) + 0.866.L_2.\cos(\theta(t)) \quad (4.9)$$

where $\theta(t) = \beta(t) - \alpha(t)$

Similar results for the femur-tibia angle with 3-D Leg Model are achieved. Way of the 2-D solutions is given in the Appendix C. The leg motion according to these results is given in the Figure 4.5.

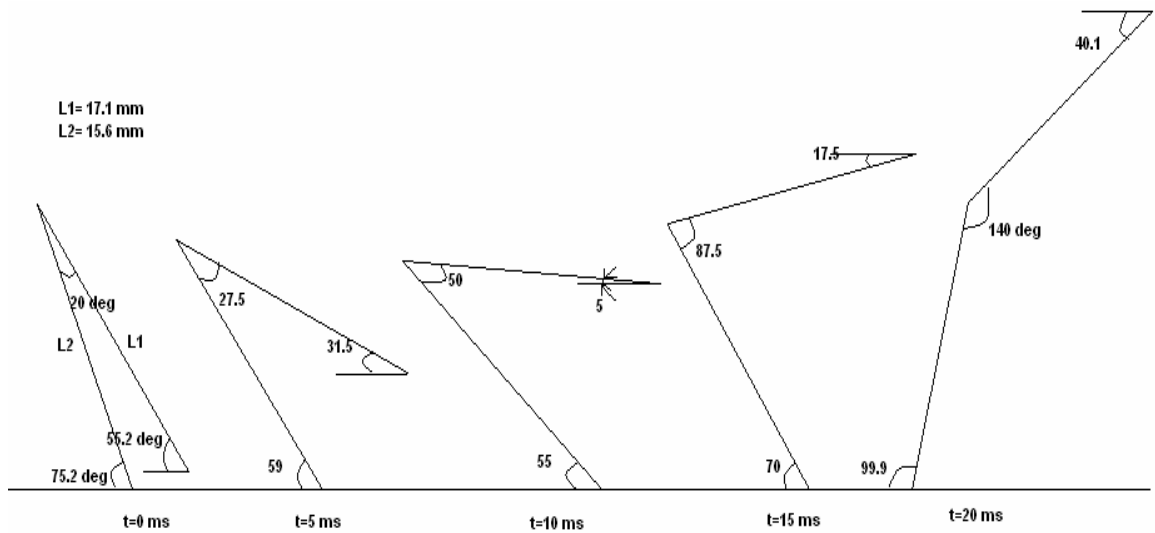


Figure 4.5 Position of a grasshopper leg until take-off

4.2.3 Dynamic Analysis

The very first step in dynamic analysis is to develop a dynamic model. Mass distribution is given in the Figure 4.6.

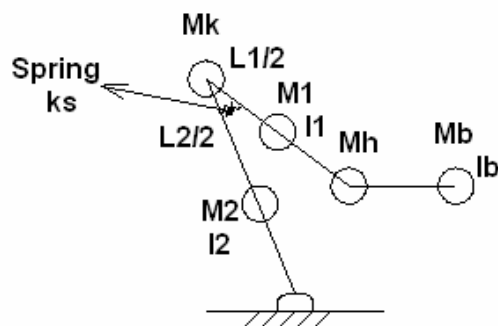


Figure 4.6 Mass distribution of the leg model

M1 and M2, limb masses, are concentrated at the mid points of the limbs. Mk represents the mass of the knee actuator and Mh is hip actuator mass. Mb is the body mass and it is concentrated at the centre of mass of the body. I1, I2 and Ib are the moments of inertia of the limbs about their centroids;

$$I1 = \frac{M1.L1^2}{12} \text{ and } I2 = \frac{M2.L2^2}{12} \quad (4.10)$$

To find the limb mass, models of the femur and tibia are given in the Appendix D.

$$M1 = \rho.V_{femur} = 1.025(kg / m^3).85.958.(10^{-3})^3(m^3) \cong 0.0881mg \quad (4.11)$$

$$M2 = \rho.V_{tibia} = 1.025(kg / m^3).4.41.(10^{-3})^3(m^3) \cong 0.00452mg \quad (4.12)$$

Consequently, M_b the mass of body (not including the legs) becomes

$$M_b = M - 2.(M1 + M2) - 4.m_{legs} = 414.65mg \quad (4.13)$$

where m_{legs} is front legs weight and it is assumed that $m_{legs} = 0.04$ mg according to experiments and total mass, M , is about 415 mg. Note that the grasshoppers have six legs; two of them are hind legs. A Lagrange's method is used for arriving at equations between joint power and foot coordinates. Elaboration solution is given in the Appendix E.

i. Using Lagrange's Method, the Torque for Knee Actuator is;

$$T_2 = G_1.\ddot{\theta}(t) + G_2.\ddot{\beta}(t) + G_3.(\dot{\beta}(t))^2 + G_4.g + G_5 \quad (4.14)$$

where

$$G_1 = (0.75(M_1 + M_h + M_b) + M_k).L_2^2 + I_2 \quad (4.15)$$

$$G_2 = -(0.375M_1 + 0.75(M_h + M_b))L_1L_2 \cos(\beta(t) - \theta(t)) \quad (4.16)$$

$$G_3 = (0.375M_1 + 0.75(M_h + M_b))L_1L_2 \sin(\beta(t) - \theta(t)) \quad (4.17)$$

$$G_4 = (0.5M_2 + M_1 + M_k + M_h + M_b)L_2 \sin(\theta(t)) \quad (4.18)$$

$$G_5 = k(\theta(t) - \beta(t)) \quad (4.19)$$

ii. Using Lagrange's Method, the Torque for Hip Actuator is;

$$T_1 = G_2.\ddot{\theta}(t) + G_6.\ddot{\beta}(t) + 2G_3.\dot{\beta}(t)\dot{\theta}(t) - G_3(\dot{\theta}(t))^2 + G_7g - G_5 \quad (4.20)$$

where

$$G_6 = (0.188M_1 + 0.75(M_h + M_b) + M_k).L_1^2 + I_1 \quad (4.21)$$

$$G_7 = -(0.5M_1 + M_h + M_b)L_1 \sin(\beta(t)) \quad (4.22)$$

4.3 RESULTS OF THE 2D AND 3D LEG MODEL

Variations of angles $\alpha(t)$, $\gamma(t)$, $\theta(t)$ ($\theta(t) = \beta(t) - \alpha(t)$), and $\beta(t)$ (rad) are given in the Figure 4.7, the position of centre of mass during take off is given in the Figure 4.8, and the body velocity is plotted in the Figure 4.9. The body height variations according to horizontal distance are plotted in Figure 4.10 to see the path of the centre of mass. All body height and femur-tibia angle values are compared with the numerical solutions via Mathcad 2000 program. The solution is given in Appendix A. Consequently, it is obtained that the found values are similar of the empirical data of Burrows and Morris, (2003).

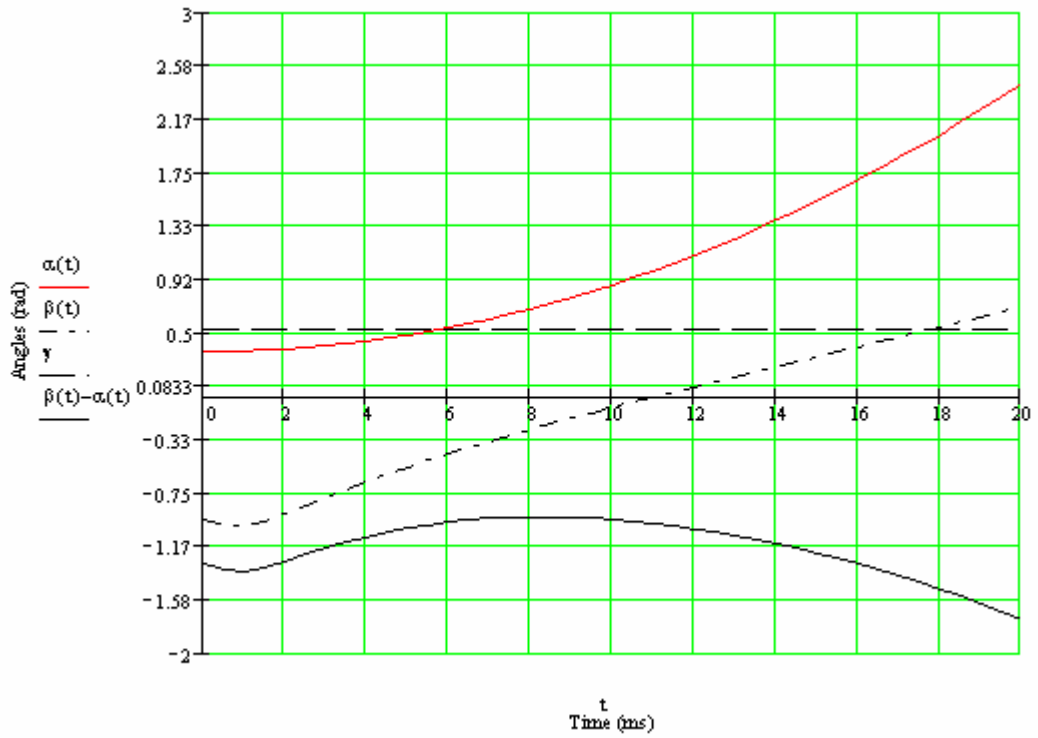


Figure 4.7 Variations of Femur-Tibia, Body-Femur, and Ground-Tibia angles until take-off

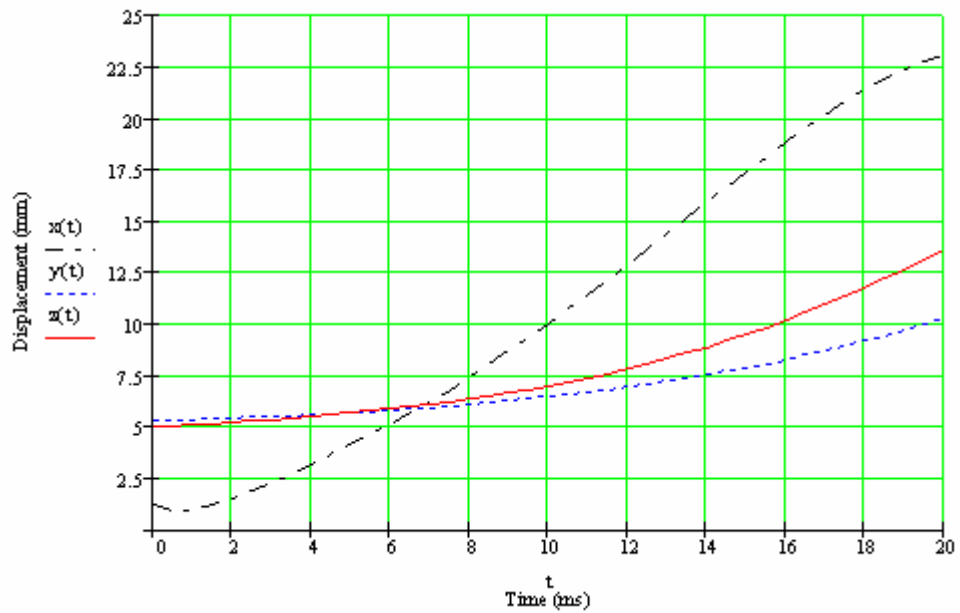


Figure 4.8 Variations of position of centre of mass coordinates until take-off

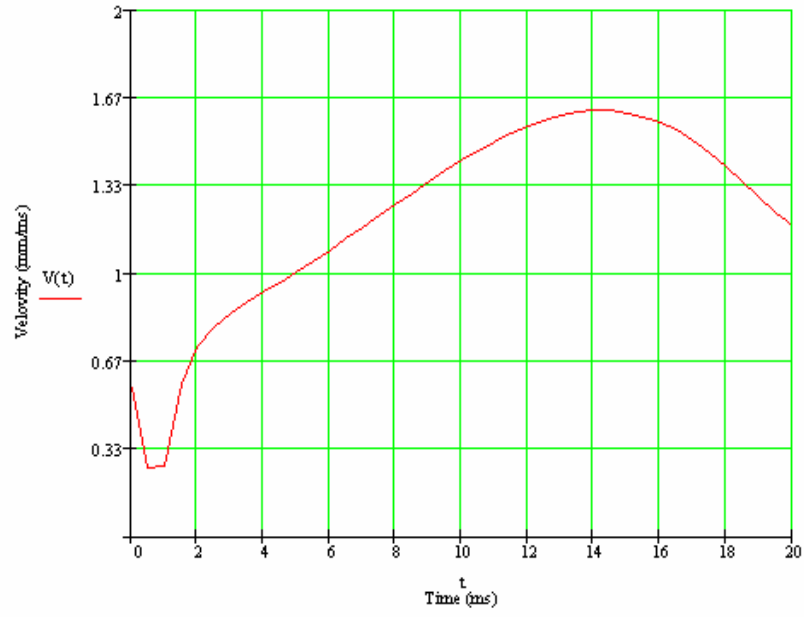


Figure 4.9 A plot of velocity until take-off



Figure 4.10 A body height variation along horizontal distance until take-off

4.4 RESULTS OF THE TORQUE ANALYSIS OF THE 2D LEG MODEL

The torque values based on 2D leg model are tabulated in Appendix F. The data given in Table F.1 are graphically shown in Figure 4.11 and Figure 4.12. The variation of torque is very small because knee actuator and hip actuator cancel each other due to their signs and magnitudes.

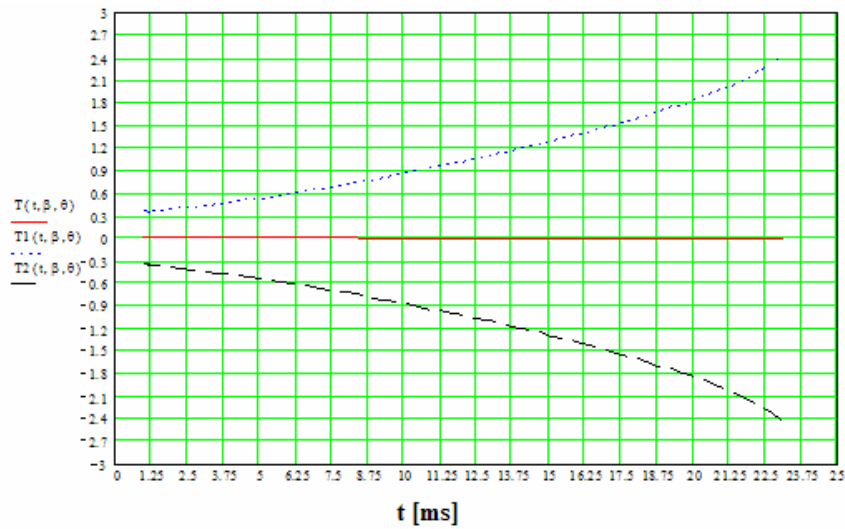


Figure 4.11 A graph of time-torque variation of 2D leg model where T is the total torque; T1 is the hip actuator torque; T2 is the knee actuator torque

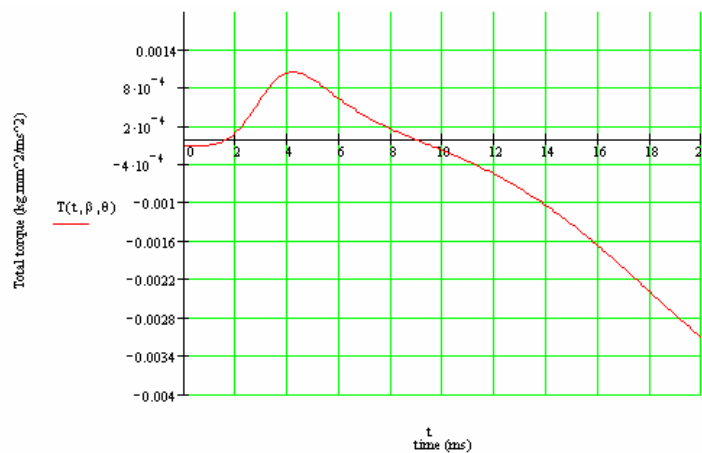


Figure 4.12 Total torque of 2D leg model

4.5 KINEMATIC ANALYSIS OF 3D LEG MODEL WITH MSC. ADAMS SIMULATION

MSC. Adams simulation software is used to obtain results of the jumping based on the presented mathematical model. In this simulation, the grasshopper given in the Figure 4.13 is assumed to be a sphere which has the same weight and parameters with the actual model.

The horizontal and vertical distances, kinetic energy and velocities are calculated by MSC. Adams analyses and the results are given in Figure 4.14 and Figure 4.15. When the results in Table 4.4 are compared to each other, it is apparent that they are close for different cases. The similarity of the results shows the validity of the simplifying assumptions.

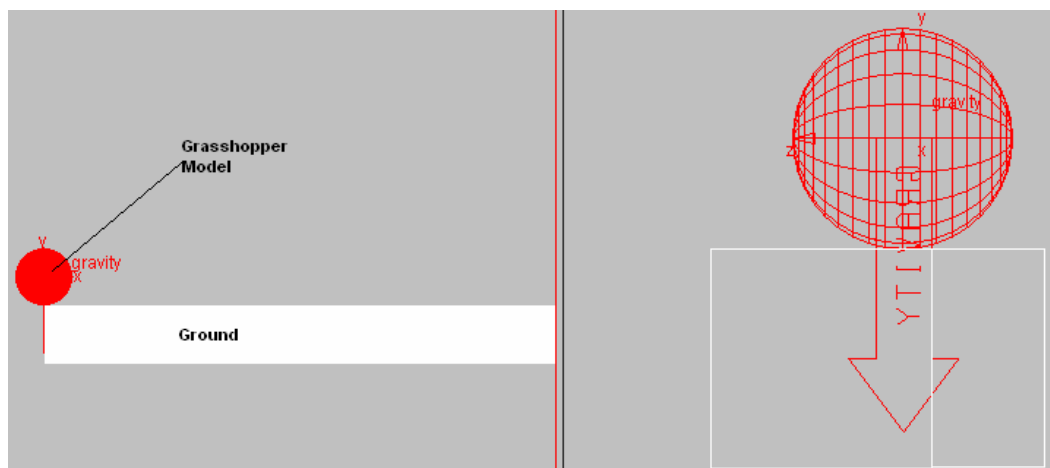


Figure 4.13 A grasshopper is modeled by using MSC. Adams Simulation Program

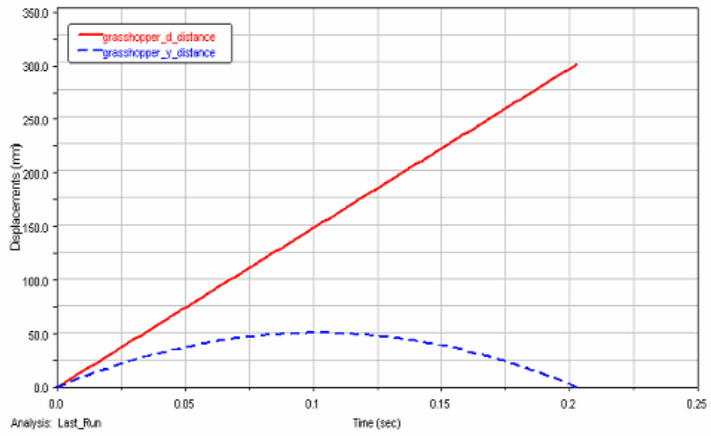
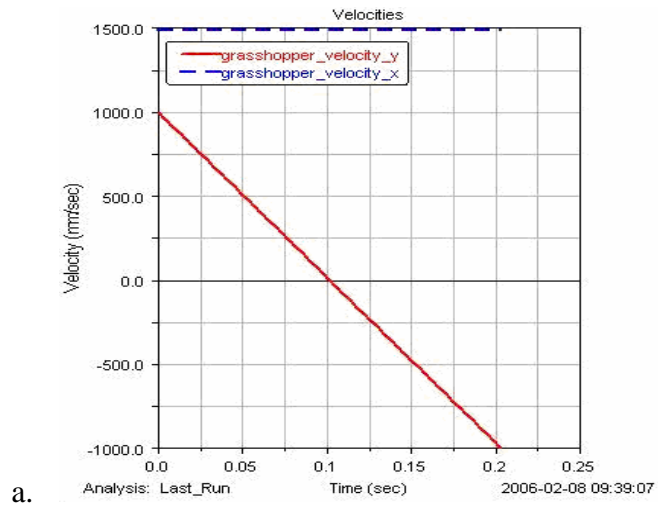
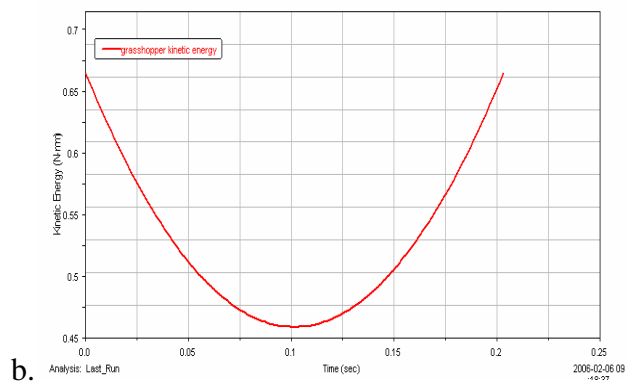


Figure 4.14 Displacement analysis of grasshopper-like by using MSC. Adams 2005



a.



b.

Figure 4.15 Like-grasshopper jumping analysis by using MSC. Adams 2005 r2
 a. Velocity Analysis, b. Kinetic energy analysis.

The results for the cases considering air resistance and without air resistance are used to obtain the numerical data tabulated in Table 4.4. The results are compared with experimental data of Burrows and Morris, (2003) for understanding the difference between the assumptions to get hold of jumping performance of Pholiptera.

Table 4.4 Jumping performance data of Pholiptera motion

	Experiment (Burrows and Morris, 2002)	Air resistance is ignored	Force is constant with air resistance	Adams Solution
Take-off velocity (m/s)	1.51	1.79	2	Input data (1.79)
Take-off time (s)	-	-	-	0.203
Take-off acceleration (m/s ²)	-	48.99	61.2	-
Peak acceleration (m/s ²)	83.4	97.98	122.32	-
Take-off force (Mn)	-	20.3	25.6	-
Extension time (ms)	30.6	36.5	30	-
Horizontal distance (mm)	Input data (302)	Input data (302)	Input data (302)	301.861
Height gained until take-off(mm)	-	4.92	4.92	-
Kinetic Energy (μJ)	470	614.74	768.43	664.1
Min. Energy requirement (μJ)	490	634.74	788.43	684.1
Power (μW)	16	36.3	51.2	-

In this chapter, mathematical models are studied according to the biomimetic design tree. 2D and 3D models are developed and take-off angles are estimated. Although there are two different models, the angles are close to each other and that of biological model. Hind leg position until take-off is evaluated with the take-off angles. Artificial muscle stroke can be obtained with this data.

Several assumptions are made for reducing the complexity. A femur-body angle, $\gamma(t)$, is assumed to be 30°. This angle variation can be added to the model as a future work. Moreover, torque analysis, using Lagrange's method, is developed. Force analysis of leg models of artificial muscles and biological muscles will be observed according to torque analysis of the hind leg. In addition to these analyses, a packet simulation program, MSC. Adams, is applied basically to concluding the jumping features of real model. All of results are used for evaluation of artificial model and preliminary design.

CHAPTER 5

ARTIFICIAL MUSCLES AND DEVELOPMENT OF A NEW ARTIFICIAL MUSCLE

The main scope of this thesis is to create a basic system that mimics aspects of the jumping mechanism of a grasshopper instead of creating models with complex structures. Better actuation and sensing technology effects the development of basic biomimetic robot structures critically (Biomimetic, 2006).

Natural muscle is a contractile organ and a simply transducer. They change the chemo-electric signal from nerves to mechanical energy. Fibers, consisted by muscles, actuate force and motion in response to nervous stimulation (Brabham, Marr, Smith and Lee, 2004).

Fourth step of the biomimetic design is an abstraction of good actuator system from biological muscles. Since the natural muscles are non-fabricated structures and they cannot be copied completely, the study of artificial muscles is the most difficult part of this study. After the literature survey on artificial muscles, a new artificial muscle is developed.

5.1 LITERATURE SURVEY ON ARTIFICIAL MUSCLES

O'Halloran and O'Malley, (2004) described that "Mammalian skeletal muscle is an incredibly elegant mechanism. Muscle is a three dimensional nanofabricated system with integrated sensors, energy delivery, waste/heat removal, local energy supplies, actuator, and repair mechanisms". Although natural muscle has a non-fabricated character, actuators and actuator systems are essential features of all robots,

providing the forces, torques and mechanical motions needed to move the joints, limbs or body (Caldwell, Medrano-Cerda, and Goodwin, 1994). Thus, research projects with huge budgets are funded for mimicking natural muscles.

There is an example of using real muscle tissue frog-like robot (Figure 5.1). In this design, using very simple control and interface design, muscles can act as a practical, controllable actuator, but this muscle tissue requires a special medium to be alive. To use such a biological muscle tissue is technologically not practical and moreover it is not sufficient for robotic applications, so an artificial muscle is necessary.

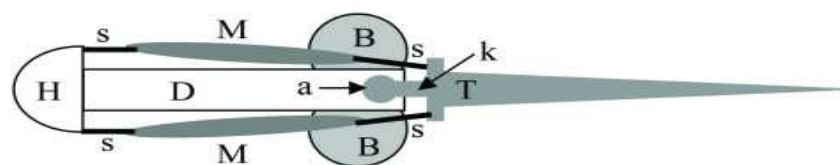
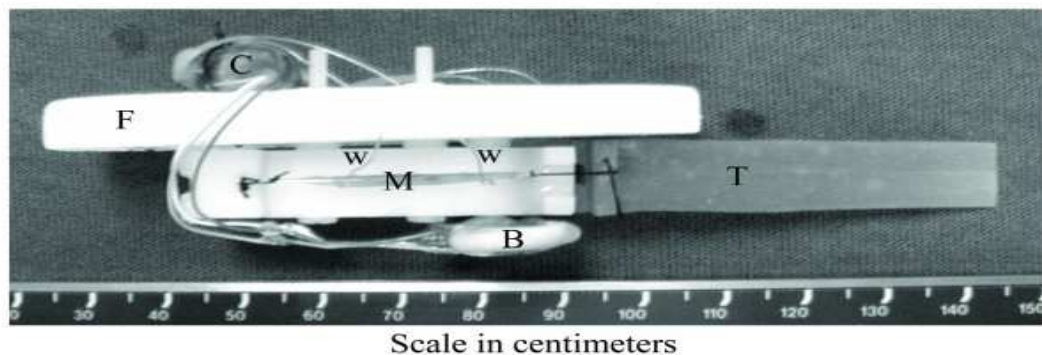


Figure 5.1 A Swimming Robot Actuated by Living Muscle Tissue (H: rigid Delrin head piece; D: rigid Delrin backbone; M: muscle; B: lithium batteries; C: encapsulated microcontroller, infra-red sensor, and stimulator unit; T: cast silicone tail; F: Styrofoam float; w: electrode wires; s: suture attachments; k: compliant hinge segment; a: cylindrical tail mounting boss) (Huge Herr, Robert, 2004)

Industrial robots usually use three primary power sources;

- Electric motors
- Hydraulic cylinders
- Pneumatic cylinders (Caldwell, Medrano-Cerda, and Goodwin, 1994).

Though electric motors have a very important and common place in robotic application areas because they are very easy to control, for example Honda's humanoid Asimo (Brown, 2004), they have some disadvantages. Firstly, motors are heavy for robotic applications. The other disadvantage is that their force-to-weight ratio is lower than that of pneumatic and hydraulic devices (Kapps, 2007). Moreover, this actuator type is not sufficient for biomimetic design approach.

Pneumatic (Kerscher, Albiez, and Berns, 2002) and hydraulic cylinder systems eliminate some of the problems associated with electric motors. These actuators also produce linear motion, which makes them more suitable to serving a role equivalent to muscle (Kingsley, 2005). However, these actuators have standard size which is too big and heavy for micro-robots.

Entire soft body is one of the essentials for robots (Lee, Shimoyama, 2002). Thus, the actuator problem is seemed to solve by soft artificial muscles (Kerscher, Albiez, and Berns, 2002). Their performance is characterized by (Caldwell, et. al, 1994);

- Power (in particular the power/weight and power/volume ratios)
- Strength
- Response rate
- Physical size
- Speed of motion
- Reliability
- Controllability
- Compliance
- Cost
- etc...

Although soft actuators have been considered recently, a number of new different type of technologies have been developed (Caldwell, Medrano-Cerda and Goodwin, 1994) and most of them are compared in Table 5.1 (Arora, 2005).

Table 5.1 Comparison of natural muscle and man-made actuator technologies (Arora, 2005; Pelrine, Kornbluh, Pei, et. al, 2002)

Actuator	Strain	Actuation Pressure	Density	Efficiency	Speed (fast AND slow)
Natural Muscle	●	●	●	●	●
Electromagnetic	●	●	○	●	○
Piezoelectric	○	●	◐	●	●
Shape Memory Alloy	◐	●	◐	○	○
Magnetostrictive	○	●	○	●	○
Electrostatic	●	○	●	●	●
Dielectric Elastomers	●	●	●	●	●
○ = Poor ◐ = Fair ● = Good					

5.1.1 Braided Pneumatic Actuators (BPA); McKibben Artificial Muscles; Air Muscles

“One of the earliest attempts at artificial muscle modeling was undertaken by an American physician, McKibben in the 1950’s Pneumatic actuators were one of the first approaches to artificial muscle modeling”, O’Halloran and O’Malley, (2004). Air muscles are soft pneumatic devices, ideally suited for robotics and bio-robotics. In addition to this their positive characters, they have similar features with rear muscles (Figure 5.2).

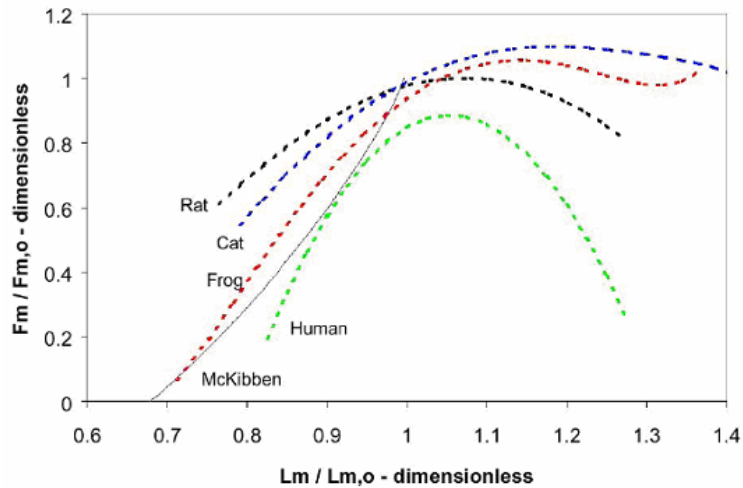


Figure 5.2 The force-length relationship of Braided Pneumatic Actuator's compared to that of muscle (F_m : Muscle force; $F_{m,o}$: Initial muscle force; L_m : Muscle length, $L_{m,o}$: Initial muscle length, (Kingsley, 2005; Colbrunn, 2000))

Braided Pneumatic Actuator (BPA), which have applications in robotics, bio-robotics, biomechanics, artificial limbs replacement and industry, consists of a rubber bladder encompassed by a tubular braided mesh (Figure 5.3.a). When the bladder is inflated, the actuator expands radial and undergoes a lengthwise contraction (Figure 5.3b and Figure 5.4). Typically air muscles can contract up to twenty five percentage of their elongated length (Biorobotic, 2006). Pneumatic actuators success is depend on compressors because the simple system uses a small air pump or compressor, which are driven by electric motors.

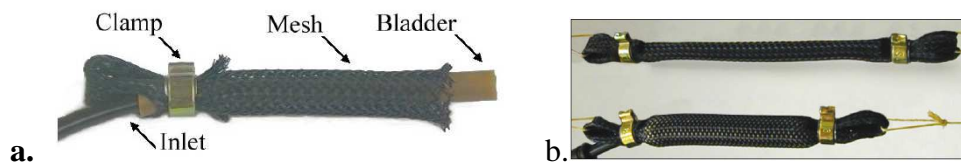


Figure 5.3 A view of BPA a. a braided pneumatic actuator (Kingsley, 2005) b. An inflated (bottom) and uninflated (top) actuator (Colbrunn, 2000)

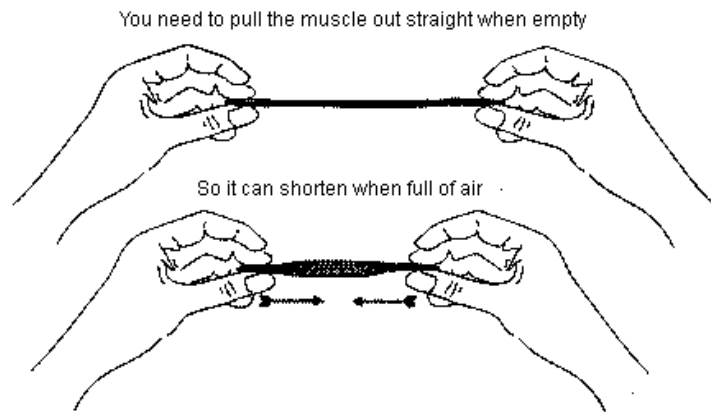


Figure 5.4 Working mechanism of a pneumatic muscle (Biorobotic, 2006).

Pneumatic cylinders (Granosik and Borenstein, 2004);

- are clean and lightweight,
- have large power output,
- have relatively low cost.

The hybrid micro robot uses braided pneumatic actuators, McKibben artificial muscles, to extend the leg segments (Figure 5.5). This robot features are given in the literature survey of bio-robots, Chapter 3.

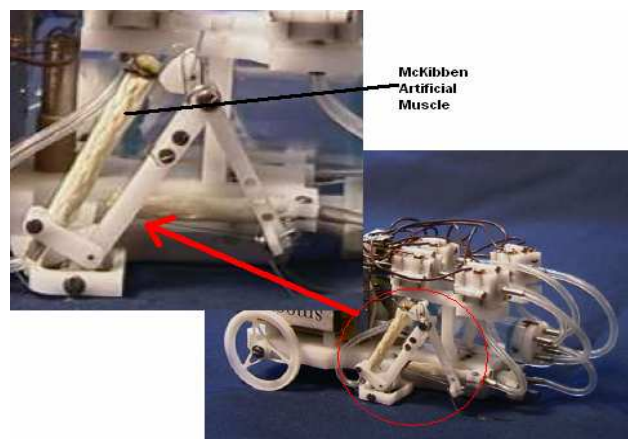


Figure 5.5 Case Western University Hybrid Robot with rear leg, its actuator is a McKibben Artificial muscle (Birch, et al., 2005)

A robotic leg, which has four degrees of freedom, was used to conclude control mechanism of braided pneumatic actuators. This leg can swing, stance and walk across a table. The hardware system and leg design are given in Figure 5.6.

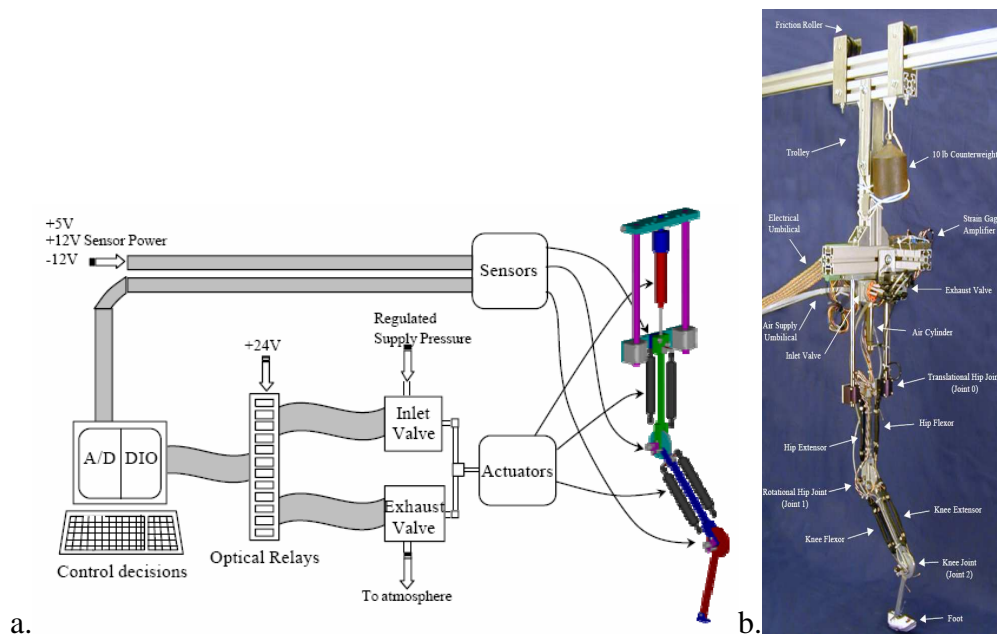


Figure 5.6 a. The hardware system of a leg design model, b. the leg model (Colbrunn, 2000)

5.1.2 Shape Memory Alloys (SMA)

Shape memory was discovered in 1932 and Nickel-Titanium alloys were found to exhibit shape memory significantly at Naval Ordnance Labs in 1962 (Virtualskies, 2007). SMA, a group of metallic materials, contracts with a thermal cycle (Lowe, 2006). SMAs contract up to ten percentage of their elongated length when heated and they return to their original length when cooled off (O'Halloran and O'Malley, 2004 (Figure 5.7)). Shape-Memory alloys can tolerate strain 3 to 25 times higher than piezoelectric can.

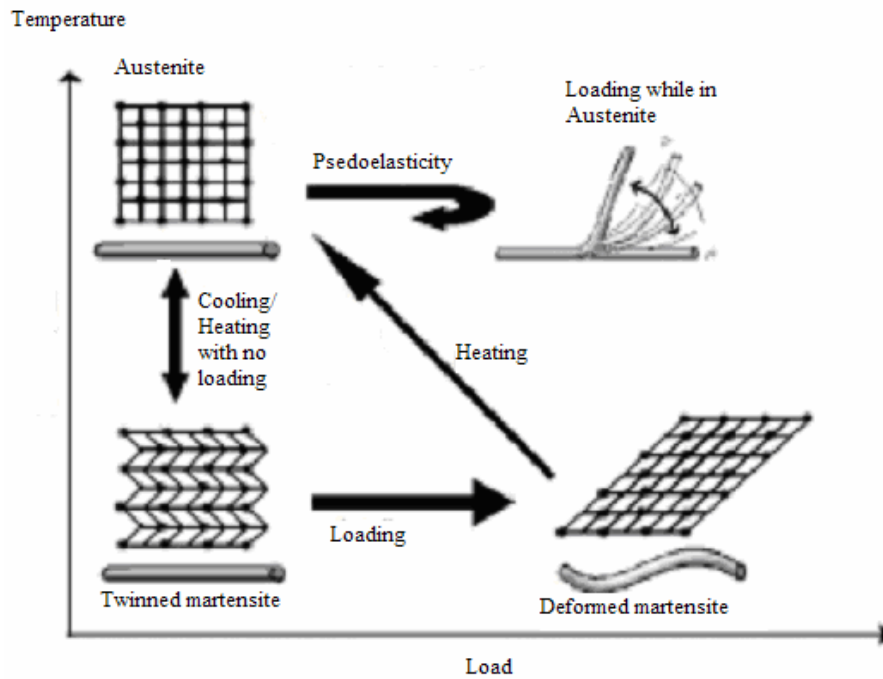


Figure 5.7 Basic Principles of SMA (Kapps, 2007)

Some Shape-Memory alloys:

- nickel-titanium (Nitinol),
- gold-cadmium,
- gold-cadmium,
- brass,
- ferromagnetic (a thin film, low bandwidth alloy).

They are sometimes inadequate although SMAs have advantages (Kapps, 2007);

- can recover from large amounts of bending and torsion,
- possess an extremely high force to weight ratio,
- are incredibly compact and simple,
- are pseudo-elasticity material (or sometimes called *super elasticity*, a pseudoelastic material may return to its previous shape after the removal of even relatively high applied strains.)

Disadvantages of SMAs;

- are unable to produce significant size displacement (only about 4-10%),
- are inefficient (only about 10% due to heating),
- are difficult to model (due to non-linear qualities in actuations),
- are somewhat expensive to manufacture,
- have relatively slow reaction time.

As a result of the fact that SMAs requires small space, have various forms; wires, tubes, sheets, etc. for using different application areas, and they have less weight than a conventional actuator, they are highly useful in situations where conventional actuators are too large, bulky, or inadaptable (Kapps, 2007). Six-legged robot, based on a spider insect, is an example of a bio-robot which is controlled with shape memory alloys to yield a walking motion. Legs contract when heat energy is increased and the legs expand when the material cools. Other examples of bio-robots which are used Shape Memory Alloys are a winged robot whose wings expand and contract to produce a flight motion, a fish robot that swims, and a snake robot that slithers (Virtualskies, 2007).

5.1.3 Electroactive Ceramics (EAC)

Polycrystalline ceramics are an example of Electroactive ceramics. Application of a high electric field at an elevated temperature is used as part of the poling process to align the microscopically small piezoelectric domains (Figure 5.8, (O'Halloran and O'Malley, 2004)).

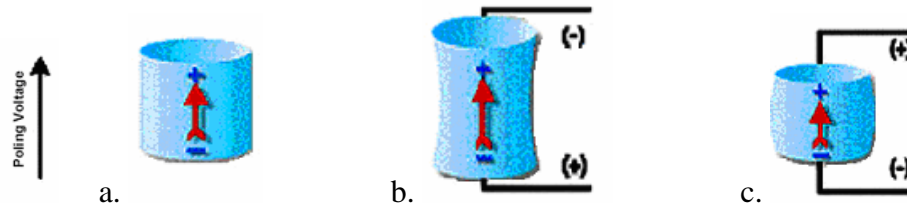


Figure 5.8 Polarisation is a result of the alignment of piezoelectric domains a. disk after polarization, b. applied voltage same polarity as poling voltage: disk lengthens, c. applied voltage opposite polarity as poling voltage: disk contracts (O’Halloran and O’Malley, 2004).

5.1.4 Electromagnetic

Lowe, (2006) represents that “Electromagnetic solutions typically consist of a motor that rotates an output shaft; it connects to a *drive train*, gear reducer transmission or other mechanical device that has several touching and moving parts, which create an *indirect* displacement”.

5.1.5 Piezoelectric

Piezoelectric (piezo means pressure in Greek) effect was discovered by the Curic brothers in the 1880’s (Stilson, 1996). If piezoelectric materials are hit with electric current, they deform; they generate electricity if they are deformed. Namely, mechanical stress causes crystals to electrically polarize and vice versa (Ashley, 2003). Piezoelectric technologies expand and contract with voltage at high frequencies (Lowe, 2006). In contrast, piezoelectric materials can generate large stress of about 10-40 MPa, but this force gives only a few nanometers. Piezoelectric actuators (Kapps, 2007);

- are very fast,
- require high voltages,
- are very accurate,
- have high repeatability,
- return to their resting state when the electric stimulus is removed,
- can withstand very broad temperature ranges.

5.1.6 Electroactive Polymer Artificial Muscle (EAP or EPAM)

Since the early 70's a new Electroactive polymer materials has grown, but the most progress was made after 1990. Drive robots with more efficient, higher power density actuation was discovered due to a new technology muscle, called Electroactive Polymer Artificial Muscle (EPAM or EAP), in the early 1990's (Figure 5.9). An EAP actuator is not only completely different from conventional electro-mechanical devices, but also separates itself from other high-tech approaches that are based on piezoelectric materials or shape-memory alloys by providing a significantly more power-dense package (Lowe, 2006; Ducheon, 2005). Energy density of actuators is given in Figure 5.10 where EM represents electro-mechanical devices.



Figure 5.9 A view of EAP, EPAM Roll Actuator from Artificial Muscle (Lowe, 2006).

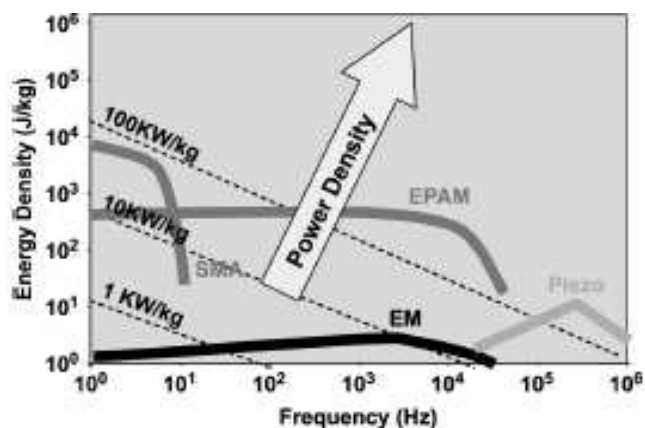


Figure 5.10 EAP actuators-energy density/frequency characteristics (Ducheon, 2005)

Electroactive polymers are resembled human muscles because EAPs expand and contract silently, based on variable voltage input levels (Prnewswire, 2006; Bar-Cohen, 2005) and they have high fracture toughness, large actuation strain and inherent vibration damping (O’Halloran and O’Malley, 2004). In contrast EAPs have a much smaller and lower weight form factor than Electromagnetic (EM) motor devices, much like the human muscle, but they provide the same level of power as EM devices (Duchon, 2005). Elements of EAP actuated devices and principle of operation is given basically in Figure 5.11. EAPs (Kapps, 2007),

- can induce strains (at least twice greater in magnitude than EACs),
- have higher response speeds, lower densities and improved resilience than SMAs,
- have low mechanical energy density,
- have low actuation forces.

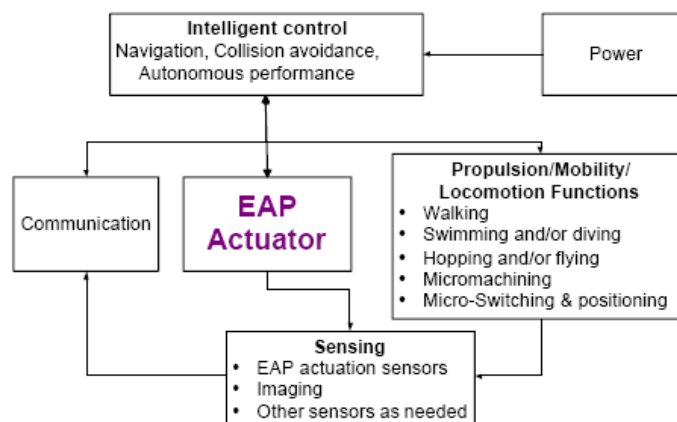


Figure 5.11 Principle of operation EAP actuated devices (Bar-Cohen, 2000).

Types of EAPs

EAPs can be sorted into two groups: ionic EAPs and electronic EAPs are given in Appendix G, Table G.1. Each of them is compared with advantages and disadvantages. Applications areas and devices of these EAPS are tabulated in Appendix G, Table G.2.

1. Ionic EAP;

Ionic polymer gels (Figure 5.12), ionomeric polymer-metal composites (IPMC, (Figure 5.13)), conductive polymers carbon nanotubes and electrorheological fluids, work on the basis of electrochemistry- the mobility or diffusion of charged ions are examples of Ionic EAPs (IEAP). They need not only a current to hold position but also wet media or flexible coating (Lowe, 2006; Ashley, 2003). IEAP materials are generally used in robotics, biotechnology and industrial applications (Shahinpoor, Kim, 2004). Multifinger grippers, an example of IPMC (Figure 5.13.b), have a great mass carrying capability (Bar-Cohen, Xue, Joffe, Lif, Shahinpoor, Simpson, Smith, and Willis, 1997). Properties of all variety of ionic EAP are tabulated according to Bar-Cohen, 2005 in Appendix G, Table G.1.

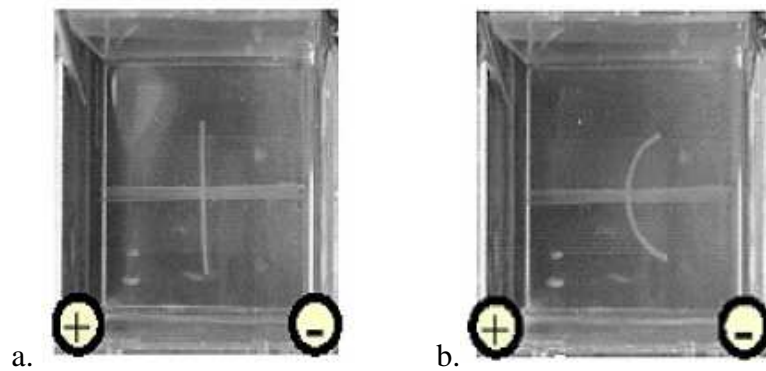


Figure 5.12 A view of Ionic EAPs, a. Ionic gel at reference state, b. activated state (O'Halloran and O'Malley, 2004; Bar-Cohen, 2004).

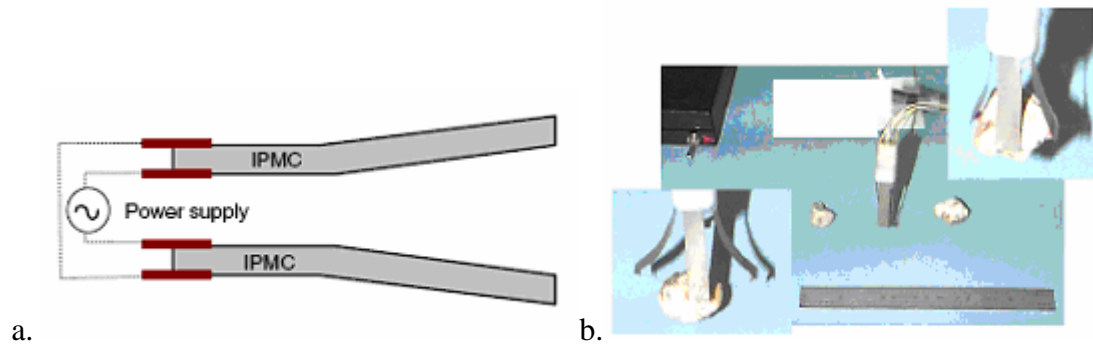


Figure 5.13 a. An illustration of the IPMC gripper concept, b. a four-finger gripper (Shahinpoor, Kim, 2004)

2. Electronic EAPs;

Electronic EAPs, such as ferroelectric polymers (Figure 5.14.a), electrets, dielectric elastomers (Figure 5.14.b) and electrostrictive graft elastomers (Figure 5.14.c), are driven by electric fields. Although electronic EAPs do not need a protective coating and required almost no current to hold position, and electronic EAPs can react quickly and deliver strong mechanical forces, they require relatively high voltages, which can cause uncomfortable electric shocks (Lowe, 2006; Ashley, 2003). Properties of all variety of electronic EAP are tabulated according to Bar-Cohen, 2005 in Appendix G.

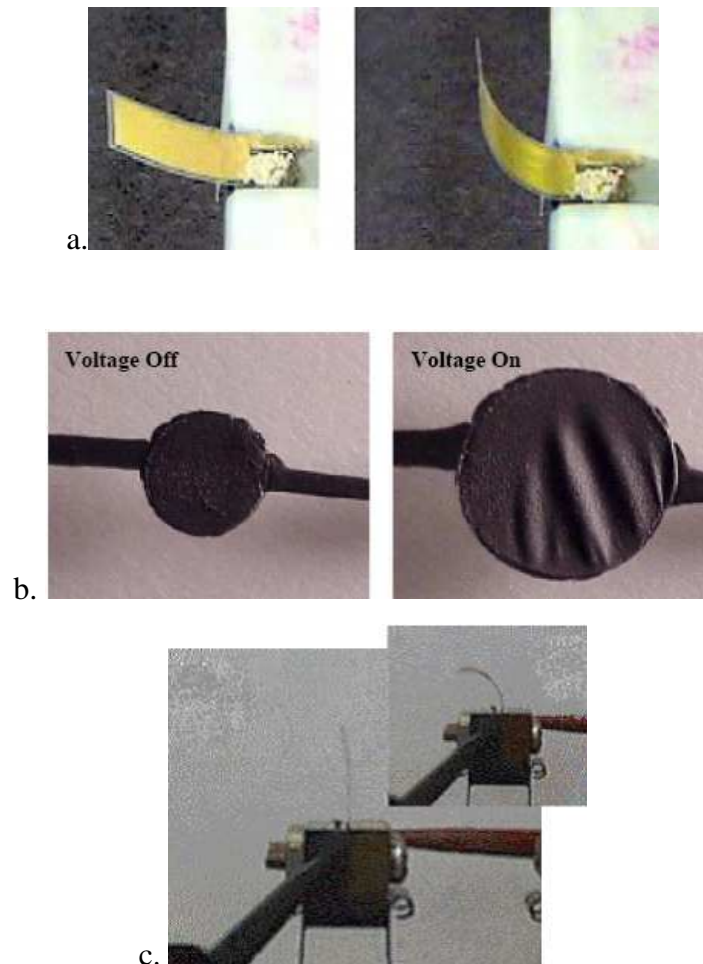


Figure 5.14 Electronic EAPs a. Ferroelectric polymer in the reference state (left) and in its actuated state (right), b. circular strain test of a dielectric elastomer with carbon grease electrodes, c. electrostrictive graft elastomer (O'Halloran and O'Malley, 2004).

Dielectric EAP, an Electronic EAPs Type,

An important type of Electronic EAPs is dielectric EAP whose basic architecture is made up of a film of an elastomer dielectric material that is coated on both sides with another expandable film of a conducting electrode. When voltage is applied to the two electrodes a Maxwell Pressure (Ducheon, 2005) is created upon the dielectric layer. Electrode pressure causes the dielectric film to become thinner; it expands in the planar directions. Thus, electrical force is converted to mechanical actuation and motion (Figure 5.15, (Ashley, 2003; Ducheon, 2005; Lowe, 2006)).

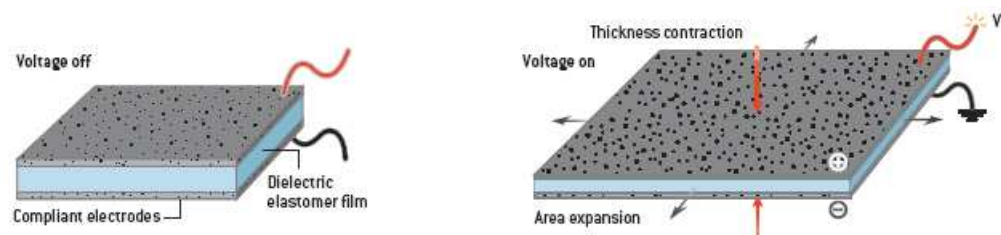


Figure 5.15 Working mechanism of Dielectric EAP (Ashley, 2003)

Dielectric elastomers can generate more strain and force than many of the competing technologies (Ashley, 2003) and they are sensitive their position, so Dielectric EAPs do not require a dedicated position sensor (Kapps, 2007). Their properties in this regard are similar to those of natural animal muscle (Figure 5.16). Another advantage of this type is that dielectric elastomer actuators require relatively high voltages (1-5 kV) to active, so devices can operate at a very low current. They also use thinner, less expensive wiring and keep fairly cool (Ashley, 2003).

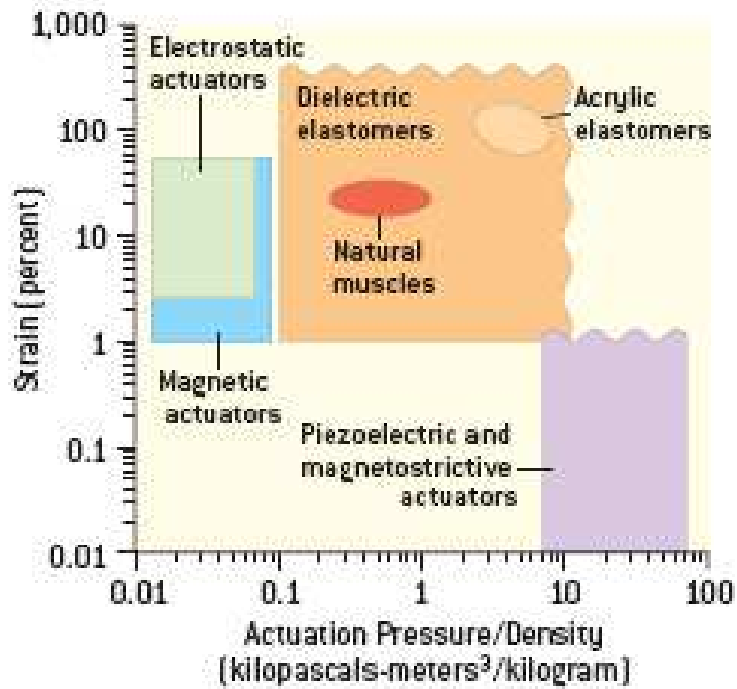


Figure 5.16 Comparison of artificial muscle properties (Ashley, 2003)

Dielectric Elastomer Actuators Configurations: Dielectric elastomer actuators expand when electrically stimulated and may work in different modes and configurations. These configurations are shown in Figure 5.17.

Bow tie actuators are linear actuators, which have been used in robotic leg applications such as the self-contained hexapod robot and an insect-inspired flapping wing robot which are driven by four silicone bow-tie actuators (O'Halloran and O'Malley, 2004).

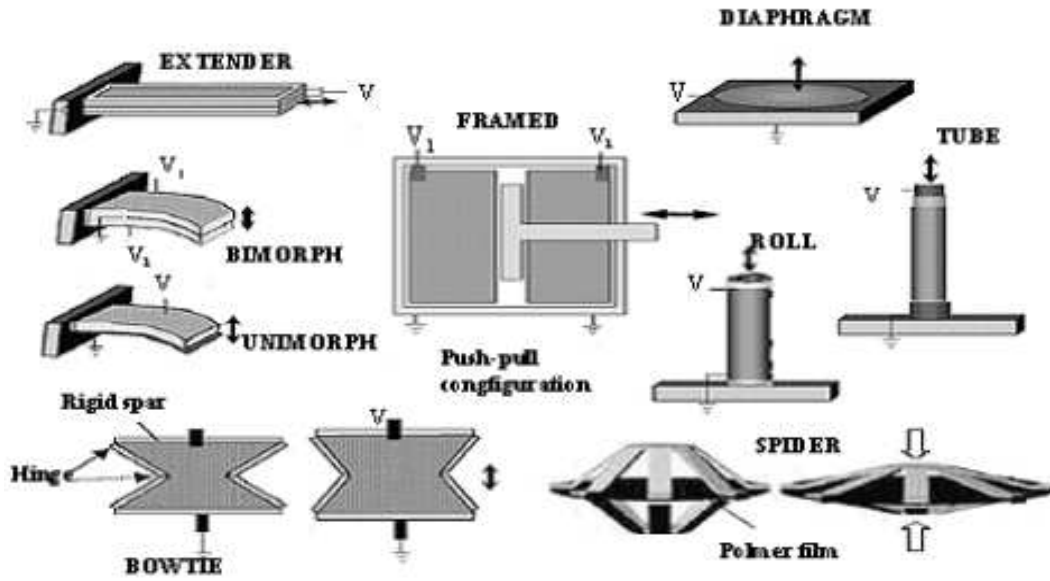


Figure 5.17 A variety of actuator configurations for dielectric elastomers, where the arrows the direction of actuation (O'Halloran and O'Malley, 2004).

Roll actuators or spring rolls can extend –or bend- with electricity (Figure 5.18). These rolls are multifunctional because they combine bending, axial extension, and position sensing (O'Halloran and O'Malley, 2004). If voltages are given on two sides, the roll extends, called as push-pull actuator. If only one half receives voltage, the other half bends, this actuator is called as bending rolls (Ashley, 2003).

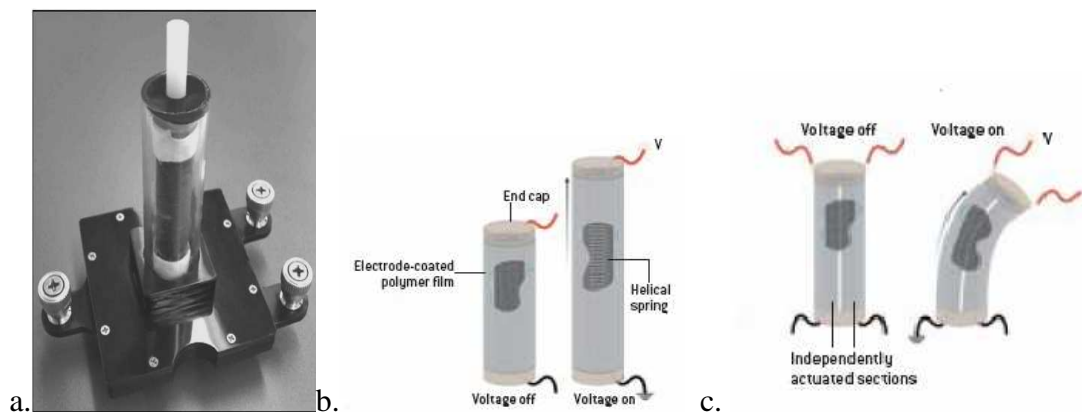


Figure 5.18 Spring Roll a. EAP roll actuator (Ducheon, 2005), b. Push-pull actuators, c. Bending rolls (Ashley, 2003)

An application of the roll actuator, aside its potential application in the development of a mechatronic muscle is as an inchworm robot. The main benefit of this project is the illustration of how a muscle like actuator can operate without the rigid support of a skeleton just as worms do in nature. Roll actuators have also seen applications as robot legs. Merbot is an example of this application (O'Halloran and O'Malley, 2004). To separate the power and integration issues from the actuator and biomimetic aspects, off-board power was used on FLEX 2 and Skitter (Figure 5.19). Powerful rolled acrylic actuators were used on these robots. Robots, biomimetic design, have a lifelike locomotion, in contrast to the rigid mechanical-type motion commonly seen in conventional, motor-driven motors. Skitter's design based on cockroach locomotion and uses six rolled actuators to provide six, single-degree-of-freedom legs (Pelrine, Kornbluh, Pei, Stanford, et. al, 2002).

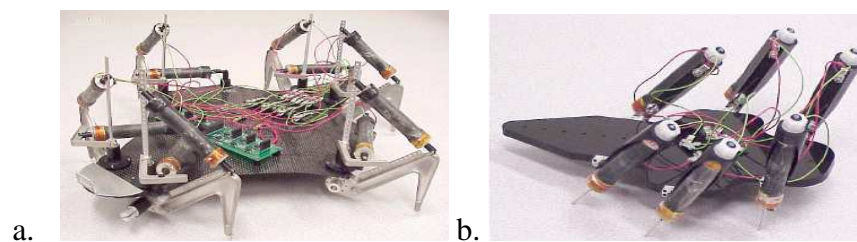


Figure 5.19 a. FLEX 2, b. Skitter (Pelrine, Kornbluh, Pei, Stanford, et. al, 2002)

Longitudinal EAP expands laterally under electro-activation. EAP film subjected to 25 V/m induced over 12% extension (Figure 5.19, (Bar-Cohen, 1997)). An example of this Longitudinal EAP, a lifter, is given in the Figure 5.20.

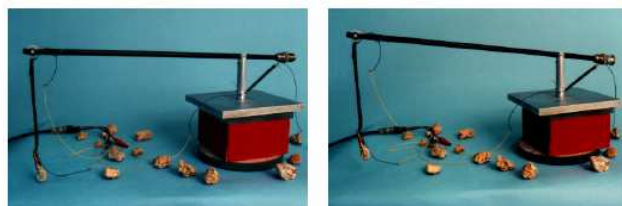


Figure 5.20 An example of the Longitudinal EAP actuator (Bar-Cohen, 1997)

5.1.7 Antagonistically-Driven Linear Actuator (ANTLA)

ANTLA, based on dielectric elastomer, has bidirectional actuation, “push-pull” type operation (Figure 5.21). ANTLA is a cost effective muscle because its fabrication process is very simple. The advantages of this actuator are high force-to-weight ratio, cost effectiveness, ease of fabrication, intrinsic softness, and disposability. Their properties in this regard are similar to those of natural animal muscle (Choi, Jung, Ryew, Nam Jeon, Koo, and Tanie, 2005)

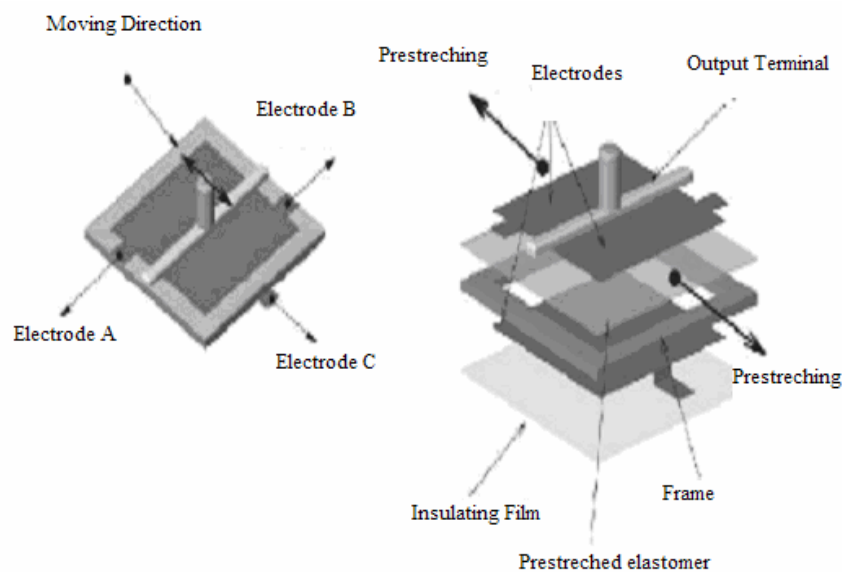


Figure 5.21 Mechanical structure of ANTLA (Choi, Jung, Ryew, et.al, 2005)

5.1.8 Baughman and Colleagues' Artificial Muscles

Methanol-powered artificial muscles have been created aiming to create battery-free robotic limbs and prosthetics. Baughman and colleagues have designed two types of artificial muscle that also act as fuel cells– converting chemical energy to mechanical movement (Merali, 2006).

- A nickel-titanium shape-memory wire coated in a platinum catalyst.
- Sheets of carbon nanotubes, coated in a catalyst.

5.1.9 A Comparison of Artificial Muscles

Some important artificial muscles are considered in this part. The chronological order of invention of an actuator and a few artificial muscles is given in Figure 5.22. EAPs and pneumatic artificial muscles are the most efficient artificial muscles for biomimetic design and their properties are much like natural muscles. In this scope, EAPs, a new artificial muscle technology, and pneumatic artificial muscles are studied particularly. The maximum stress-strain and maximum strain-power characteristics of the actuators are given in Figure 5.23 and Figure 5.24.

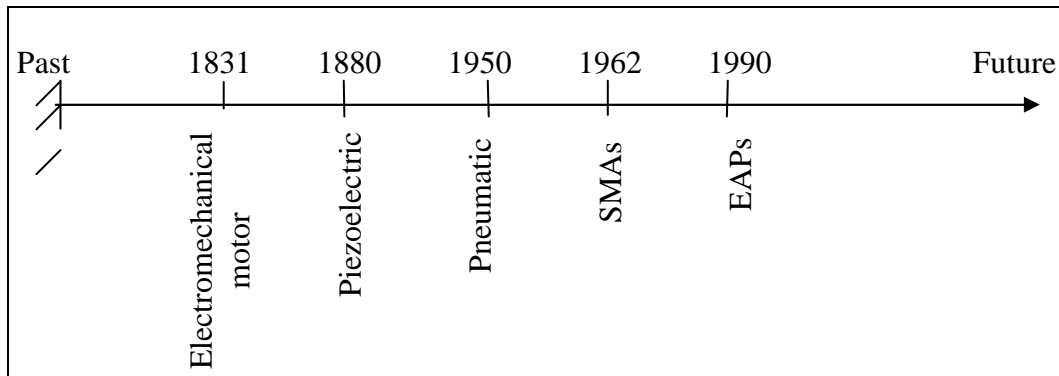


Figure 5.22 Chronological order of invention of a few actuators/artificial muscles

“Current actuation technologies are based either on high modulus – low strain materials, such as piezoceramics and magnetostrictors, or on multi-component systems, such as hydraulic, pneumatic or electromagnetic devices”, Huber et.al, (1997). Piezoelectric materials can generate large stress of about 10-40 MPa, but this force gives only a few nanometers. It makes piezoelectric be a weak material as an artificial muscle. Although shape memory alloys (SMAs) deliver both high forces and large displacements, the response times and longevity of these materials require optimization. EAPs systems are in the middle of the performance indices of mechanical actuators, between the high stress-low strain and the low stress-high strain groups. It is clear that dielectric elastomer has a higher strain-power ratio than that of others and natural muscles have. Some important artificial muscles and a natural muscle are compared with empirical data in Table 5.2 from different sources.

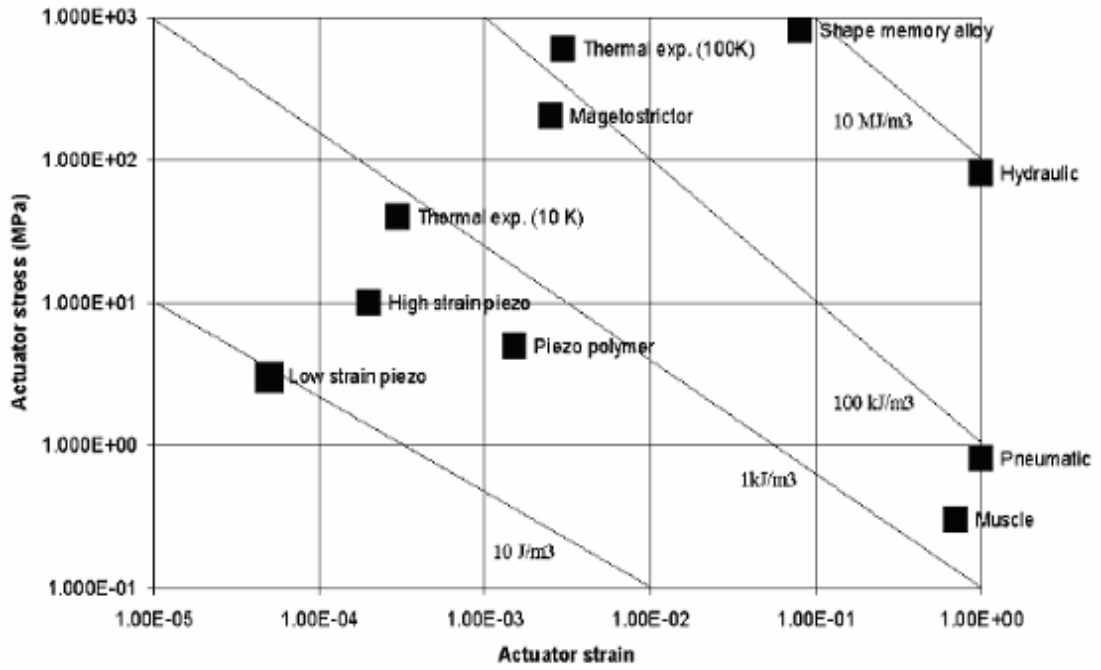


Figure 5.23 Max. Stress-Strain Graph for Actuator Materials. The sloping lines from left to right give an indication of the energy storage capacity per unit volume of the various actuators (Bonser, Harwin, Hayes, et.al, 2004)

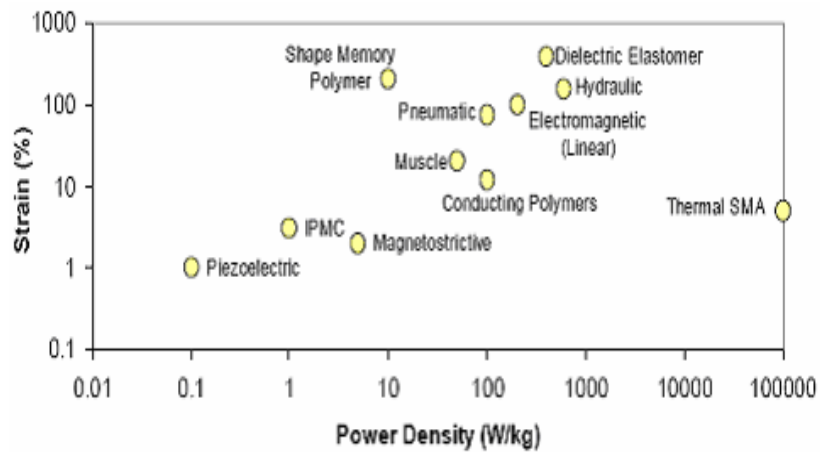


Figure 5.24 Actuator Max. Strain-Power Density Graph (Kapps, 2007)

Table 5.2 Some Artificial Muscles and a Natural Muscle Comparison

	Natural Muscle	Pneumatic	DC	Pneumatic Cylinder	SMA's	SM Polymer	EABs	EAC	Piezoelectric			Electromagnetic	Electrostatic
									Ceramic	Single crystal	Polymer		
Force to weight ratio		400:1 ⁺	16:1 ⁺	16:1 ⁺									
Contraction in length	20(40)% ^c	20-25% ⁺			<8% ⁺		10-15% #			1% [^]	1% [^]		
Max. Actuation strain(%)	>40 [·]				5 ⁺	100 [:]	>10% ⁺	0.1-0.3%		0.2 [·]	1.7 [·]	0.1 [·]	100 ⁺
Max. Pressure Force (Mpa)	0.1(0.35) [·]	6-8 (bar) [·]			>200 ⁺⁺	4 [~]	0.1-25 ⁺	30-40 ⁺		110 [·]	131 [·]	4.8 [·]	0.2 ⁺
Specific Density	0.08(J/g) [·] or 1 ⁺				5-6 g/cc ⁺	1 [·]	1-2.5 g/cc	6-8 g/cc ⁺	7.7	7.7	7.7	1.8	1.5 g/cc
Drive Voltage			0--		5 V ⁺		50-800V Ionic; 1-7 V ⁺ Electronic; 10-150V ⁺	50-800 V ^{+/g}					144V/ μ m
Consumed power					Watts ⁺		m-Watts ⁺⁺	Watts ⁺					
Fracture behaviour					Resilient, elastic ⁺		Resilient, elastic ⁺	Fragile ⁺					Large Fracture toughness ^s
Elastic Energy density (J/cm ³)	0.08(W/g) or 0.07 [·]				>100 [·]	2 [~]	0.5-3.5 [·]	6-8 g/cc [·]		0.1 [·]	1.0 [·]	0.0024 [·]	0.015 ⁺
Coupling efficiency (k ²) (%)					5 [·]		60-70 [·]			52 [·]	81 [·]	7 [·]	50 ⁺
Max. Efficiency (%)	>35 ⁻ (20% [·])				<10 [~]	<10 [~]	60-90 [·]			>90 [·]	>90 [·]		>90 ⁺
Reaction speed (full cycle)	Medium [·]		Fast #		msec to min (slow) ⁺⁻	Slow [·]	msec to sec (Fast) ⁺⁻	msec to sec ⁺		Fast [·]	Fast [·]	Fast [·]	msec (Fast) ⁺

References:

- [·] Aron, 2005
- [·] Ashley, 2003
- [·] Bar-Cohen, 2005
- # Bar-Cohen, 2007
- ^o Boser, Harvin, Hayes, Jeronimakis, Mitchell, and Santilli, 2004
- [·] Festo, 2003
- [·] Hollman and Malley, 2004
- ^{\$} Kornhub, Fehrer, Ederle, Joseph, 1998
- [^] Love, 2006

5.2 STUDIES ON ARTIFICIAL MUSCLES

After literature survey on actuators and artificial muscles, the fourth step of the biomimetic design, is considered, two ready-made artificial muscles are selected as a grasshopper-like jumping mechanism actuator. The first alternative is an EAP muscle whose properties are much like animal muscles. EAP muscles are soft actuators and have high strain-stress ratios and high response speeds. Although it is seen that EAPs is sufficient for the jumping mechanisms, this type is not used as an actuator for the system because EAPs are new artificial muscles and their behavior is not known properly for such a study. Because of the fact that EAPs require time for progress, this type is not preferred for the mechanism as an actuator.

Another alternative is a pneumatic artificial muscle. The pneumatic artificial muscle has a lot of advantages. Firstly, its physical characters are known exactly. The muscle behaves like a spring with a changing external force: the displacement is in direction of the applied force (Figure 5.25).

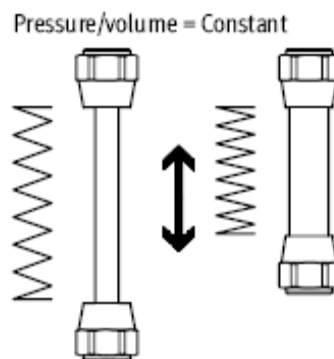


Figure 5.25 Pneumatic artificial muscle model (Festo, 2006)

Secondly, the contraction properties have similar features with biological muscles. Other important features of the pneumatic artificial muscle are; light weight and large power output, and low cost. In addition to these positive features, there is a huge negative character; the ready-made pneumatic muscles size is too large. A

complex winding work-bench or machine is necessary to produce a small pneumatic muscle, so the budget of bio-robot system would be increased.

A grasshopper-like leg set-up of pneumatic artificial muscle is designed and manufactured as given in Figure 5.26. The smallest Festo pneumatic artificial muscle has the following dimensions; 10 mm inner diameter, 14 mm outer diameter, and 4 cm length and set-up size is 25x30x2.5 cm. Festo pneumatic artificial muscle (fluidic muscle) characteristic curve is given in Figure 5.27 and working mechanism is shown in Figure 5.28. When the valve is turned to position 1, the flexor artificial muscle is inflated; the actuator expands in the radial direction and undergoes a lengthwise contraction. Thus, tibia is pulled and the angle between femur and tibia decreases. When the valve is turned to position 2, the flexor artificial muscle air exits from the exhaust pipe in the valve and the extensor artificial muscle is filled with air, not only the actuator contracts but also tibia extends suddenly. The necessary take-off force for the body is obtained. Although these muscles have a good contraction performance (25%), a grasshopper-like leg's size with these muscles is too big for mini (volume is nearly 1 dm³ (Başaran, 2003)) robots.

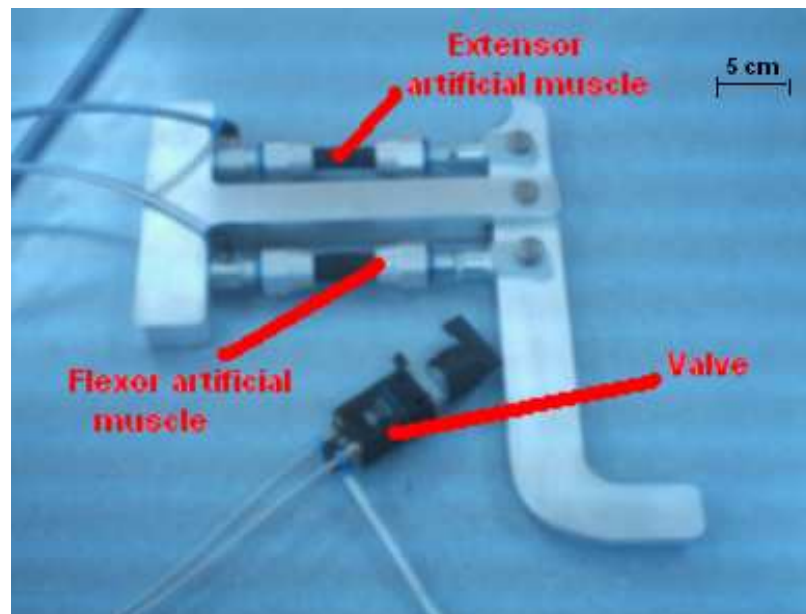


Figure 5.26 A view of set-up with Festo Pneumatic (McKibben) Artificial Muscle (Atılım University, Biomimetic Design Laboratory)

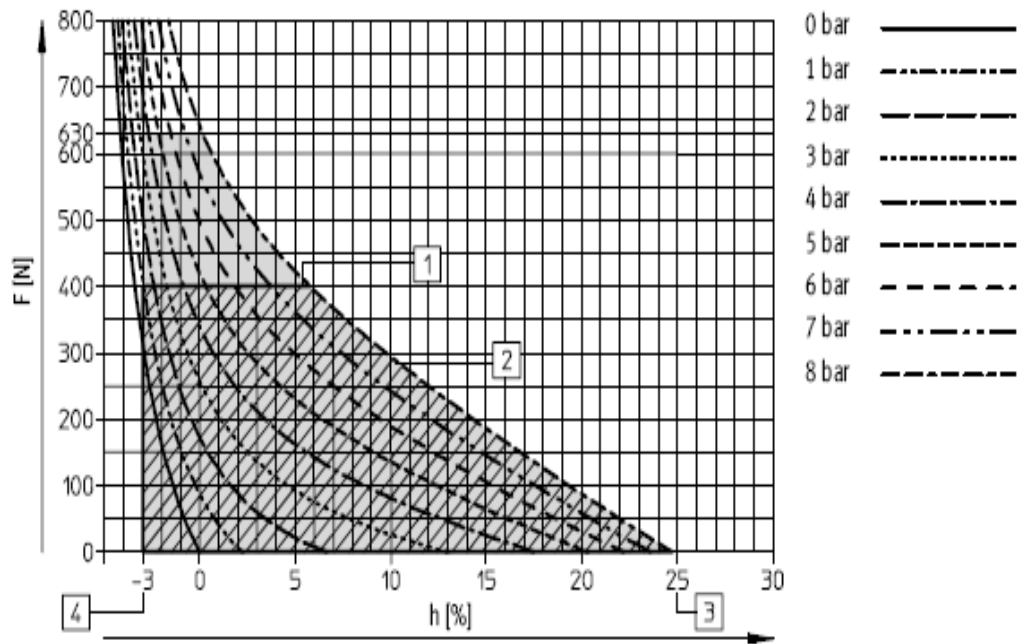


Figure 5.27 A characteristic curve of Festo MAS 10 pneumatic muscles where 1. Force compensation, 2. Max. operating pressure, 3. Max. Deformation, 4. Max. Pretensioning (Festo, 2006)

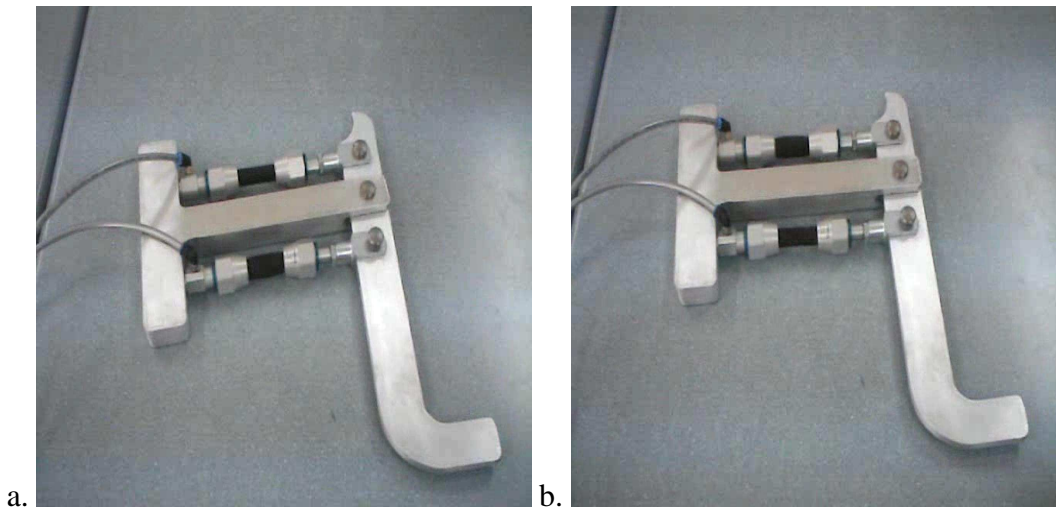


Figure 5.28 Working mechanism of grasshopper-like leg set-up of Festo pneumatic artificial muscle a. flexor artificial muscle is inflated, b. extensor artificial muscle is inflated (Atılım University, Biomimetic Design Laboratory)

5.2.1 A New Artificial Muscle Design and Manufacture

Because of the fact that the size of pneumatic artificial muscles not appropriate for mini bio-robots and a smaller one cannot be produced, a new artificial muscle design and manufacture is considered. An explosion due to electric discharge between the electrodes is constructed in a piston-cylinder system as an actuator for jumping mechanism of mini grasshopper-like robot. The system consists of a piston, a cylinder, and wire electrodes as given in Figure 5.29.a. The cylinder is filled with dielectric liquid which provides the discharge between electrodes. This muscle is activated by an electrical current with the discharge between electrodes (Figure 5.29.b and 5.29.c). The discharge is generated in a small electrode gap in the cylinder with use of charge circuit of an Electro-Discharge Machine (EDM) as a power supply. Thus, the dielectric liquid is exploded and the piston is pushed outwards of the cylinder as given in Figure 5.29.d. This working mechanism is different from the other artificial muscles; the muscle does not contract but it extends only.

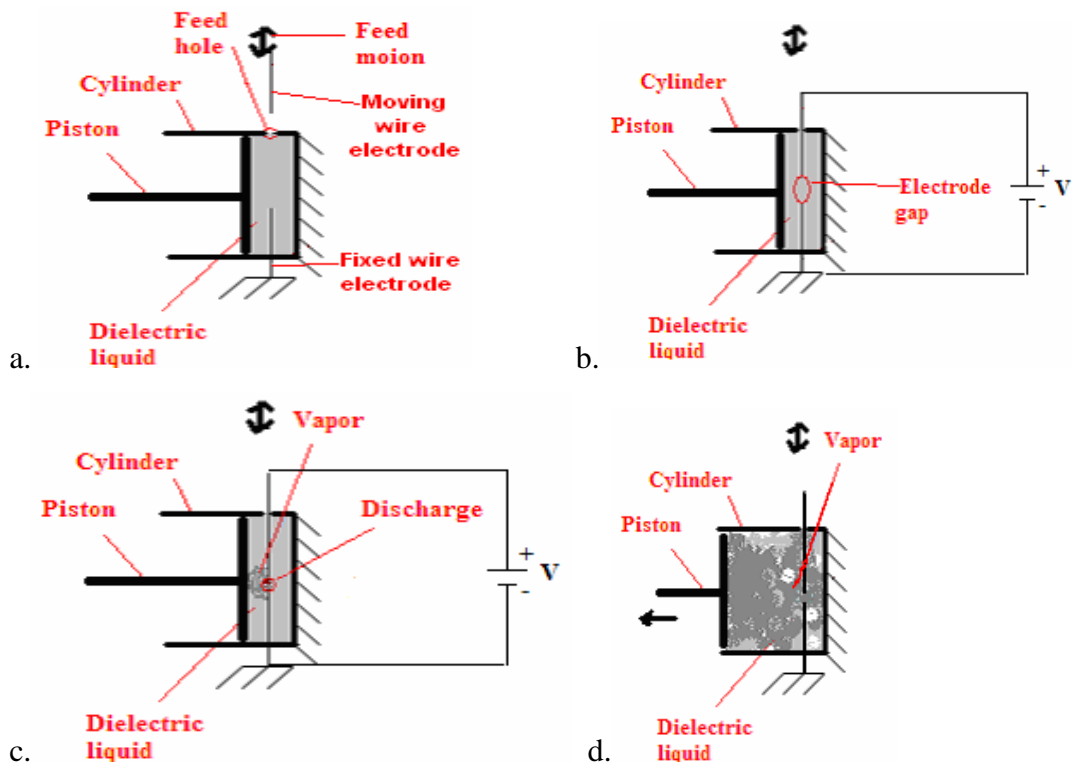


Figure 5.29 A schematic view of the artificial muscle working mechanism

Three type piston and cylinder systems are designed and manufactured at the beginning of this study; these systems are given in Figure 5.30. First of all, a metal cylinder/piston part was worked on. The cylinder has two small (nearly 1 mm) electrode holes and since the electrical isolation cannot be provided this system does not work. Secondly, delrin (a plastic nonconductor material) cylinder and metal piston were produced. Although the delrin-metal system was able to produce necessary force for pushing the piston, the working system was assembled on an EDM (Figure 5.31) and this cause reduction of mobility of the mechanism. The voltage given by EDM electrical circuit is transferred with cables from the machine; a view of the set-up is given in Figure 5.32. A feed motion of electrode is not given in this set-up. The gap between electrodes in the cylinder is fixed at nearly 50 μm . As a result, since the discharge power is weak, the necessary force to push the piston cannot be obtained.

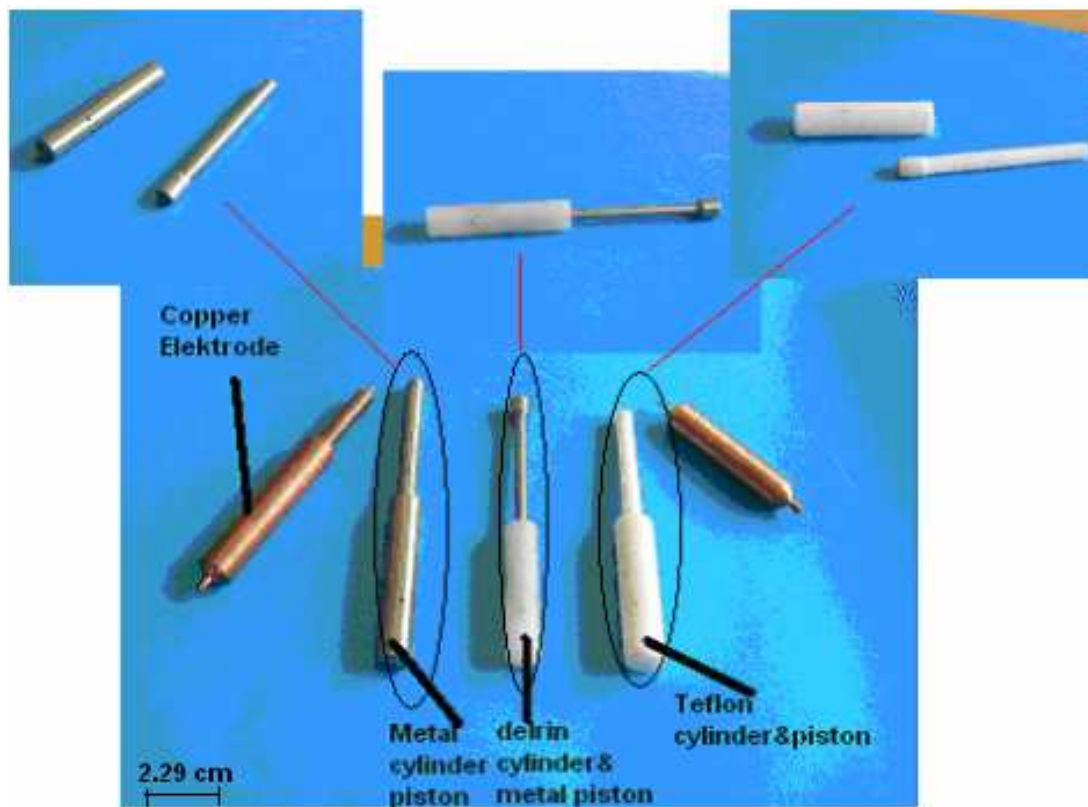


Figure 5.30 Piston and cylinder systems

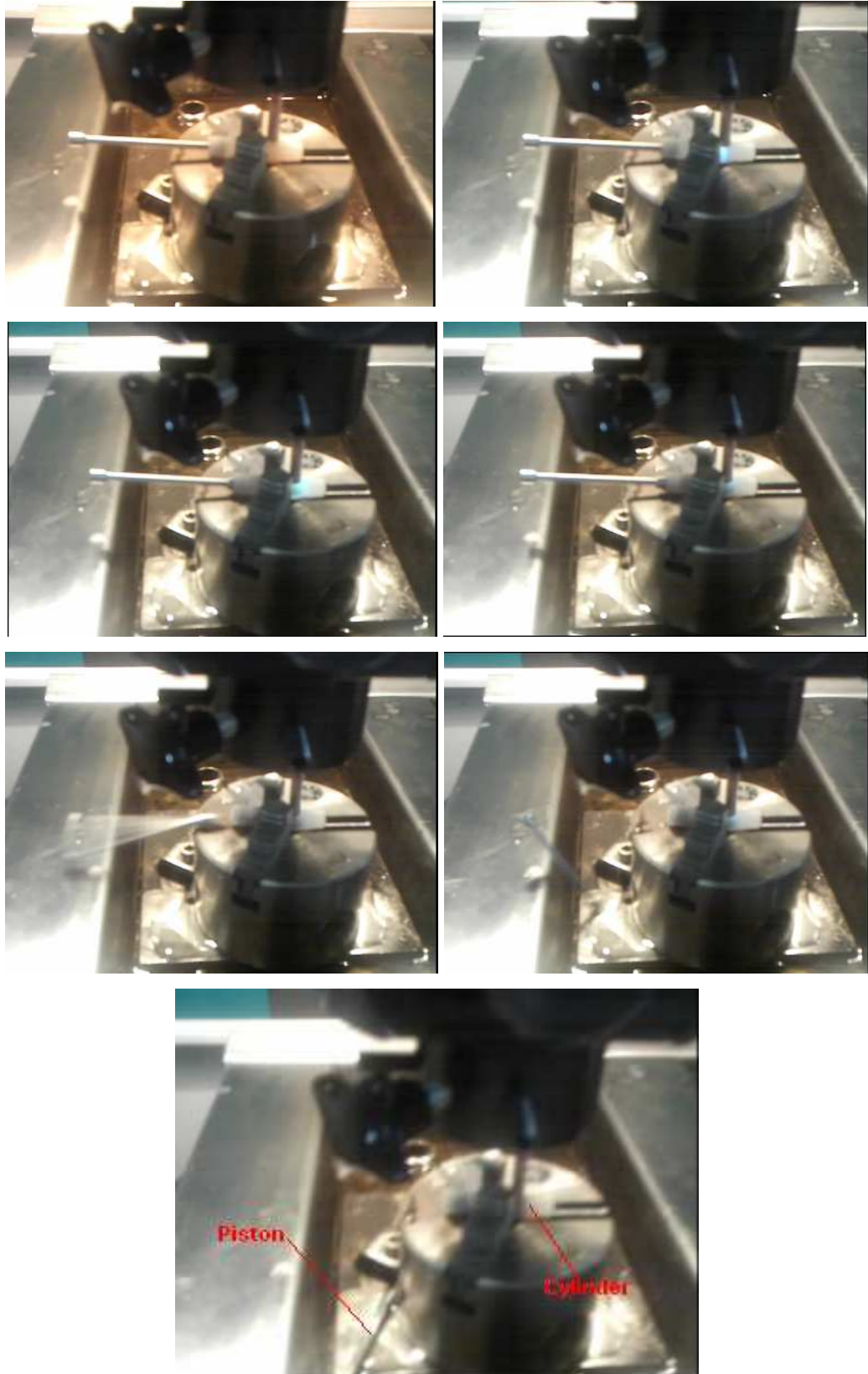


Figure 5.31 A view of explosion due to electric discharge in the piston-cylinder artificial muscle (Atılım University, Machine Shop)

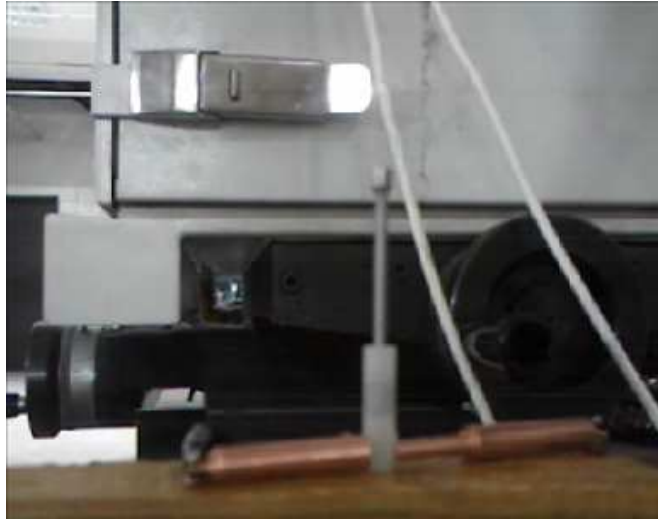


Figure 5.32 A view of a vertical piston position set-up whose circuit is detached from the EDM (Atılım University, Machine Shop)

Thirdly, teflon piston and cylinder were worked on. While these piston and cylinder systems materials were tested, the artificial muscle system was tried to detach from EDM. A simple RC circuit is used on some experimental set-ups (Figure 5.33). First set-up includes a conventional micrometer to adjust the discharge gap distance and to feed electrode wire with a horizontal sliding motion (Figure 5.33.a). There are some disadvantages of this set-up; electrical isolation is a main problem, micrometer is not sensitive for gap adjustment, and discharge is occurred at different electrode gaps when the other parameters are kept fixed.

Because of the disadvantages of the first set-up, a second set-up is designed and constructed (Figure 5.33.b). Although this set-up has a high sensitivity, RC circuit does not give powerful discharge for the necessary movement of the piston because of the lacking of high voltage power supply. The maximum output voltage of the power supply is 50 V and different resistance and capacitance values are used for the set-ups. A smaller plastic cylinder, the outer and inner diameters are 4.78-3.78 mm and the length of the cylinder is 33.08 and teflon piston, the diameters are 3.78 and 3 mm and the length of the piston is 30 mm, are prepared to use on EDM (Figure 5.34). This system gives better results than others.

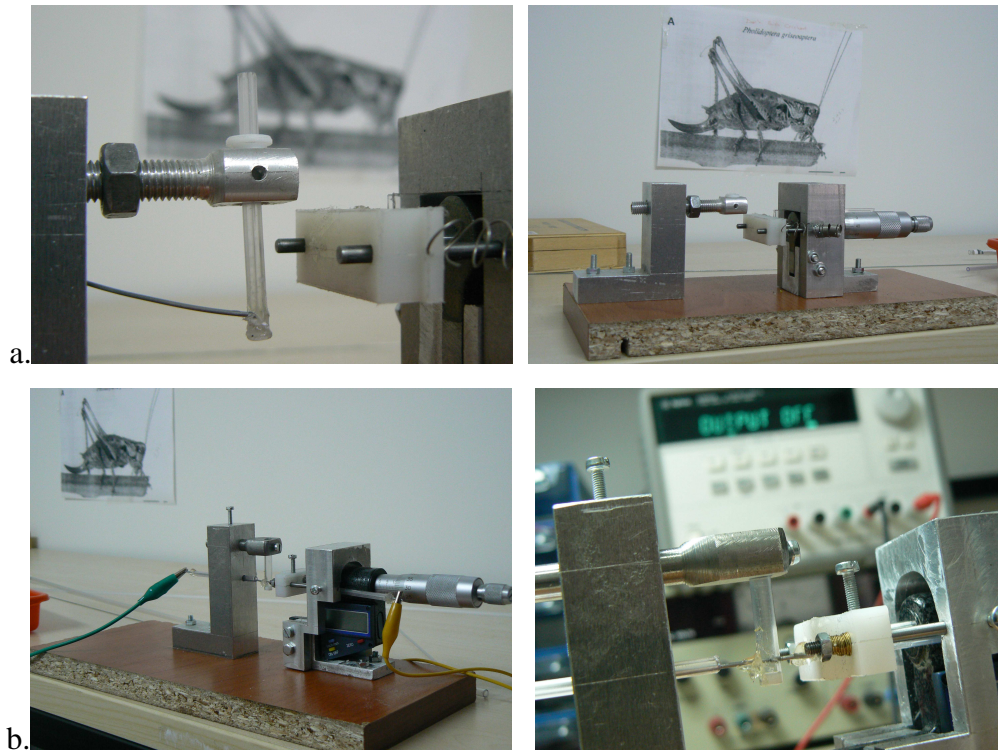


Figure 5.33 RC circuit set-ups a. with conventional micrometer and without isolation for electrical wire, b. with digital micrometer and electrical isolation (Atılım University, Biomimetic Design Laboratory)

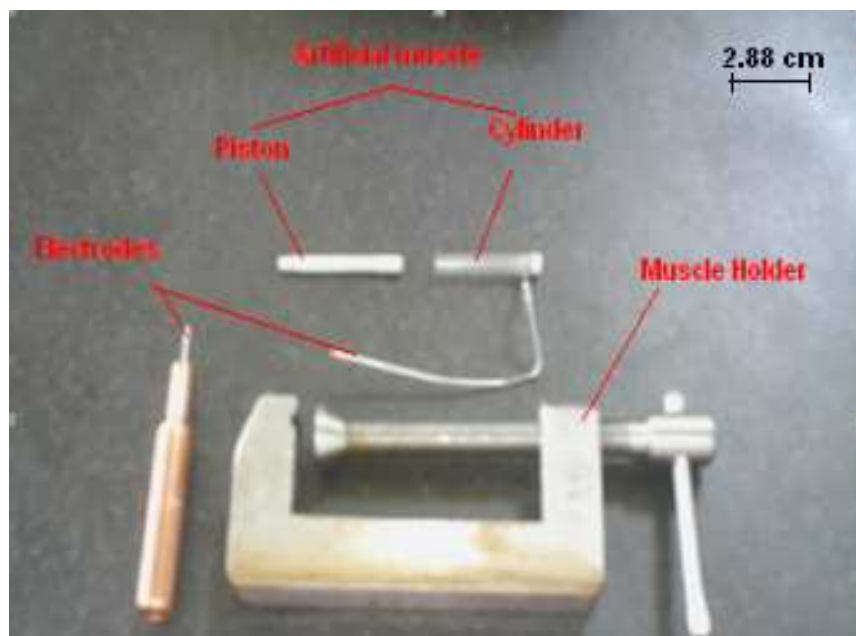


Figure 5.34 A plastic cylinder-teflon piston system and its apparatus for using on EDM (Atılım University, Machine Shop)

5.2.2 Characteristics of Force Sensor Set-up Used in the New Artificial Muscle

A biosensor piezoelectric force sensor is selected. “A biosensor is an analytical tool consisting of biologically active material used in close conjunction with a device that will convert a biochemical signal into a quantifiable electrical signal”, Kumar, (2000). Piezoelectric crystals can also be used in measuring an instantaneous change in the force (dynamic forces). “A piezoelectric effect states that when asymmetrical, elastic crystals are deformed by a force, an electrical potential will be developed within the distorted crystal lattice. This effect is reversible. That is, if a potential is applied between the surfaces of the crystal, it will change its physical dimensions”, Lynch, Peshkin, Eren, et.al, (2002).

The advantages of piezoelectric sensors compared with other types of sensors (Kuratle and Signer, 2007) are:

- Long life without aging
- High sensitivity
- Low threshold
- Large measuring range
- Practically displacement-free measurement
- High natural frequency
- Wide temperature range

A force sensor set-up; a Kistler piezoelectric low level force sensor, Type 9205 (Figure 5.35.a), a coupling element, Type 9405 (Figure 5.35.b), a charge meter and a software program is selected for measuring the actuation force of the new artificial muscle as given in Figure 5.36. The coupling element is used to reduce the effect of transverse forces and bending moments acting on the sensor. Low Level Force Sensors in the range of less than 1 mN up to 50 N are universally applicable, highly sensitive force sensors for measurement of quasistatic and dynamic tensile and compressive forces. The sensor element consists of a package of three piezoelectric crystal rods between two pressure distributions parts (Kistler data sheet, 2005) Technical data of this sensor is given in Table 5.3

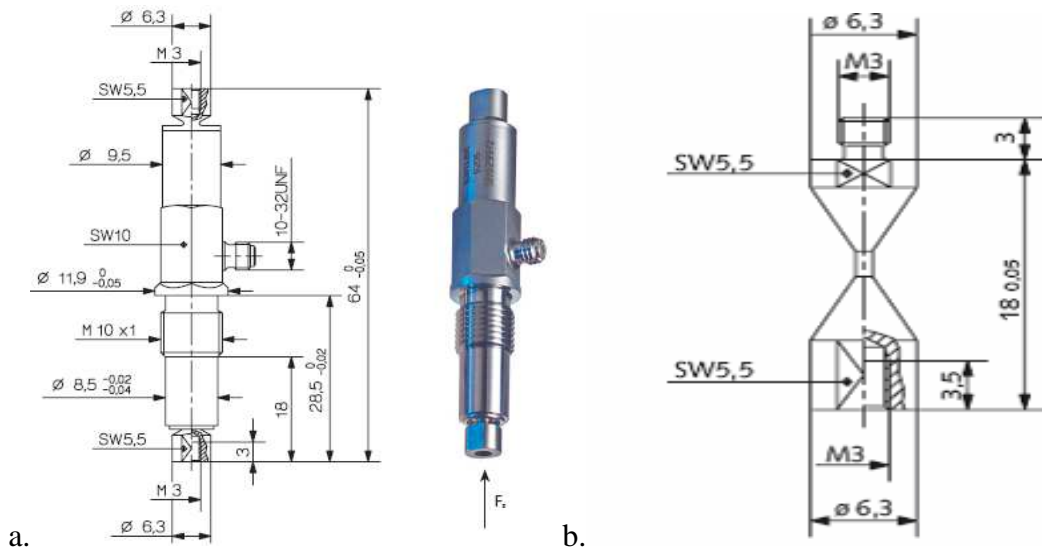


Figure 5.35 The general construction of a. Kistler 9205 type force sensor, b. coupling element where SW 5.5 is a fork wrench (Kistler data sheet, 2005)

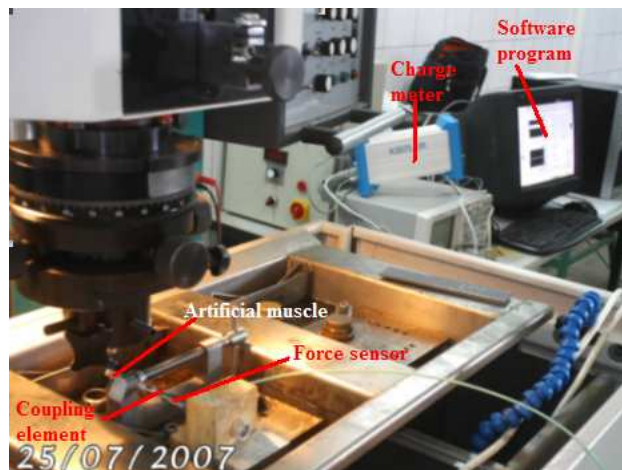


Figure 5.36 A view of Kistler force sensor set-up (Atılım University, Machine Shop)

It is a highly sensitive sensor intended mainly for the laboratory and research with the following characteristics:

- For tensile and compressive forces
- Very high sensitivity and resolution
- Very low temperature sensitivity

Table 5.3 Kistler, Type 9205 Low Force Sensor Technical Data
(Kistler data sheet, 2005)

Measuring range	F_z	N	-50 ... 50
Overload	F_z	N	-75/150
Calibrated measuring ranges			
100 %	F_z	N	-50 ... 50
10 %	F_z	N	-5 ... 5
1 %	F_z	N	-0,5 ... 0,5
Threshold	F_z	N	$<0,5 \cdot 10^{-3}$
Sensitivity	F_z	pC/N	≈ -115
Linearity, all measuring ranges		%FSO	$\leq \pm 1$
Hysteresis, all measuring ranges		%FSO	$\leq 0,5$
Transverse force ¹⁾ , max.	F_{xy}	N	10
Transverse force sensitivity	$F_{xy} \rightarrow F_z$	N/N	$\leq \pm 0,05$
Bending moment, max.	M_{xy}	N·m	0,25
Sensitivity to bending moment	$M_{xy} \rightarrow F_z$	N/N·m	$\leq \pm 3$
Torque, max.	M_z	N·m	0,15
Rigidity	c_z	N/ μ m	≈ 4
Natural frequency		kHz	> 10
Acceleration sensitivity			
axial		N/g	$< 0,03$
radial		N/g	$< 3 \cdot 10^{-3}$
Operating temperature range		°C	-50 ... 150
Temperature coefficient of sensitivity			
-50 ... 150 °C		%/°C	$\approx -0,02$
Insulation resistance, at 20 °C		Ω	$> 10^{13}$
Capacitance		pF	≈ 26
Connector (ceramic insulator)		KIAG 10-32 neg.	
Degree of protection (with cable connected)		EN60529	IP65
Case material		DIN	1.4542
Weight		g	19
Tightening torque, max.			
M10x1		N·m	10
M3		N·m	0,2

¹⁾ Force application in the plane of the cylindrical front end.

Basic Principle of the Experimental Procedure:

When the tensile/compressive force changes, the sensor produces an electric charge. The charge signal is converted by the charge meter into a proportional output voltage, which can be picked off with evaluation electronics and recorded. Although the force sensor can measure dynamic small force, the set-up software program does not work in real time because of its connection cable. A real time GPIB connecting card system, an oscilloscope, and a basic free Agilent program leads the capture data, measured from the artificial muscle. The artificial muscle mechanism (Figure 5.37) with a coupling element, a force sensor and the force analysis set-up constructions are given in Figure 5.38 and Figure 5.39 and their dimensions are shown in a technical drawing, Figure 5.40 where all dimensions in mm. An output screen for the experiment is given Figure 5.41 where time is limited by 200 ms. The voltage input is supplied from the EDM and force is observed in mV from the artificial muscle. During the experiment, the EDM is programmed with some level on the panel of the EDM that power level is 1, arc time is 5, arc interim is 6 and withdraw is 1. From the empirical data, the new artificial muscle gives nearly 600 mV (≈ 300 mN) when the height of dielectric liquid is 25.7 mm and voltage output scaling is 0.5 N/V which is set by the charge meter.

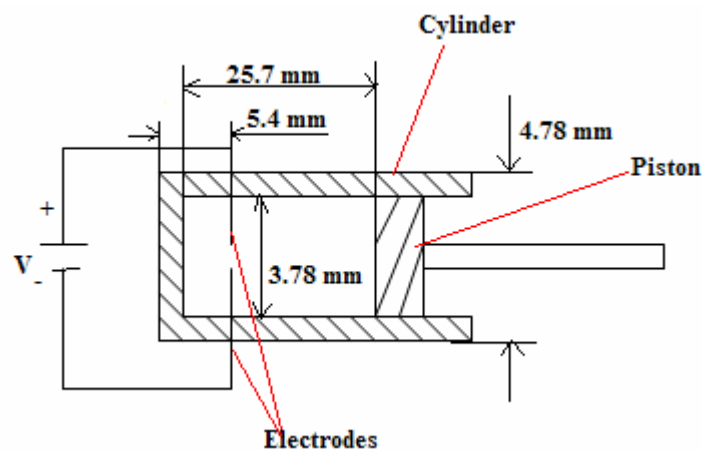


Figure 5.37 The artificial muscle mechanism

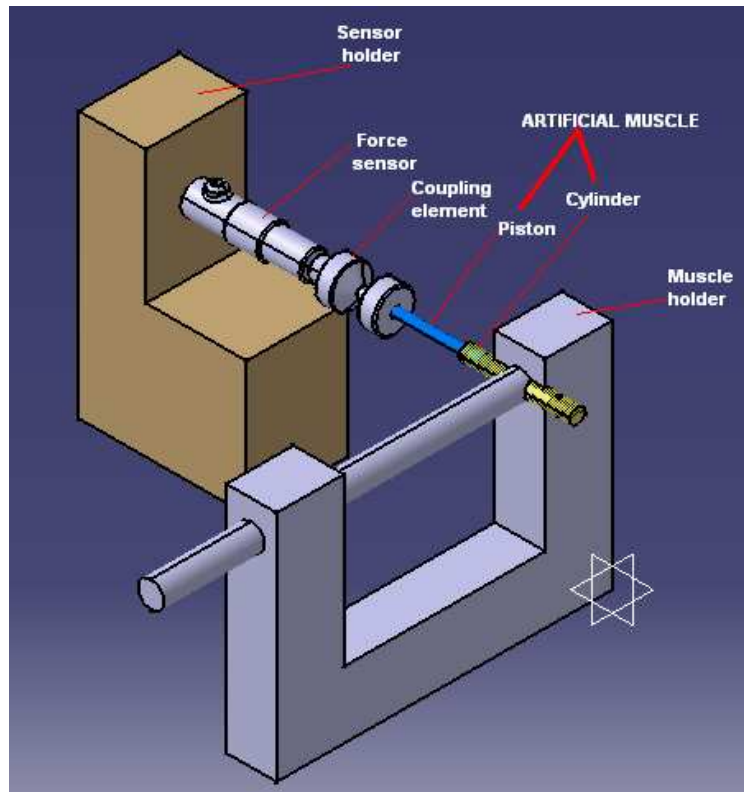


Figure 5.38 The artificial muscle mechanism with a coupling element and a force sensor, Catia P3V5R10

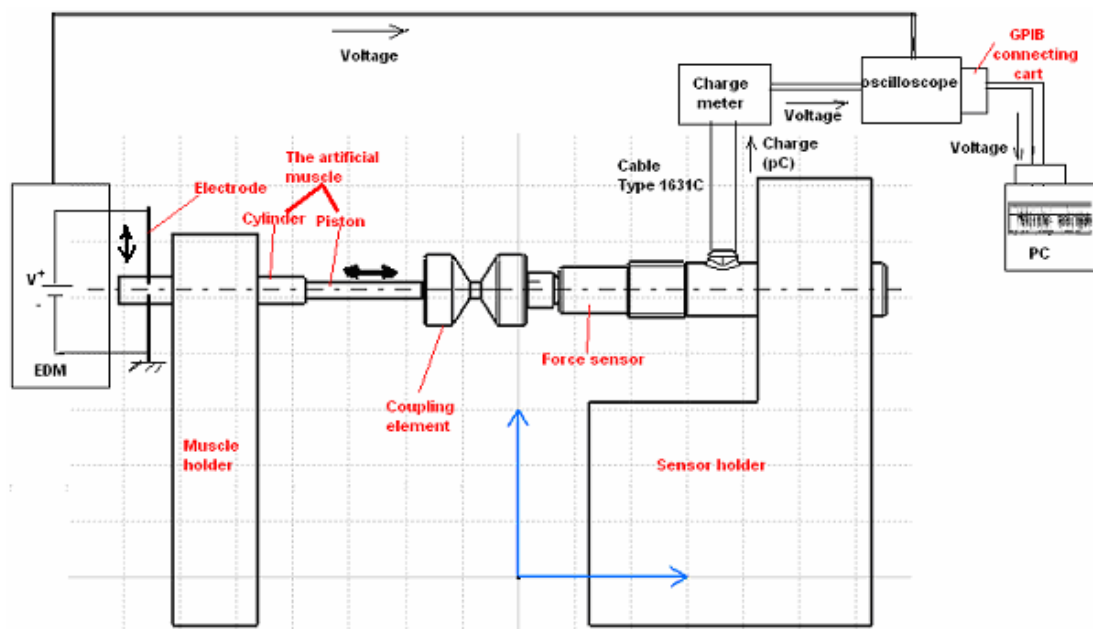


Figure 5.39 The construct of artificial muscle mechanism, coupling element and force sensor and the force analysis set-up

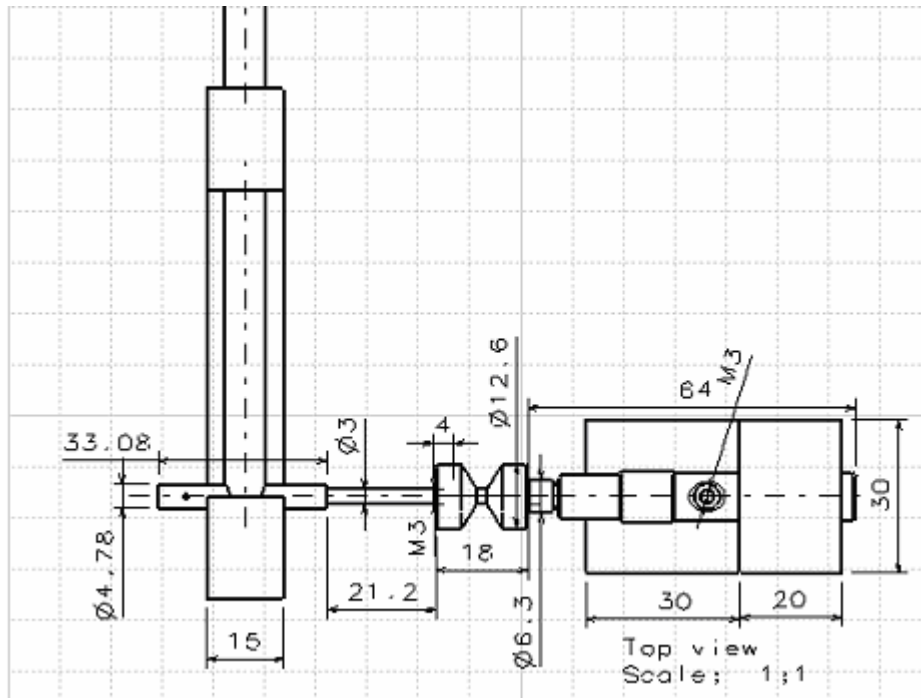


Figure 5.40 A top view of the artificial muscle and the force sensor technical drawing with dimensions, Catia P3V5R10

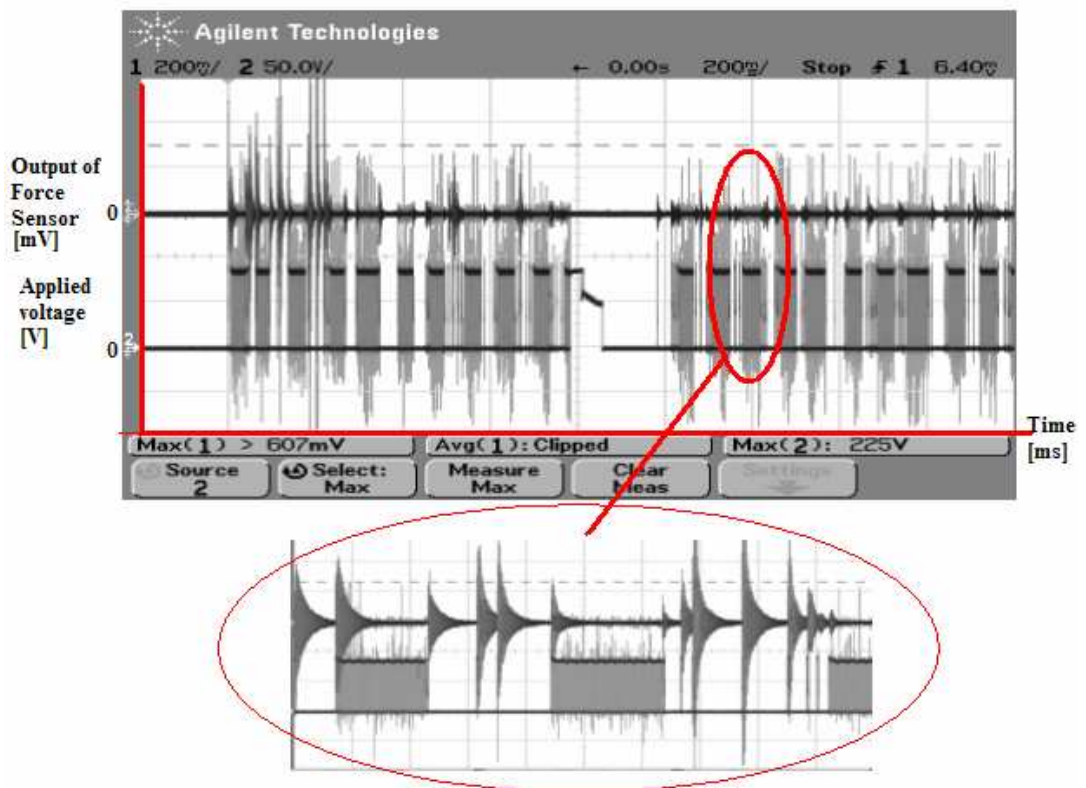


Figure 5.41 An output screen showing force sensor and applied voltage using Agilent software for the experiments

The disadvantage of muscle is that the muscle is not a soft actuator unlike the natural muscle. Advantages of this artificial muscle;

- Lighter weights of loads will reduce cost,
- easier manufacturing will also decrease cost,
- using water as an explosive will protect environment,
- using electric as an trigger mechanism will reduce cost,
- linear motion is obtained.

Although there is a limited number of artificial muscles in literature, a few of them are selected for grasshopper-like jumping mechanism because of the fact that most of them either have large size or are not sufficient for biomimetic design. A new artificial muscle is developed and a nearly 300 mN linear force is evaluated.

CHAPTER 6

PRELIMINARY DESIGN OF JUMPING MECHANISM OF GRASSHOPPER-LIKE ROBOT

Although grasshoppers have an exactly non-mimic jumping mechanism, the jumping mechanism is imitated basically by using artificial muscle technology and mechatronic components. For this purpose, anatomy of jumping mechanism is studied and an artificial muscle is developed. In addition, a preliminary design is developed and a prototype mechanism is manufactured according to the biomimetic design in this chapter. A grasshopper-like bio-robot model is developed and both the force of the new artificial muscle and the force of its leg model are compared with the force derived from the mathematical model.

6.1 DESIGN OF JUMPING MECHANISM OF GRASSHOPPER-LIKE ROBOT MODEL

According to mathematical 2D and 3D models and based on same experimental data obtained from literature survey, a preliminary design of a grasshopper-like bio-robot is developed using Catia P3V5R10. The design is given in Figure 6.1. In this figure, yellow part represents the bio-robot body, red parts and blue limbs show femur and tibia of jumping leg mechanisms respectively. The femur-tibia joint is a pin connected hinge joint like in the biological structure. Green small parts at the end of the tibia represent spurs, and finally black parts shows tarsus; they are designed as metallic curved plates for energy storage until take-off. Both front and middle legs of the body are designed as passive elements. Artificial muscles can be emplaced on femur and electronic circuit is placed on the body.

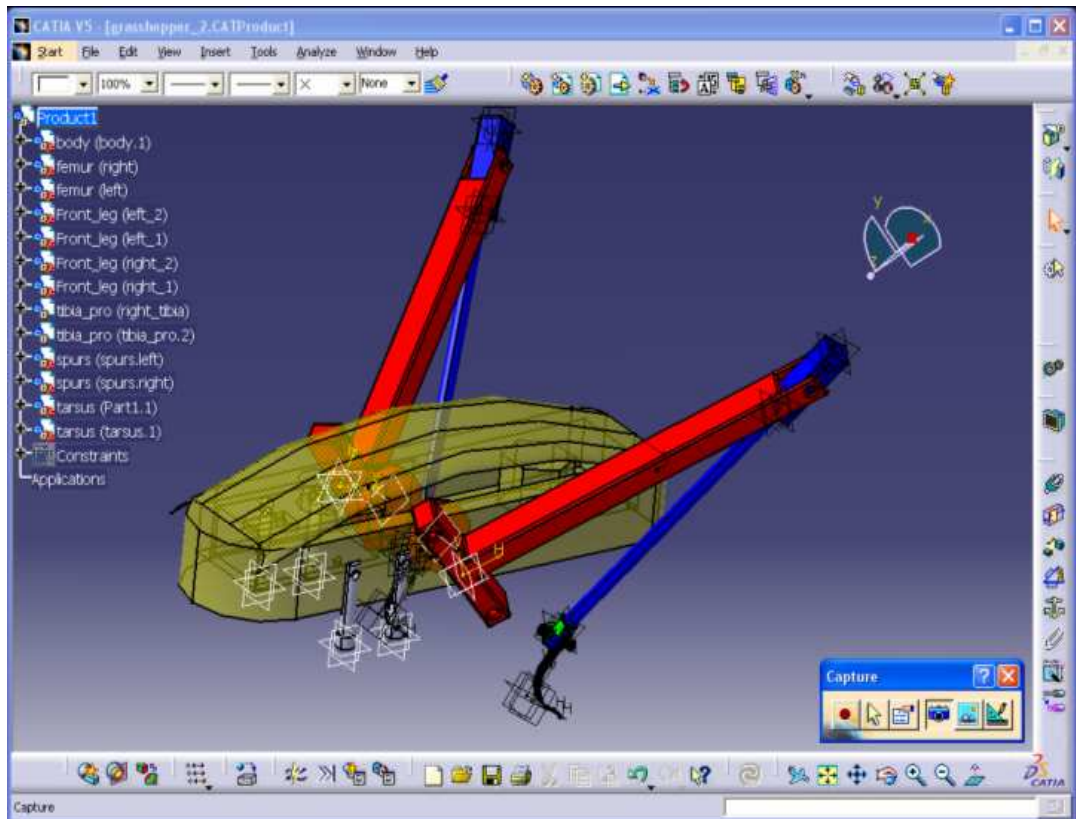


Figure 6.1 A view of grasshopper-like bio-robot, Catia P3V5R10 drawing

Two leg models are manufactured as prototypes of grasshopper-like jumping mechanism. One of them is developed to show artificial muscles working mechanism as given in Figure 6.2. An extra artificial muscle and a torsion spring are placed in the working mechanism prototype design but cannot be implemented on the prototype. For a future work a second artificial muscle is designed. The use of this design the muscle force throwing the body can be evaluated. The artificial muscle of this prototype cannot work automatically because the charge circuit is not able to detach from EDM. The other prototype is designed and manufactured according to center of mass position, obtained from take-off angles, until take-off (Figure 6.3). Hind leg position of the mathematical leg model until take-off is observed due to this prototype leg model. In this prototype, a slot placed on the wall. The canal path obtained from the Figure 4.10. With the use of this path the position of grasshopper leg until take-off as shown in Figure 4.5 given to the mechanism.

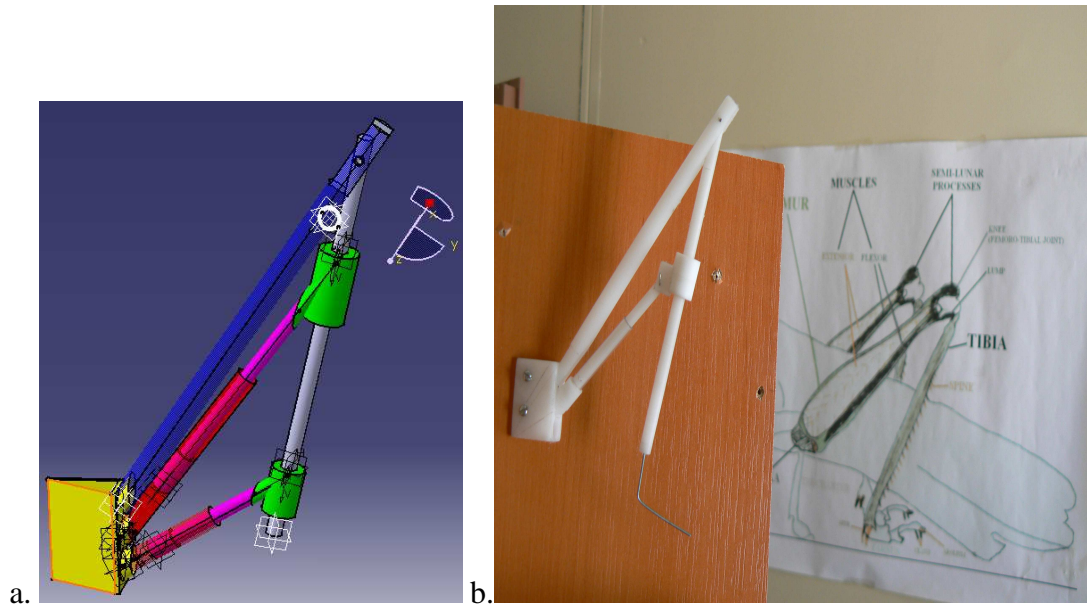


Figure 6.2 a. A view of prototype design of leg model, Catia P3V5R10, b. The working mechanism of new artificial muscle prototype in a jumping leg model (Atılım University, Biomimetic Design Laboratory)



Figure 6.3 Position of center of mass prototype in a jumping leg model until take-off (Atılım University, Biomimetic Design Laboratory)

6.2 DISCUSSION ON THE ARTIFICIAL MUSCLE FORCE

A 2D mathematical leg model using femur-tibia and body-femur angles was developed in Chapter 4 and the torques of the joints were determined (Figure 6.4). The maximum torque of femur-tibia joint (knee) is evaluated 2.440 Nm for 20 ms when the jumping starts. All joints of these models are hinge joints, grey elliptic part is the body and the tibia part is fixed to the ground. If the distance between muscle-tibia and knee joints, s , is taken as 2 mm, then the muscle force, F , is calculated as 305 mN. A leg model with the artificial muscle is designed as shown in Figure 6.5. The muscle force, F_a , is determined as 488 mN if the distance, s_a , is taken as 5 mm for the same joint. A 300_mN linear force was obtained from the experiments in Chapter 5. That force compensates the force of the biological muscle model given in Figure 6.4. Although the force of single artificial muscle model given in Figure 6.5 is not enough for jumping by taking $s_a=5$ mm, it would be possible to obtain jumping by increasing the distance between muscle-tibia and knee joints, s_a . However, the leg model with a large distance is not a good design from the point of view of biomimetic approach.

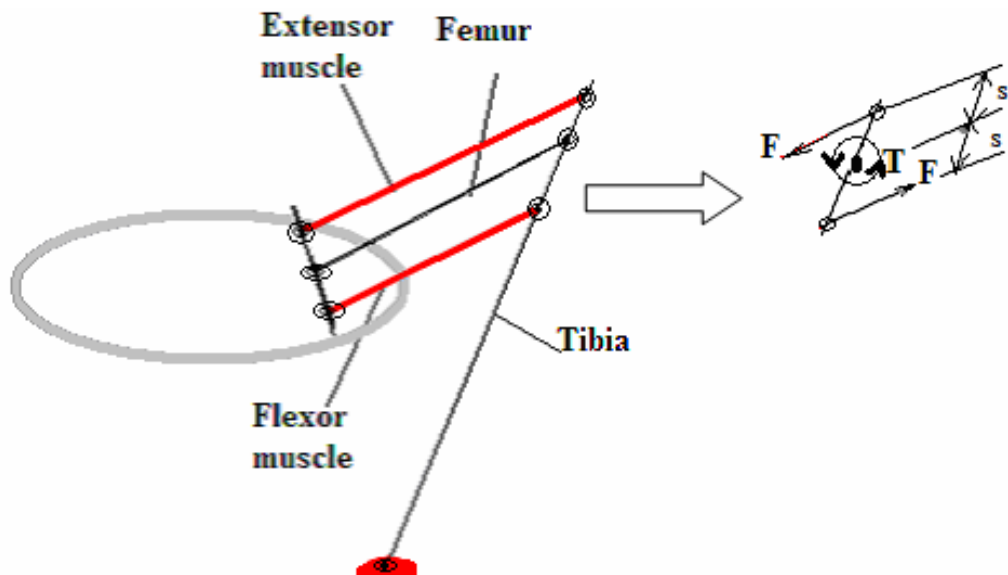


Figure 6.4 A view of leg model with extensor and flexor biological muscles

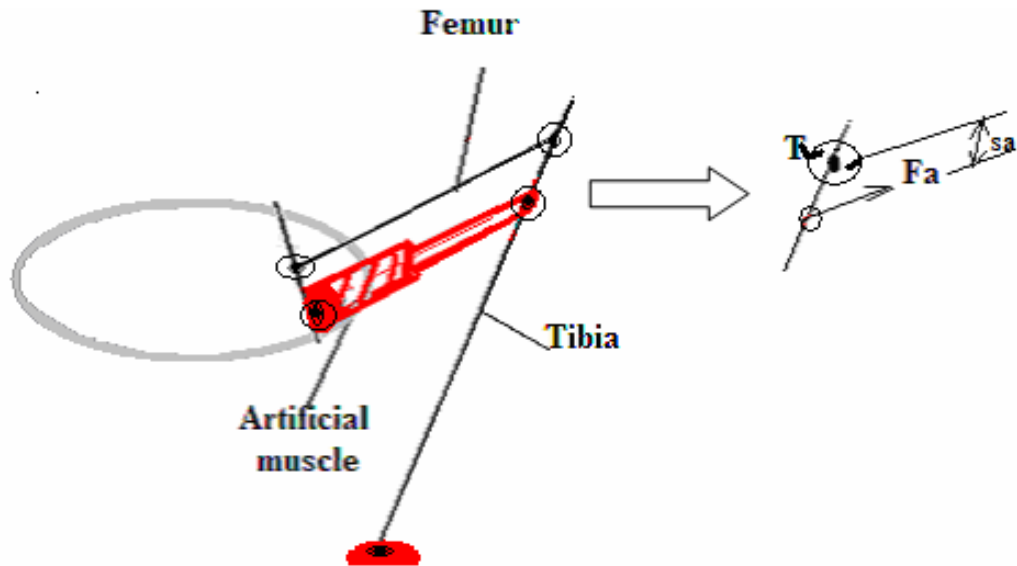


Figure 6.5 A view of leg model using single artificial muscle

In this chapter, a pre-design of grasshopper-like bio-robot is evaluated using both mathematical model and literature survey on grasshoppers. Although artificial muscles designed to be placed on the femur in this model, the muscles are not implemented. This design may be simulated and dynamic analysis can be evaluated in MSC. Adams program to obtain torque and force data, these data would be utilized to compare with mathematical and biological models.

Two prototypes for leg models are also manufactured to observe working mechanism of the artificial muscle and position of centre of mass. Three segments, femur, tibia and tarsus, are included in the prototypes. One of prototypes represents the position of centre of mass and hind leg using a canal on the wall (Figure 6.3). The other one is produced to show the artificial muscle working mechanism. However, the muscle cannot work automatically, because the lack of charge circuit apart from the EDM.

CHAPTER 7

CONCLUSIONS AND FURTHER RECOMMENDATIONS

As the conclusion of this thesis, discussion of the whole work is presented and the suggestions for future work are given.

7.1 DISCUSSION AND CONCLUSIONS

The aim of this thesis is to design a grasshopper-like jumping mechanism using biomimetic design approach. Constraints on the design of grasshopper-like jumping mechanism are specified in this study. A literature survey is conducted on the anatomy of jumping mechanism of grasshoppers. In addition, an apteral type of grasshoppers, *Isophya nervosa*, is studied as a biological observation part of the biomimetic design. Because of the lack of special set-ups to observe the motion of insects, the study on the anatomy is limited with the literature survey.

Since biomimetic study has become widespread, more universities worked on bio-robots which are mimicked insects or other animals intensively. Literature survey on bio-robots is evaluated while the mathematical model of the jumping leg mechanism is studied. All mathematical solution is compared with different methods. The position of the centre of mass of the body and the torque of hip and knee joints are developed using 2D and 3D leg models. The constructed mathematical model is used for production of prototypes and design of a new artificial muscle.

An electrical discharge system is used to have a light and small actuator. An explosion due to electric discharge between two electrodes constructed in a piston-cylinder system is used as an actuator. The cylinder is filled with dielectric liquid as a fuel because of the low cost and environmental aspects. With this system, a new

artificial muscle is developed as an actuator for jumping mechanism of grasshopper-like bio-robot in the thesis though there are several alternative artificial muscles which have constraints with their size and application areas.

A piston-cylinder system with 4.78 mm outer and 3.78 mm inner diameter filled with 25.7 mm dielectric liquid height can give 300 mN on the average. The weight of the designed piston-cylinder system is about 0.8 gr giving a force to weight ratio of the artificial muscle developed about 38:1. That ratio is smaller than the ratio for pneumatic artificial muscles but it is larger than the ratio for electrical motors and pneumatic cylinders. The artificial muscle percentage elongation is expected to be higher compared to that of natural muscles and the other artificial muscles due to explosion in the cylinder and that percentage gives higher than SMAs and piezoelectric artificial muscles, but that is not close to natural muscles. The muscle reaction speed is fast giving reaction in msec, which would be comparable with that of natural muscles and the other artificial muscles.

The measured force of the new artificial muscle is compared with the force obtained from the mathematical leg model. The average experimental force of the artificial muscle is close to that of mathematical leg model. However, the force obtained from the leg design which is driven by an artificial muscle, cannot give necessary jumping force. An extra artificial muscle implementation to the system is necessary to supply jumping mechanism as a future study.

Two prototypes are developed to verify the mathematical and artificial muscle models while a grasshopper-like bio-robot is designed. One of the prototypes is used to represent the working mechanism of artificial muscle and the other shows the path of the body centre of mass of grasshopper until take-off. Legs positions and body-femur, femur-tibia and tibia-ground angles can be observed by using the prototype. If the production of an electrical circuit separates from EDM, the prototypes can be worked with artificial muscles.

As conclusion;

- By applying electric voltage to the electrodes with a small gap in a piston-cylinder arrangement filled with a dielectric fluid, it is shown that it is possible to get an explosion which gives force for the actuation of leg mechanism for jumping.
- For a 3.78-mm piston-cylinder diameter and a 25.7-mm fluid height, for 235 V applied, a 300 mN force on the average can be obtained.
- For the designed muscle, a force to weight ratio of 38:1 can be obtained
- An extra artificial muscle or more powerful muscle implementation to the system is necessary to supply jumping mechanism of the grasshopper with 500 mgr weight.
- If the production of an electrical circuit is separated from EDM, the leg model of the prototypes can be worked with the artificial muscles.

7.2 SUGGESTIONS FOR FUTURE WORK

- In the mathematical model, one of the femur-tibia angles, $\gamma(t)$, is set constant at 30° . Although the angle has a small change during lift-off and the effect of that angle may be added in mathematical model as a future study.
- MSC. Adams program is used with a simple spherical model for determining the horizontal distance, kinetic energy, etc. This simulation program can be utilized for analyzing kinematics of the grasshopper-like bio-robot design, given in Chapter 5.

The linear motion of artificial muscle has been accomplished but further development of its performance can be improved. Those can be listed as follows:

- The piston-cylinder mechanism must be a closed system. If this closed system can be constructed, the discharge and vaporization effects will increase. The feed motion gap of the movable electrode on the cylinder causes vapor to escape which must push the piston. However, the closed

system prevents the feed motion of electrodes because the feed motion gap is closed; discharge features in a closed system may be obstructed.

- Because of the fact that EDM has still driven the discharge process, the force capacity of the developed muscle is limited. A more powerful power supply is to be used and RC circuit should be improved by a large size capacitor.
- The artificial muscle is not a soft actuator; this system may be moved in a soft tube as a future work, so it becomes softer tissue like the natural muscle.

REFERENCES

1. Arora, S., 2005, "Development of dielectric elastomer based prototype fiber actuators", Thesis, North Carolina State University
<http://www.lib.ncsu.edu/theses/available/etd-07282005-145223/unrestricted/etd.pdf>
(Download Date: 26.12.2006)
2. Ashley, 2003, "Artificial Muscles", Scientific American, www.sciam.com
(Download Date: 04.07.2006)
3. Bar-Cohen, Y., 1997, "Low Mass Muscle Actuators (LoMMAs)",
<http://ndea.jpl.nasa.gov/nasa-nde/lommas/lommas97.pdf>
(Download date: 30.06.2006)
4. Bar-Cohen, Y., Xue, T., Joffe, B., Lif, S. S., Shahinpoor, M., Simpson, J., Smith, J., and Willis, P., 1997, "Electroactive Polymers (EAP) Low Mass Muscle Actuators", Proceedings of SPIE--Volume 3041, Smart Structures and Materials 1997: Smart Structures and Integrated Systems, Mark E. Regelbrugge, Editor, June 1997, pp. 697-701
5. Bar-Cohen, Y., Leary, S., Yavrouian, A., Oguro, K., Tadokoro, S., Harrison, J., Smith, J., and Su, J., 1999, "Challenges to the Transition of IPMC Artificial Muscle Actuators to Practical Application", MRS Symposium: FF: Electroactive Polymers, Nov. 29 to Dec. 1, 1999 at Boston, MS Document ID: 31295.
6. Bar-Cohen, Y., 2000, "Electroactive polymers as artificial muscles -capabilities, potentials and challenges", Handbook on Biomimetics, Yoshihito Osada (Chief Ed.), Section 11, in Chapter 8, "Motion" paper #134, publisher: NTS Inc., Aug. 2000

7. Bar-Cohen, Y., 2004, "Electroactive Polymers (EAP) as actuators for potential future planetary mechanisms", Proceedings of the 2004 NASA/DoD Conference on Evolution Hardware (EH'04).
8. Bar-Cohen, Y., 2005, "Electroactive Polymers as Artificial Muscles Reality, Potential and Challenges", SPIE EAPAD-Short Course, March 6, San Diego, California.
9. Bar-Cohen, Y., 2006, "Biomimetics-using nature to inspire human innovation", Bioinsp. Biomim. 1, P1-P12.
10. Başaran, D., 2003, "Design, Production and development of mini/micro robots to form a cooperative colony", Middle east Technical University, Department of Mechanical Engineering Master Thesis, pg 98
11. Bennet-Clark, H.C., 1975, "The energetics of the jump of the locust *Schistocerca gregaria*", J. Exp. Biol., 63, 53-83
12. Biomimetic, 2006, "Abstract"
<http://www-cdr.stanford.edu/biomimetics/pdf/biomimetics.pdf>
(Download Date: 27.06.2006)
13. Biorobotics, 2006, "Biorobotics - Build Your Own Robotic Air Muscle Actuator"
<http://www.imagesco.com/articles/airmuscle/AirMuscleDescription01.html>
(Download date: 27.06.2006)
14. Birch, M.C., Quinn, R.D., Hahm, G., Phillips, S.M., Drennan, B., Fife, A., Beer, R.D. and Hiten, V., 2000, "Design of a Cricket Microrobot", Proceedings of the 2000 IEEE International Conference on Robotics and Automation (ICRA'00), San Francisco, CA

15. Birch, M.C., Quinn, R.D., Hahm, G., Phillips, S.M., Drennan, B., Fife, A., Beer, R.D., Yu, X., Garverick, S.L., Laksanacharoen, S., Pollack, A.J. and Ritzmann, R.E., 2005, "A Miniature Hybrid Robot Propelled by Legs", Case Western University,
16. Bonser, R.H.C., Harwin, W.S., Hayes, W., Jeronimidis, G., Mitchell, G.R., and Santulli, C., 2004, "EAP-based artificial muscles as an alternative to space mechanisms"
<http://ndeaa.jpl.nasa.gov/ndeaa-pub/Japan/biomimetic-polymers-handbook.pdf>
(Download Date: 25.07.2006)
17. Brabham, K., Marr, M., Smith, A., and Lee, P., 2004, "Artificial Muscle",
http://web.cecs.pdx.edu/~mperkows/CLASS_ROBOTICS/FEBR26-2004/ArtificialMusclePresentation.ppt#1
(Download date: 18.10.2006)
18. Brown, C., 2004, "Getting a grip on artificial muscles",
<http://www.eetimes.com/showArticle.jhtml?articleID=49400133>
(Download date: 04.07.2006)
19. Burrows, M. and Morris, G., 2001, "The Kinematics and Neural Control of high speed kicking movements in the locust", *J. Exp. Biol.*, 204:3471-3481.
20. Burrows, M. and Morris, O., 2002, "Jumping in a winged stick insect", *J. Exp. Biol.*, 206:1035-49.
21. Burrows, M. and Morris, O., 2003, "Jumping and kicking in bush crickets", *J. Exp. Biol.*, 205:2399-412.

22. Caldwell, D.G., Medrano-Cerda, G.A., and Goodwin, M., 1994, "Characteristics and Adaptive Control of Pneumatic Muscle Actuators for a Robotic Elbow", IEEE

23. Choi, H. R., Jung, K., Ryew, S., Nam, J., Jeon, J., Koo, J. C., and Tanie, K., 2005, "Biomimetic soft actuator: design, modeling, control, and applications", IEEE/ASME Transactions on Mechatronics, vol. 10, no. 5, October 2005

24. Colbrunn, R.W., 2000, "Design and control of a robotic leg with braided pneumatic actuators", Case Western Reserve University, Department of Mechanical and Aerospace Engineering Master Thesis

25. Delcomyn, F., and Nelson, M.E., 2000, "Architectures for a biomimetic hexapod robot", Robotics and Autonomous Systems 30 (2000) 5–15

26. Ducheon, C., 2005, "Robots will be of service with muscles, not motors", Industrial Robot: An International Journal 32/6 452-455

27. Elliott, C. J. H., Zumstein, N., Forman, O., Nongthomba, U. and Sparrow, J.C., 2004, "Distance and force production during jumping in wild-type and mutant *Drosophila melanogaster*", J. Exp.Biol., 207: 3515-3522

28. Emporia State University, 2005," A grasshopper jumping",
<http://www.emporia.edu/egps/tales/grasshoppers2.htm>
 (Download Date: 27.07.2005)

29. Enchanted Learning, 1999, Enchanted Learning, (1999), "Grasshopper",
<http://www.enchantedlearning.com/subjects/insects/orthoptera/Grasshopperprintout.html>
 (Download Date: 13.07.2005)

30. Espenscheid, K.S., Quinn, R.D., Beer, R.D. and Chiel, H.J., 1993 “Leg coordination mechanisms in the stick insect applied to hexapod robot locomotion”, The Massachusetts Institute of Technology, Adaptive Behavior, Vol.1, No.4:455-468
31. Fauske, G. M., 2002, “Anatomy of a Grasshopper”,
<http://www.ndsu.nodak.edu/entomology/hopper/anatomy.htm>
(Download Date: 13.07.2005)
32. Festo, 2006, “Fluidic Muscles; DMSP-../ MAS-..”, Operating instructions.
33. Granosik, G., and Borenstein, J., 2004, “Minimizing Air Consumption of Pneumatic Actuators in Mobile Robots”, IEEE International Conference on Robotics and Automation, New Orleans, LA., April 26-May 1, pp. 3634-3639.
34. Halloran, A.O., and Malley, F.O., 2004, “Materials and technologies for artificial muscle: a review for the mechatronic muscle project”, P.J. Prendergast and P.E. McHugh (Eds.), Topics in Bio-Mechanical Engineering, pp. 184-215.
35. Heitler, W.J., 2005, “How grasshoppers jump”,
<http://www.st-andrews.ac.uk/~wjh/jumping/index.html>
(Download Date: 01.07.2005)
36. Hugel, D. Robert G., 2004, “A Swimming Robot Actuated by Living Muscle Tissue”, Journal of NeuroEngineering and Rehabilitation, October 28
37. Kapps, M., 2007, “Smart-Material Mechanisms as Actuation Alternatives for Aerospace Robotics and Automation”,
http://isdc2.xisp.net/~kmiller/isdc_archive/fileDownload.php/?link=fileSelect&file_id=295
(Download date: 25.07.2006)

38. Kerscher, T., Albiez, J., and Berns, K., 2002, "Joint control of the Six-Legged Robot AirBug Driven by Fluidic Muscles", Third International Workshop on Robot Motion and Control, November 9-11.
39. Kikuchi, F., Ota, Y., and Hirose, S., 2003, "Basic Performance Experiments for Jumping Quadruped", Proceedings of the 2003 IEEE/RSJ InU Conference on Intelligent Robots and Systems Las Vegas, Nevada October
40. Kinglesley, D.A., 2005, "A Cockroach Inspired Robot with Artificial Muscles", Case Western Reserve University, Department of Mechanical and Aerospace Engineering Thesis
41. Kistler data sheet, 2005, "Low Level Force Sensor", Instruction Manual.
42. Konez, A., Erden, A., and Akkök, M., 2006, "Preliminary Design Analysis of Like-grasshopper Jumping Mechanism", The 12th International Conference on Machine Design and Production, Volume II, pg. 829, September, Kuşadası, Turkey
43. Kornbluh, R., Pelrine, R., Eckerle, J., Joseph J., 1998, "Electrostrictive polymer artificial muscle actuators", Proceedings of the 1998 IEEE International Conference on Robotics & Automation Leuven, Belgium, May
44. Kumar, A., 2000, "Biosensors Based on Piezoelectric Crystal Detectors: Theory and Application", The Minerals, Metals & Materials Society,
<http://www.tms.org/pubs/journals/JOM/0010/Kumar/Kumar-0010.html>
(Download date: 25.07.2007)

45. Kuratle R. H. and Signer, A., “The Basic of Piezoelectric Measurement Technology”,
<http://www.kistler.com/medias/izS408kP5EZxP85D8YwBEd-30.pdf>
(Download date: 25.07.2007)
46. Lambrecht, B.G. A., Horchler, A.D., and Quinn R.D., 2005, “A Small, Insect-Inspired Robot that Runs and Jumps”, Proceedings of the 2005 IEEE International Conference on Robotics and Automation Barcelona, Spain, April 2005
47. Laksanacharoen, S., Pollack, A. J., Nelson, G. M., Quinn, R. D. and Ritzmann, R. E., 2005, “Biomechanics and simulation of cricket for Microrobot design”, Case Western Reserve University
48. Lee, Y.K., Shimoyama, I., 2002, “A Multi-Channel Micro Valve for Micro Pneumatic Artificial Muscle”, IEEE.
49. Leeuwen, M.V. and Vreeken, J., 2004, “A philosophy of minimalist biomimetic robotics”,
http://www.karlaspelund.com/biomimes/biomime_links.htm
(Download Date: 22.07.2005)
50. Lowe, M., 2006, “Elastomers: Powerful Polymer”,
http://www.appliancedesign.com/CDA/Articles/Feature_Article/4adb4f336188b010VgnVCM100000f932a8c0____
(Download date: 27.10.2006)
51. Lynch, K. M., Peshkin, M. A., Eren, H., Elbestawi, M. A., Garshelis, I. J., Thorn, R., Norris, P. M., Hosticka, B., Figueroa, J. F., Everett, H. R. (Bart), Ipson, S.S., and Liu, C., 2002, “Mechatronics Handbook”, Chapter 19, Sensors, CRC Press LLC

52. Merali, Z., 2006, "Methanol-powered artificial muscles start to flex",
<http://www.newscientist.com/article.ns?id=dn8859>
(Download date: 30.06.2006)
53. Morrey, J.M., Lambrecht, B., Horchler, A.D., Ritzmann, R.E., and Quinn, R.D.,
2003, "Highly Mobile and Robust Small Quadruped Robots", Proceedings of the
2003 IEEURSI Intl. Conference on Intelligent Robots and Systems Las Vegas,
Nevada October 2003
54. O'Halloran, A. and O'Malley, F., 2004, "Materials and Technologies For
Artificial Muscle: A Review For The Mechatronic Muscle Project", P.J.
Prendergast and P.E. McHugh (Eds.), Topics in Bio-Mechanical Engineering, pp.
184-215
55. Pelrine, R., Kornbluh, R., Pei, Q., Stanford, S., Oh, S., Eckerle, J., Full, R.,
Rosenthal, M., and Meijer, K., 2002, "Dielectric Elastomer Artificial Muscle
Actuators: Toward Biomimetic Motion", Smart Structures and Materials 2002:
Electroactive Polymer Actuators and Devices (EAPAD), 126 Yoseph Bar-Cohen,
Editor, Proceedings of SPIE Vol. 4695
56. Pfadt, R. E., 2002, "Field Guide to Common Western Grasshoppers", Wyoming
Agricultural Experiment Station, Bulletin 912, Third Edition
57. Pnewswire, 2006, "Artificial Muscle Introduces World's First Line of Standard
Electroactive Polymer (EAP) Linear Actuators",
[http://www.pnewswire.com/cgi-bin/stories.pl?ACCT=104&STORY
=/www/story/01-25-2006/0004267359&EDATE=](http://www.pnewswire.com/cgi-bin/stories.pl?ACCT=104&STORY=/www/story/01-25-2006/0004267359&EDATE=)
(Download date: 27.06.2006)
58. Raibert, M.H., 1986 "Legged Robots That Balance", MIT Press: Cambridge,
Massachusetts.

59. Raibert, M.H., 1993, "Legged Robots", Biological Neural Networks in Invertebrate Neuroethology and Robotics. Academic Press, Inc: New York.
60. Ringrose, R., 1997, "Self Stabilizing Running", Proceedings of the 1997 IEEE International Conference on Robotics and Automation, Albuquerque, NM.
61. Safak, K.K., Adams G.G., 2002, "Modeling and simulation of an artificial muscle and its application to biomimetic robot posture control", Robotics and Autonomous Systems 41 (2002) 225–243
62. Savant, A., 2003, "Leg design of walking robots", Fr. C. Rodrigues Institute of Technology, Mumbai University, Mechanical Engineering Department, Bs Report
63. Shahinpoor, M., and Kim, K. J., 2004, "Ionic polymer–metal composites: IV. Industrial and medical applications", Smart Mater. Struct. 14, 197–214
64. Stanford, 2005, "Biomimetic Robots", <http://www-cdr.stanford.edu/biomimetics/>
(Download date: 13.06.2006)
65. Stilson T., 1996, "Piezoelectric Sensors",
<http://soundlab.cs.princeton.edu/learning/tutorials/sensors/node7.html>
(Download date: 25.07.2007)
66. Titech, 2006, "Jumping Quadruped driven by pneumatic power "AirHopper""
http://www-robot.mes.titech.ac.jp/robot/walking/airhopper/airhopper_e.html
(Download date: 20.04.2007)
67. University of Reading, 1992, "The Centre for Biomimetics Brochure"
<http://www.rdg.ac.uk/Biomim/home.htm>
(Download date: 10.06.2006)

68. Virtualskies, 2007, "Shape-Memory Alloys",
<http://virtualskies.arc.nasa.gov/research/youDecide/shapeMemAlloys.html>
(Download date: 27.06.2007)
69. Webb,B. and Harrison,R.R., 2005, "Integrating sensorimotor systems in a robot model of cricket behavior",
<http://www.stir.ac.uk/staff/psychology/bhw1/phonotaxis/spie.pdf>
(Download Date: 26.07.2005)
70. Wei, T.E., Nelson, G.M., Quinn, R.D., Verma, H. and Garverick, S.L., 2005, "Design of a 5-cm Monopod Hopping Robot", Case Western Reserve University

APPENDICES

APPENDIX A

ANALYTICAL SOLUTION OF BODY HEIGHT AND BODY-FEMUR ANGLE

A. 1. Calculation of Body Height

If the body height and femur-tibia angle changes are assumed to be zero between the time -80 ms and -20 ms in the Figure 4.2 in Chapter 4, the body height (according to body centre of mass position) ($z(t)$) can be represented analytically by using the empirical data obtained from the Figure A.1. Moreover, -20ms is shifted to origin for positive time interval. It is assumed that body height ($z(t)$) polynomial is third degree.

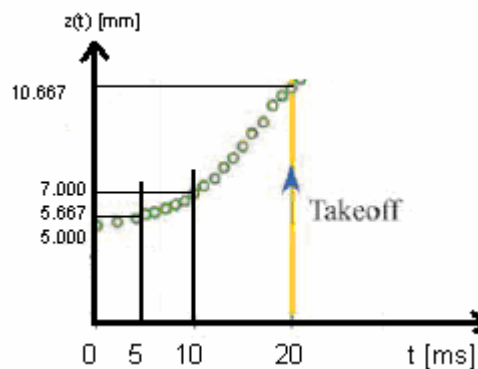


Figure A.1 Body height ($z(t)$) of body movement of a Pholidoptera male before take-off for positive time definite

According to this figure initial conditions are;

$$t=0 \text{ ms} \quad \Rightarrow \quad z(t)=5 \text{ mm} \quad (\text{A.1})$$

$$t=5 \text{ ms} \quad \Rightarrow \quad z(t)=5.667 \text{ mm} \quad (\text{A.2})$$

$$t=10 \text{ ms} \quad \Rightarrow \quad z(t)=7 \text{ mm} \quad (\text{A.3})$$

$$t=20 \text{ ms} \quad \Rightarrow \quad z(t)=10.667 \text{ mm} \quad (\text{A.4})$$

A.1.1 Polynomial Solution

If body height ($z(t)$) polynomial is assumed to be third degree, it is represented with

$$z(t) = at^3 + bt^2 + ct + d \quad (\text{A.5})$$

If the first initial condition is substituting into the equation of A.5, it is gotten,

$$t=0 \text{ ms} \quad \Rightarrow \quad z(t)=5 \text{ mm} \quad \Rightarrow \quad d=5 \quad (\text{A.6})$$

Substituting (A.6) into the (A.2)

$$5c = 0.667 - 125a - 25b \quad (\text{A.7})$$

Similarly, substituting (A.6) and (A.7) into the conditions (A.3) and (A.4), it is gotten,

$$0.666 = 750a + 50b \quad (\text{A.8})$$

$$2.999 = 7500a + 300b \quad (\text{A.9})$$

Consequently, body height becomes

$$z(t) = -0.00332333t^3 + 0.018305t^2 + 0.05018333t + 5 \quad (\text{A.10})$$

A.1.2 Lagrange Interpolating Polynomials Solution

$$f_n(x) = \sum_{i=0}^n L_i(x) \cdot f(x_i) \quad (\text{A.11})$$

$$L_i(x) = \prod_{j=0, j \neq i}^n \frac{(x - x_j)}{(x_i - x_j)} \quad (\text{A.12})$$

For third order polynomial and interval of time, the formulation is

$$z_3(t) = \sum_{i=0}^3 L_i(t) \cdot f(t_i) = L_0(t) \cdot z(t_0) + L_1(t) \cdot z(t_1) + L_2(t) \cdot z(t_2) + L_3(t) \cdot z(t_3) \quad (\text{A.13})$$

Thus, body height is

$$\begin{aligned} z_3(t) = & \frac{(t-5)(t-10)(t-20)}{(0-5)(0-10)(0-20)} * 5 + \frac{(t-0)(t-10)(t-20)}{(5-0)(5-10)(5-20)} * 5.667 \\ & + \frac{(t-0)(t-5)(t-20)}{(10-0)(10-5)(10-20)} * 7 + \frac{(t-0)(t-5)(t-10)}{(20-0)(20-5)(20-10)} * 10.667 \end{aligned} \quad (\text{A.14})$$

From the equation (A.14), body height becomes

$$z(t) = -0.00332334t^3 + 0.01830501t^2 + 0.0501833t + 5 \quad (\text{A.15})$$

A.1.3 Least Square Regression, Polynomial Regression Solution

$$z(t) = a_3t^3 + a_2t^2 + a_1t + a_0 \quad (\text{A.16})$$

$$\frac{\partial S_r}{\partial a_0} = na_0 + a_1 \sum t_i + a_2 \sum t_i^2 + a_3 \sum t_i^3 = \sum z_i \quad (\text{A.17})$$

...

Thus, we get four formulae

$$na_0 + a_1 \sum t_i + a_2 \sum t_i^2 + a_3 \sum t_i^3 = \sum z_i \quad (\text{A.18})$$

$$a_0 \sum t_i + a_1 \sum t_i^2 + a_2 \sum t_i^3 + a_3 \sum t_i^4 = \sum t_i z_i \quad (\text{A.19})$$

$$a_0 \sum t_i^2 + a_1 \sum t_i^3 + a_2 \sum t_i^4 + a_3 \sum t_i^5 = \sum t_i^2 z_i \quad (\text{A.20})$$

$$a_0 \sum t_i^3 + a_1 \sum t_i^4 + a_2 \sum t_i^5 + a_3 \sum t_i^6 = \sum t_i^3 z_i \quad (\text{A.21})$$

Table A.1 Time and body height values according to initial conditions

i	ti	yi	ti*yi	ti^2	(ti^2)*yi	ti^3	(ti^3)*yi	ti^4	ti^5	ti^6
1	0	5	0	0	0	0	0	0	0	0
2	5	5,667	28,335	25	141,675	125	708,375	625	3125	15625
3	10	7	70	100	700	1000	7000	10000	100000	1000000
4	20	10,667	213,34	400	4266,8	8000	85336	160000	3200000	64000000
Total	35	28,334	311,675	525	5108,475	9125	93044,38	170625	3303125	65015625

Mathcad 2000 Solution is given.

%Least square Regression, polynomial regression

$$M := \begin{pmatrix} 4 & 35 & 525 & 9125 \\ 35 & 525 & 9125 & 170625 \\ 525 & 9125 & 170625 & 3303125 \\ 9125 & 170625 & 3303125 & 65015625 \end{pmatrix} \quad V := \begin{pmatrix} 28.334 \\ 311.675 \\ 5108.475 \\ 93044.38 \end{pmatrix}$$

soln := lsolve(M, V)

$$\text{soln} = \begin{pmatrix} 4.999995 \\ 0.0501942222 \\ 0.01830325 \\ -0.0003322722 \end{pmatrix}$$

Body height becomes

$$z_3(t) := (-0.0003322722) \cdot t^3 + (0.01830325) \cdot t^2 + (0.0501942222) \cdot t + (4.999995) \quad (\text{A.22})$$

A.1.4 Result of the Body Height Analysis

The graph of the body height according to difference analytical and numerical solutions is given in the given Figure 4.11.

i. Polynomial Solution;

$$z_1(t) = (-0.000332334)t^3 + (0.01830501)t^2 + (0.0501833)t + 5 \quad (4.23)$$

ii. Lagrange Interpolating Polynomials Solution;

$$z_2(t) = (-0.000332333)t^3 + (0.018305)t^2 + (0.05018333)t + 5 \quad (4.24)$$

iii. Least Square Regression Solution;

$$z_3(t) = (-0.0003322722)t^3 + (0.01830325)t^2 + (0.0501942222)t + (4.999995) \quad (4.25)$$

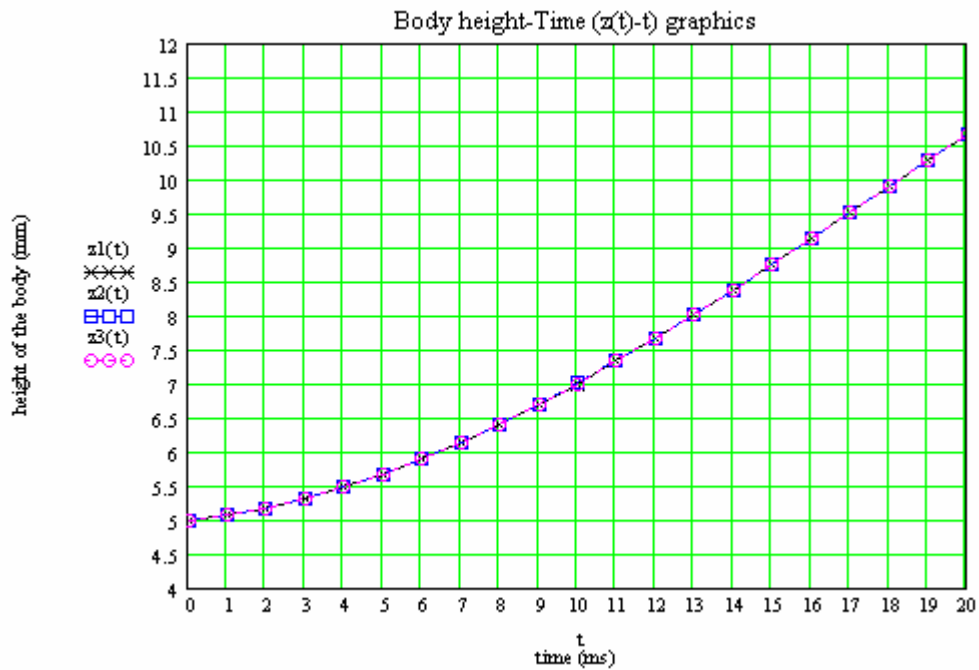


Figure A.2 Mathcad 2000 body height solutions, polynomial, Lagrange and least square methods solutions

A. 2. Calculation of Femur-Tibia (Knee) Angle

If the body height and femur-tibia angle changes are assumed to be zero between the time -80 ms and -20 ms in the Figure 4.2 in Chapter 4, the Femur-Tibia angle ($\alpha(t)$) can be represented analytically by using the empirical data obtained from the Figure

A.2. Moreover, -20ms is shifted to origin for positive time interval. It is assumed that the Femur-Tibia angle ($\alpha(t)$) polynomial is third degree like body height polynomial.

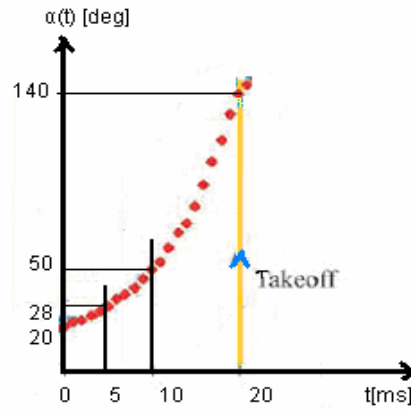


Figure A.3 Femur-Tibia angle ($\alpha(t)$) of body movement of a Pholidoptera male before take-off for positive time definite

According to this figure initial conditions are;

$$t=0 \text{ ms} \quad \Rightarrow \quad \alpha(t)=20 \text{ deg} \quad (\text{A.23})$$

$$t=5 \text{ ms} \quad \Rightarrow \quad \alpha(t)=28 \text{ deg} \quad (\text{A.24})$$

$$t=10 \text{ ms} \quad \Rightarrow \quad \alpha(t)=50 \text{ deg} \quad (\text{A.25})$$

$$t=20 \text{ ms} \quad \Rightarrow \quad \alpha(t)=140 \text{ deg} \quad (\text{A.26})$$

A.2.1 Polynomial Solution

If Femur-Tibia angle ($\alpha(t)$) polynomial is third degree, it is represented with

$$\alpha(t) = et^3 + ft^2 + gt + h \quad (\text{A.27})$$

If similar way with body height is used, femur-tibia angle becomes

$$\alpha(t) = 0.00133333t^3 + 0.26t^2 + 0.26666675t + 20 \quad (\text{A.28})$$

A.2.2 Lagrange Interpolating Polynomials

For third order polynomial and interval of time, the formulation of Femur-tibia angle is

$$\alpha_3(t) = \sum_{i=0}^3 L_i(t) \cdot \alpha(t_i) = L_0(t) \cdot \alpha(t_0) + L_1(t) \cdot \alpha(t_1) + L_2(t) \cdot \alpha(t_2) + L_3(t) \cdot \alpha(t_3) \quad (\text{A.29})$$

Thus, femur-tibia angle is

$$\begin{aligned} \alpha_3(t) = & \frac{(t-5)(t-10)(t-20)}{(0-5)(0-10)(0-20)} * 20 + \frac{(t-0)(t-10)(t-20)}{(5-0)(5-10)(5-20)} * 28 \\ & \frac{(t-0)(t-5)(t-20)}{(10-0)(10-5)(10-20)} * 50 + \frac{(t-0)(t-5)(t-10)}{(20-0)(20-5)(20-10)} * 140 \end{aligned} \quad (\text{A.30})$$

From the equation (8), angle polynomial becomes

$$\alpha(t) = 0.001333337t^3 + 0.25999994t^2 + 0.2666669t + 20 \quad (\text{A.31})$$

A.2.3 Least Square Regression, Polynomial Regression

$$\alpha(t) = a_3t^3 + a_2t^2 + a_1t + a_0 \quad (\text{A.32})$$

Thus, we get four formulae

$$na_0 + a_1 \sum t_i + a_2 \sum t_i^2 + a_3 \sum t_i^3 = \sum \alpha_i \quad (\text{A.33})$$

$$a_0 \sum t_i + a_1 \sum t_i^2 + a_2 \sum t_i^3 + a_3 \sum t_i^4 = \sum t_i \alpha_i \quad (\text{A.34})$$

$$a_0 \sum t_i^2 + a_1 \sum t_i^3 + a_2 \sum t_i^4 + a_3 \sum t_i^5 = \sum t_i^2 \alpha_i \quad (\text{A.35})$$

$$a_0 \sum t_i^3 + a_1 \sum t_i^4 + a_2 \sum t_i^5 + a_3 \sum t_i^6 = \sum t_i^3 \alpha_i \quad (\text{A.36})$$

Table A.2 Time and the angle values according to initial conditions

i	ti	αi	ti*αi	ti^2	(ti^2)*αi	ti^3	(ti^3)*αi	ti^4	ti^5	ti^6
1	0	20	0	0	0	0	0	0	0	0
2	5	28	140	25	700	125	3500	625	3125	15625
3	10	50	500	100	5000	1000	50000	10000	100000	1000000
4	20	140	2800	400	56000	8000	1120000	160000	3200000	64000000
Total	35	238	3440	525	61700	9125	1173500	170625	3303125	65015625

Mathcad 2000 Solution is given.

%Least square Regression, polynomial regression

$$M := \begin{pmatrix} 4 & 35 & 525 & 9125 \\ 35 & 525 & 9125 & 170625 \\ 525 & 9125 & 170625 & 3303125 \\ 9125 & 170625 & 3303125 & 65015625 \end{pmatrix} \quad V := \begin{pmatrix} 238 \\ 3440 \\ 61700 \\ 1173500 \end{pmatrix}$$

soln := lsolve(M, V)

$$\text{soln} = \begin{pmatrix} 20 \\ 0.2666666667 \\ 0.26 \\ 0.0013333333 \end{pmatrix}$$

Femur-Tibia (Knee) angle becomes

$$\alpha_3(t) := (0.0013333333) \cdot t^3 + (0.26) \cdot t^2 + (0.2666666667) \cdot t + 20 \quad (\text{A.37})$$

A.2.4 Result of the Femur-Tibia Angle Analysis

The graph of the femur-tibia angle according to difference analytical and numerical solutions is given in the given Figure A.3.

i. Polynomial Solution;

$$\alpha_1(t) = (0.001333333)t^3 + (0.26)t^2 + (0.2666675)t + 20 \quad (4.26)$$

ii. Lagrange Interpolating Polynomials Solution;

$$\alpha_2(t) = (0.001333337)t^3 + (0.25999994)t^2 + (0.2666669)t + 20 \quad (4.27)$$

iii. Least Square Regression Solution;

$$\alpha_3(t) = (0.0013333333)t^3 + (0.26)t^2 + (0.2666666667)t + 20 \quad (4.28)$$

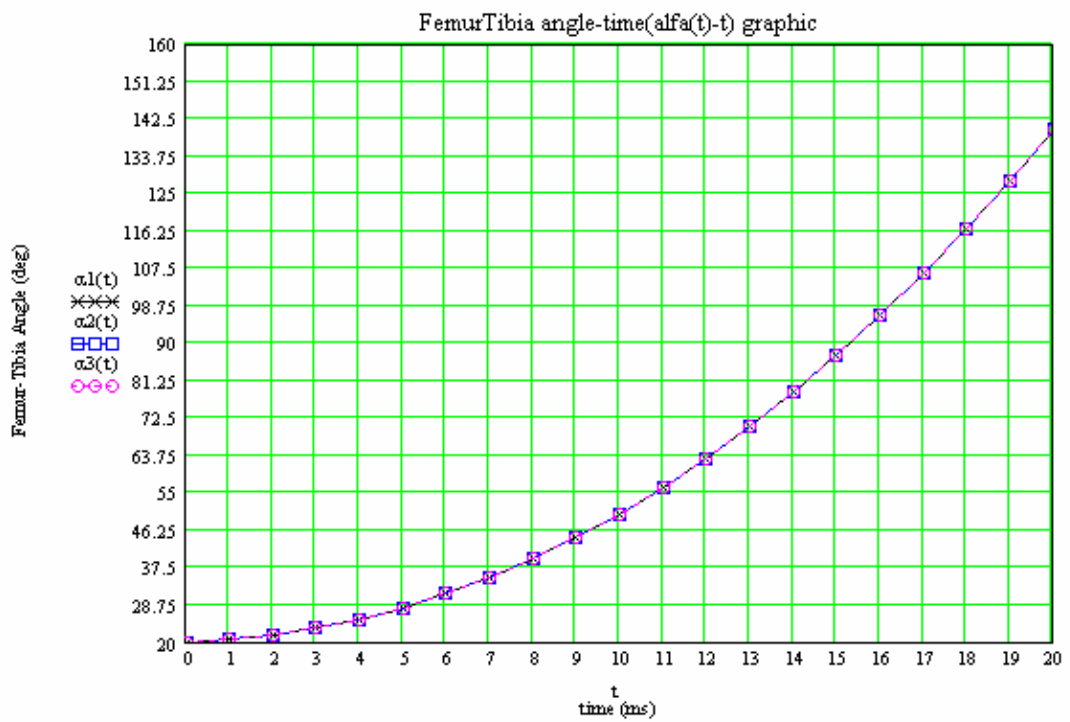


Figure A.4 Mathcad 2000 femur-tibia angle solutions, polynomial, Lagrange and least square methods solutions

APPENDIX B

CALCULATION OF BODY-FEMUR ANGLE

$\beta(t)$ can be determined from the equations (4.1), (4.2) and (4.3) in Chapter 4.

$$\begin{aligned} z(t) &= -0.866.L_1.\cos(\beta(t)) + 0.866.L_2.\cos(\beta(t) - \alpha(t)) \\ &= [-0.866.L_1 + 0.866.L_2 \cos(\alpha(t))]\cos(\beta(t)) + [0.866.L_2.\sin(\alpha(t))]\sin(\beta(t)) \end{aligned} \quad (\text{B.1})$$

If

$$[-0.866.L_1 + 0.866.L_2 \cos(\alpha(t))] = C + D.\cos(\alpha(t)) = E.\cos(\delta(t)) \quad (\text{B.2})$$

and

$$[0.866.L_2.\sin(\alpha(t))] = D.\sin(\alpha(t)) = E.\sin(\delta(t)) \quad (\text{B.3})$$

Thus,

$$z(t) = E.[\cos(\beta(t)).\cos(\delta(t)) + \sin(\beta(t)).\sin(\delta(t))] \quad (\text{B.4})$$

$$z(t) = E.[\cos(\beta(t) - (\delta(t)))] \quad (\text{B.5})$$

Finally, body-femur angle can be found as

$$\beta(t) = \delta(t) + a \cos\left(\frac{z(t)}{E(t)}\right) \quad (\text{B.6})$$

where $E(t) = \sqrt{(C + D.\cos(\alpha(t)))^2 + (D.\sin(\alpha(t)))^2}$;

$$\delta(t) = a \tan\left(\frac{D.\sin(\alpha(t))}{C + D.\cos(\alpha(t))}\right);$$

$$C = -L1.\cos(\gamma(t))$$

and

$$D = L2.\cos(\gamma(t))$$

APPENDIX C

2D LEG MODEL RESULTS

Table C.1 2D Leg Model Angles Results

time	Alfa (deg)	Beta (deg)	Teta= Beta-alfa (deg)	x(t) (mm)	z(t) (mm)	Velocity (mm/ms ²)
0.000	20,0	-55,2	-75,2	1.175	5.000	0.562
0.500	20,1	-57,6	-77,7	0.968	5.051	0.258
1.000	20,3	-57,7	-78	0.970	5.104	0.269
1.500	20,7	-55,5	-76,2	1.183	5.160	0.579
2.000	21,2	-52,3	-73,5	1.508	5.219	0.723
2.500	21,9	-48,7	-70,6	1.884	5.281	0.797
3.000	22,7	-45,1	-67,8	2.290	5.348	0.847
3.500	23,7	-41,5	-65,2	2.718	5.420	0.888
4.000	24,8	-38,0	-62,8	3.165	5.496	0.927
4.500	26,1	-34,7	-60,8	3.631	5.579	0.965
5.000	27,5	-31,5	-59	4.115	5.667	1.005
5.500	29,0	-28,4	-57,4	4.618	5.762	1.045
6.000	30,8	-25,4	-56,2	5.141	5.864	1.087
6.500	32,7	-22,6	-55,3	5.685	5.974	1.130
7.000	34,7	-19,8	-54,5	6.248	6.093	1.173
7.500	36,9	-17,2	-54,1	6.832	6.219	1.217
8.000	39,2	-14,6	-53,8	7.436	6.355	1.261
8.500	41,6	-12,1	-53,7	8.060	6.501	1.304
9.000	44,3	-9,7	-54	8.704	6.657	1.346
9.500	47,1	-7,3	-54,4	9.367	6.823	1.387
10.000	50,0	-5,0	-55	10.048	7.001	1.427
10.500	53,0	-2,7	-55,7	10.745	7.190	1.464
11.000	56,3	-0,4	-56,7	11.458	7.392	1.498
11.500	59,7	1,9	-57,8	12.184	7.606	1.529
12.000	63,2	4,1	-59,1	12.921	7.833	1.556
12.500	66,9	6,4	-60,5	13.667	8.074	1.579
13.000	70,7	8,6	-62,1	14.419	8.329	1.597
13.500	74,6	10,8	-63,8	15.174	8.599	1.609
14.000	78,8	13,1	-65,7	15.928	8.884	1.615
14.500	83,1	15,3	-67,8	16.678	9.185	1.615
15.000	87,5	17,5	-70	17.419	9.502	1.608
15.500	92,1	19,8	-72,3	18.147	9.835	1.593
16.000	96,8	22,0	-74,8	18.857	10.186	1.571
16.500	101,7	24,3	-77,4	19.542	10.554	1.541
17.000	106,7	26,6	-80,1	20.198	10.940	1.503
17.500	111,9	28,8	-83,1	20.817	11.345	1.457
18.000	117,2	31,1	-86,1	21.394	11.770	1.405
18.500	122,7	33,3	-89,4	21.919	12.213	1.347
19.000	128,3	35,6	-92,7	22.386	12.677	1.286
19.500	134,1	37,9	-96,2	22.785	13.162	1.227
20.000	140,0	40,1	-99,9	23.107	13.668	1.176

APPENDIX D

CALCULATION OF MASSES AND VOLUMES OF FEMUR-TIBIA

To find the limb mass, models of the femur and tibia are given in the Figure D.1.

Masses of the femur and tibia:

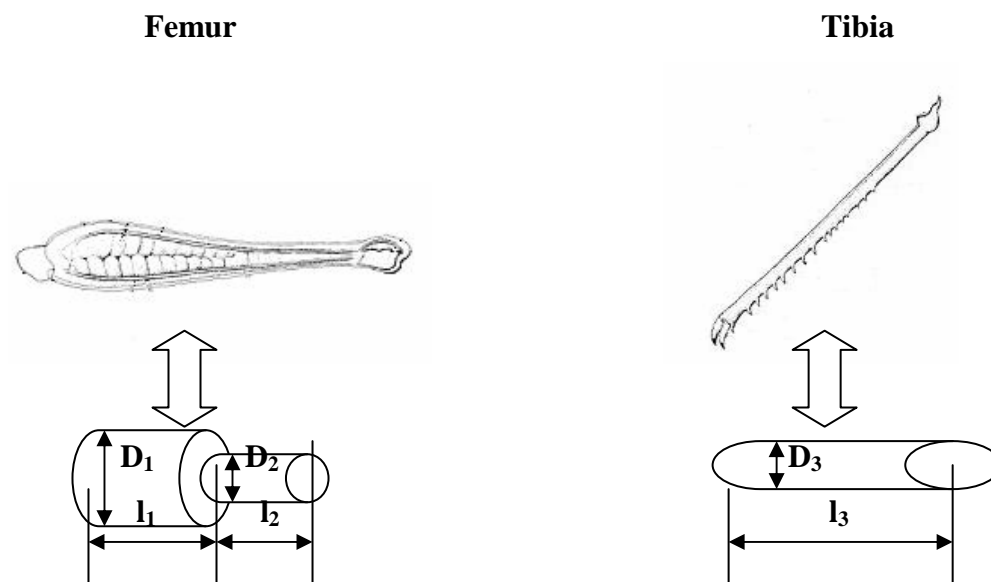


Figure D.1 Mathematical models of the femur and tibia.

Where

$$l_1 = 10.26 \text{ mm}; \quad D_1 = 3.2 \text{ mm}$$

$$l_2 = 6.84 \text{ mm}; \quad D_2 = 0.8 \text{ mm}$$

$$l_3 = 15.6 \text{ mm}; \quad D_3 = 0.6 \text{ mm}$$

Volume of the femur and tibia:

$$V_{femur} = \frac{\pi.D_1^2}{4}.l_1 + \frac{\pi.D_2^2}{4}.l_2 = 85.958mm^3 \quad (D.1)$$

$$V_{tibia} = \frac{\pi.D_3^2}{4}.l_3 = 4.41mm^3 \quad (D.2)$$

$$M1 = \rho.V_{femur} = 1.025(kg / m^3).85.958.(10^{-3})^3(m^3) = 88.107.10^{-9}(kg) \quad (D.3)$$

$$M2 = \rho.V_{tibia} = 1.025(kg / m^3).4.41.(10^{-3})^3(m^3) = 4.52.10^{-9}(kg) \quad (D.4)$$

APPENDIX E

DYNAMIC MODEL OF THE GRASSHOPPER LEG

A Lagrange's method is used for arriving at equations between joint power and foot coordinates. For assumed mass distribution;

a. Kinetic Energy;

Kinetic Energy of M1 is;

$$K_1 = \frac{1}{2} M_1 (\dot{x}_1^2 + \dot{z}_1^2) \quad (\text{E.1})$$

where

$$x_1 = 0.866 \cdot \frac{L_1}{2} \cdot \sin(\beta(t)) - 0.866 \cdot L_2 \cdot \sin(\theta(t)) \quad (\text{E.2})$$

$$z_1 = -0.866 \cdot \frac{L_1}{2} \cdot \cos(\beta(t)) + 0.866 \cdot L_2 \cdot \cos(\theta(t)) \quad (\text{E.3})$$

and

$$\dot{x}_1 = 0.433 \cdot L_1 \cdot \cos(\beta(t)) \cdot \dot{\beta}(t) - 0.866 \cdot L_2 \cdot \cos(\theta(t)) \cdot \dot{\theta}(t) \quad (\text{E.4})$$

$$\dot{z}_1 = 0.433 \cdot L_1 \cdot \sin(\beta(t)) \cdot \dot{\beta}(t) - 0.866 \cdot L_2 \cdot \sin(\theta(t)) \cdot \dot{\theta}(t) \quad (\text{E.5})$$

Substituting these equations into the equation;

$$K_1 = \frac{1}{2} M_1 \left[0.188.L_1^2 \dot{\beta}(t)^2 + 0.75L_2^2 \dot{\theta}(t)^2 - 0.75L_1L_2 \cos(\beta(t) - \theta(t)).\dot{\beta}(t).\dot{\theta}(t) \right] \quad (\text{E.6})$$

Kinetic Energy of M2 is;

$$K_2 = \frac{1}{2} M_2 \left(\frac{L_2}{2} \right)^2 \left[\frac{d}{dt} (90 + \theta(t)) \right]^2 = 0.125.M_2.L_2^2.\dot{\theta}^2 \quad (\text{E.7})$$

Kinetic Energy of Mh is;

$$K_h = \frac{1}{2} M_h (\dot{x}_h^2 + \dot{z}_h^2) \quad (\text{E.8})$$

where

$$x_h = 0.866.L_1.\sin(\beta(t)) - 0.866.L_2.\sin(\theta(t)) \quad (\text{E.9})$$

$$z_h = -0.866.L_1.\cos(\beta(t)) + 0.866.L_2.\cos(\theta(t)) \quad (\text{E.10})$$

and

$$\dot{x}_h = 0.866.L_1.\cos(\beta(t)).\dot{\beta}(t) - 0.866.L_2.\cos(\theta(t)).\dot{\theta}(t) \quad (\text{E.11})$$

$$\dot{z}_h = 0.866.L_1.\sin(\beta(t)).\dot{\beta}(t) - 0.866.L_2.\sin(\theta(t)).\dot{\theta}(t) \quad (\text{E.12})$$

Substituting these equations into the equation;

$$K_h = \frac{1}{2} M_h \left[0.75.L_1^2 \dot{\beta}(t)^2 + 0.75L_2^2 \dot{\theta}(t)^2 - 1.5L_1L_2 \cos(\beta(t) - \theta(t)).\dot{\beta}(t).\dot{\theta}(t) \right] \quad (\text{E.13})$$

Kinetic Energy of Mb is;

$$K_b = \frac{1}{2} M_b (\dot{x}_b^2 + \dot{z}_b^2) \quad (\text{E.14})$$

where

$$x_b = 0.866.L_1.\sin(\beta(t)) - 0.866.L_2.\sin(\theta(t)) + 0.27 \quad (\text{E.15})$$

$$z_b = -0.866.L_1.\cos(\beta(t)) + 0.866.L_2.\cos(\theta(t)) \quad (\text{E.16})$$

and

$$\dot{x}_b = 0.866.L_1.\cos(\beta(t)).\dot{\beta}(t) - 0.866.L_2.\cos(\theta(t)).\dot{\theta}(t) \quad (\text{E.17})$$

$$\dot{z}_b = 0.866.L_1.\sin(\beta(t)).\dot{\beta}(t) - 0.866.L_2.\sin(\theta(t)).\dot{\theta}(t) \quad (\text{E.18})$$

Substituting these equations into the equation;

$$K_b = \frac{1}{2} M_b \left[0.75.L_1^2 \dot{\beta}(t)^2 + 0.75.L_2^2 \dot{\theta}(t)^2 - 1.5L_1L_2 \cos(\beta(t) - \theta(t)).\dot{\beta}(t).\dot{\theta}(t) \right] \quad (\text{E.19})$$

Kinetic Energy of Mk is;

$$K_k = \frac{1}{2} M_k .L_2^2 .\dot{\theta}^2 \quad (\text{E.20})$$

Kinetic Energy of I2 is;

$$K_{I2} = \frac{1}{2} I_2 .\dot{\theta}^2 \quad (\text{E.21})$$

Kinetic Energy of I1 is;

$$K_{I1} = \frac{1}{2} I_1 \cdot \dot{\beta}^2 \quad (\text{E.22})$$

Kinetic Energy of Ib is;

$$K_{Ib} = 0 \quad (\text{E.23})$$

b. Potential Energy;

$$P = -M_2 g \frac{L_2}{2} \cos(\theta(t)) - M_k g L_2 \cos(\theta(t)) - M_1 g \left[L_2 \cos(\theta(t)) - \frac{L_1}{2} \cos(\beta(t)) \right] \\ - (M_h + M_b) g [L_2 \cos(\theta(t)) - L_1 \cos(\beta(t))] + \frac{1}{2} k (\beta(t) - \theta(t))^2 \quad (\text{E.24})$$

Thus,

$$P = -(0.5M_2 + M_k + M_1 + M_h + M_b) L_2 \cos(\theta(t)) g \\ + (0.5M_1 + M_h + M_b) L_1 \cos(\beta(t)) g + \frac{1}{2} k (\beta(t) - \theta(t))^2 \quad (\text{E.25})$$

c. Using Lagrange's Method for Knee Actuator (Mk);

$$T_2 = \frac{d}{dt} \left(\frac{\partial L_a}{\partial \dot{\theta}} \right) - \frac{\partial L_a}{\partial \theta} \quad (\text{E.26})$$

$$\frac{\partial L_a}{\partial \theta} = \frac{\partial}{\partial \theta} (K - P) = \frac{\partial K_1}{\partial \theta} + \frac{\partial K_2}{\partial \theta} + \frac{\partial K_h}{\partial \theta} + \frac{\partial K_b}{\partial \theta} + \frac{\partial K_k}{\partial \theta} + \frac{\partial K_{I2}}{\partial \theta} + \frac{\partial K_{I1}}{\partial \theta} - \frac{\partial P}{\partial \theta} \quad (\text{E.27})$$

$$\frac{\partial K_1}{\partial \theta} = -0.375 M_1 L_1 L_2 \sin(\beta(t) - \theta(t)) \cdot \dot{\beta}(t) \cdot \dot{\theta}(t) \quad (\text{E.28})$$

$$\frac{\partial K_2}{\partial \theta} = \frac{\partial K_k}{\partial \theta} = \frac{\partial K_{I2}}{\partial \theta} = \frac{\partial K_{I1}}{\partial \theta} = 0 \quad (\text{E.29})$$

$$\frac{\partial K_h}{\partial \theta} = -0.75M_h L_1 L_2 \sin(\beta(t) - \theta(t)) \cdot \dot{\beta}(t) \cdot \dot{\theta}(t) \quad (\text{E.30})$$

$$\frac{\partial K_b}{\partial \theta} = -0.75M_b L_1 L_2 \sin(\beta(t) - \theta(t)) \cdot \dot{\beta}(t) \cdot \dot{\theta}(t) \quad (\text{E.31})$$

$$\frac{\partial P}{\partial \theta} = (0.5M_2 + M_k + M_1 + M_h + M_b)L_2 \sin(\theta(t))g + k(\theta(t) - \beta(t)) \quad (\text{E.32})$$

$$\begin{aligned} \frac{\partial L_a}{\partial \theta} = & -(0.375M_1 + 0.75(M_h + M_b))L_1 L_2 \sin(\beta(t) - \theta(t)) \cdot \dot{\beta}(t) \cdot \dot{\theta}(t) \\ & - (0.5M_2 + M_k + M_1 + M_h + M_b)L_2 \sin(\theta(t))g + k(\theta(t) - \beta(t)) \end{aligned} \quad (\text{E.33})$$

$$\frac{\partial L_a}{\partial \dot{\theta}} = \frac{\partial}{\partial \dot{\theta}} (K - P) = \frac{\partial K_1}{\partial \dot{\theta}} + \frac{\partial K_2}{\partial \dot{\theta}} + \frac{\partial K_h}{\partial \dot{\theta}} + \frac{\partial K_b}{\partial \dot{\theta}} + \frac{\partial K_k}{\partial \dot{\theta}} + \frac{\partial K_{I2}}{\partial \dot{\theta}} + \frac{\partial K_{I1}}{\partial \dot{\theta}} - \frac{\partial P}{\partial \dot{\theta}} \quad (\text{E.34})$$

$$\frac{\partial K_1}{\partial \dot{\theta}} = 0.75M_1 L_2^2 \cdot \dot{\theta}(t) - 0.375M_1 L_1 L_2 \cos(\beta(t) - \theta(t)) \dot{\beta}(t) \quad (\text{E.35})$$

$$\frac{\partial K_2}{\partial \dot{\theta}} = 0.25M_2 L_2^2 \cdot \dot{\theta}(t) \quad (\text{E.36})$$

$$\frac{\partial K_h}{\partial \dot{\theta}} = 0.75M_h L_2^2 \cdot \dot{\theta}(t) - 0.75M_h L_1 L_2 \cos(\beta(t) - \theta(t)) \dot{\beta}(t) \quad (\text{E.37})$$

$$\frac{\partial K_b}{\partial \dot{\theta}} = 0.75M_b L_2^2 \cdot \dot{\theta}(t) - 0.75M_b L_1 L_2 \cos(\beta(t) - \theta(t)) \dot{\beta}(t) \quad (\text{E.38})$$

$$\frac{\partial K_k}{\partial \dot{\theta}} = M_k L_2^2 \cdot \dot{\theta}(t) \quad (\text{E.39})$$

$$\frac{\partial K_{I_2}}{\partial \dot{\theta}} = I_2 \cdot \dot{\theta}(t) \quad (\text{E.40})$$

$$\frac{\partial K_{I_1}}{\partial \dot{\theta}} = \frac{\partial P}{\partial \dot{\theta}} = 0 \quad (\text{E.41})$$

$$\begin{aligned} \frac{\partial L_a}{\partial \dot{\theta}} &= 0.75(M_1 + M_h + M_b)L_2^2 \cdot \dot{\theta}(t) \\ &\quad - [0.375M_1 + 0.75(M_h + M_b)]L_1L_2 \cos(\beta(t) - \theta(t))\dot{\beta}(t) + (M_k L_2^2 + I_2)\dot{\theta} \end{aligned} \quad (\text{E.42})$$

$$\begin{aligned} \frac{d}{dt} \left(\frac{\partial L_a}{\partial \dot{\theta}} \right) &= [(0.75(M_1 + M_h + M_b) + M_k)L_2^2 + I_2]\ddot{\theta}(t) \\ &\quad - [0.375M_1 + 0.75(M_h + M_b)]L_1L_2 [-\sin(\beta(t) - \theta(t))(\dot{\beta}(t) - \dot{\theta}(t))\dot{\beta}(t) + \cos(\beta(t) - \theta(t))\ddot{\beta}(t)] \end{aligned} \quad (\text{E.43})$$

Thus, torque becomes,

$$T_2 = G_1 \ddot{\theta}(t) + G_2 \ddot{\beta}(t) + G_3 (\dot{\beta}(t))^2 + G_4 g + G_5 \quad (\text{E.44})$$

where

$$G_1 = (0.75(M_1 + M_h + M_b) + M_k)L_2^2 + I_2 \quad (\text{E.45})$$

$$G_2 = -(0.375M_1 + 0.75(M_h + M_b))L_1L_2 \cos(\beta(t) - \theta(t)) \quad (\text{E.46})$$

$$G_3 = (0.375M_1 + 0.75(M_h + M_b))L_1L_2 \sin(\beta(t) - \theta(t)) \quad (\text{E.47})$$

$$G_4 = (0.5M_2 + M_1 + M_k + M_h + M_b)L_2 \sin(\theta(t)) \quad (\text{E.48})$$

$$G_5 = k(\theta(t) - \beta(t)) \quad (\text{E.49})$$

d. Using Lagrange's Method for Hip Actuator (Mh);

$$T_1 = \frac{d}{dt} \left(\frac{\partial L_a}{\partial \dot{\beta}} \right) - \frac{\partial L_a}{\partial \beta} \quad (\text{E.50})$$

$$\frac{\partial L_a}{\partial \beta} = \frac{\partial}{\partial \beta} (K - P) = \frac{\partial K_1}{\partial \beta} + \frac{\partial K_2}{\partial \beta} + \frac{\partial K_h}{\partial \beta} + \frac{\partial K_b}{\partial \beta} + \frac{\partial K_k}{\partial \beta} + \frac{\partial K_{I2}}{\partial \beta} + \frac{\partial K_{I1}}{\partial \beta} - \frac{\partial P}{\partial \beta} \quad (\text{E.51})$$

$$\frac{\partial K_1}{\partial \beta} = -0.375M_1L_1L_2 \sin(\beta(t) - \theta(t)) \cdot \dot{\beta}(t) \cdot \dot{\theta}(t) \quad (\text{E.52})$$

$$\frac{\partial K_2}{\partial \theta} = \frac{\partial K_k}{\partial \theta} = \frac{\partial K_{I2}}{\partial \theta} = \frac{\partial K_{I1}}{\partial \theta} = 0 \quad (\text{E.53})$$

$$\frac{\partial K_h}{\partial \theta} = -0.75M_hL_1L_2 \sin(\beta(t) - \theta(t)) \cdot \dot{\beta}(t) \cdot \dot{\theta}(t) \quad (\text{E.54})$$

$$\frac{\partial K_b}{\partial \theta} = -0.75M_bL_1L_2 \sin(\beta(t) - \theta(t)) \cdot \dot{\beta}(t) \cdot \dot{\theta}(t) \quad (\text{E.55})$$

$$\frac{\partial P}{\partial \theta} = -(0.5M_1 + M_h + M_b)L_1 \sin(\beta(t))g + k(\beta(t) - \theta(t)) \quad (\text{E.56})$$

$$\begin{aligned} \frac{\partial L_a}{\partial \theta} = & -(0.375M_1 + 0.75(M_h + M_b))L_1L_2 \sin(\beta(t) - \theta(t)) \cdot \dot{\beta}(t) \cdot \dot{\theta}(t) \\ & + (0.5M_1 + M_h + M_b)L_1 \sin(\beta(t))g - k(\beta(t) - \theta(t)) \end{aligned} \quad (\text{E.57})$$

$$\frac{\partial L_a}{\partial \dot{\beta}} = \frac{\partial}{\partial \dot{\beta}} (K - P) = \frac{\partial K_1}{\partial \dot{\beta}} + \frac{\partial K_2}{\partial \dot{\beta}} + \frac{\partial K_h}{\partial \dot{\beta}} + \frac{\partial K_b}{\partial \dot{\beta}} + \frac{\partial K_k}{\partial \dot{\beta}} + \frac{\partial K_{I2}}{\partial \dot{\beta}} + \frac{\partial K_{I1}}{\partial \dot{\beta}} - \frac{\partial P}{\partial \dot{\beta}} \quad (\text{E.58})$$

$$\frac{\partial K_1}{\partial \dot{\theta}} = 0.188M_1L_1^2 \cdot \dot{\beta}(t) - 0.375M_1L_1L_2 \cos(\beta(t) - \theta(t)) \dot{\theta}(t) \quad (\text{E.59})$$

$$\frac{\partial K_2}{\partial \dot{\beta}} = \frac{\partial K_k}{\partial \dot{\beta}} = \frac{\partial K_{I2}}{\partial \dot{\beta}} = \frac{\partial P}{\partial \dot{\beta}} = 0 \quad (\text{E.60})$$

$$\frac{\partial K_h}{\partial \dot{\beta}} = 0.75M_h L_1^2 \cdot \dot{\beta}(t) - 0.75M_h L_1 L_2 \cos(\beta(t) - \theta(t)) \dot{\theta}(t) \quad (\text{E.61})$$

$$\frac{\partial K_b}{\partial \dot{\beta}} = 0.75M_b L_1^2 \cdot \dot{\beta}(t) - 0.75M_b L_1 L_2 \cos(\beta(t) - \theta(t)) \dot{\theta}(t) \quad (\text{E.62})$$

$$\frac{\partial K_{I1}}{\partial \dot{\beta}} = I_1 \dot{\beta}(t) \quad (\text{E.63})$$

$$\begin{aligned} \frac{\partial L_a}{\partial \dot{\beta}} &= (0.188M_1 + 0.75(M_h + M_b))L_1^2 + I_1 \cdot \dot{\beta}(t) \\ &\quad - [0.375M_1 + 0.75(M_h + M_b)]L_1 L_2 \cos(\beta(t) - \theta(t)) \dot{\theta}(t) \end{aligned} \quad (\text{E.64})$$

$$\begin{aligned} \frac{d}{dt} \left(\frac{\partial L_a}{\partial \dot{\beta}} \right) &= [(0.188M_1 + 0.75(M_h + M_b))L_1^2 + I_1] \ddot{\beta}(t) \\ &\quad + [0.375M_1 + 0.75(M_h + M_b)]L_1 L_2 \left[\sin(\beta(t) - \theta(t)) (\dot{\beta}(t) \dot{\theta}(t) - (\dot{\theta}(t))^2) - \cos(\beta(t) - \theta(t)) \ddot{\theta}(t) \right] \end{aligned} \quad (\text{E.65})$$

Thus, torque becomes,

$$T_1 = G_2 \cdot \ddot{\theta}(t) + G_6 \ddot{\beta}(t) + 2G_3 \dot{\beta}(t) \dot{\theta}(t) - G_3 (\dot{\theta}(t))^2 + G_7 g - G_5 \quad (\text{E.66})$$

where

$$G_6 = (0.188M_1 + 0.75(M_h + M_b) + M_k) \cdot L_1^2 + I_1 \quad (\text{E.67})$$

$$G_7 = -(0.5M_1 + M_h + M_b) L_1 \sin(\beta(t)) \quad (\text{E.68})$$

APPENDIX F

TORQUE RESULTS OF 2D LEG MODEL

Table F.1 Torque Results

Time (ms)	T1 (Nm)	T2 (Nm)	T (Nm)
0.000	0.351	-0.350	1.590e-3
0.500	0.354	-0.351	2.130e-3
1.000	0.357	-0.355	2.086e-3
1.500	0.363	-0.362	1.445e-3
2.000	0.372	-0.370	1.152e-3
2.500	0.383	-0.382	1.021e-3
3.000	0.397	-0.397	9.282e-4
3.500	0.414	-0.414	8.432e-4
4.000	0.434	-0.433	7.597e-4
4.500	0.456	-0.455	6.768e-4
5.000	0.481	-0.480	5.944e-4
5.500	0.508	-0.508	5.126e-4
6.000	0.538	-0.538	4.309e-4
6.500	0.571	-0.571	3.490e-4
7.000	0.606	-0.606	2.662e-4
7.500	0.644	-0.644	1.817e-4
8.000	0.685	-0.685	9.457e-5
8.500	0.728	-0.728	4.012e-6
9.000	0.774	-0.774	-9.087e-5
9.500	0.822	-0.822	-1.910e-4
10.000	0.873	-0.873	-2.971e-4
10.500	0.926	-0.927	-4.100e-4
11.000	0.983	-0.983	-5.303e-4
11.500	1.041	-1.042	-6.587e-4
12.000	1.103	-1.103	-7.957e-4
12.500	1.167	-1.168	-9.416e-4
13.000	1.233	-1.234	-1.097e-3
13.500	1.302	-1.304	-1.261e-3
14.000	1.374	-1.376	-1.434e-3
14.500	1.449	-1.450	-1.616e-3
15.000	1.526	-1.527	-1.806e-3
15.500	1.605	-1.607	-2.005e-3
16.000	1.688	-1.690	-2.210e-3
16.500	1.772	-1.775	-2.421e-3
17.000	1.860	-1.863	-2.638e-3
17.500	1.950	-1.953	-2.860e-3
18.000	2.043	-2.046	-3.085e-3
18.500	2.138	-2.142	-3.313e-3
19.000	2.236	-2.240	-3.544e-3
19.500	2.337	-2.341	-3.780e-3
20.000	2.440	-2.444	-4.022e-3

APPENDIX G

ARTIFICIAL MUSCLES

Table G.1 Illustration the advantages and disadvantages of electronic and ionic EAPs as outlined by Halloran and Malley, 2004 and Bar-Cohen, 2004

EAP type	Advantages	Disadvantages
Electronic	<ul style="list-style-type: none"> - can operate in room conditions for a long time - rapid response (msec levels) - can hold strain under dc activation - induces relatively large actuation forces 	<ul style="list-style-type: none"> - requires high voltages (~150MV/m) - requires compromise between strain and stress - glass transition temperature is inadequate for low temperature actuation tasks and in the case of Ferroelectric EAP, high temperature applications are limited by the Curie temperature - Mostly, producing a monopolar actuation independent of the voltage polarity due to associated electrostriction effect.
Ionic	<ul style="list-style-type: none"> - produces large bending displacements - requires low voltage - natural bi-directional actuation that depends on the voltage polarity 	<ul style="list-style-type: none"> - except for CPs and NTs, ionic EAPs do not hold strain under dc voltage - slow response (fraction of a second) - bending EAPs induce a relatively low actuation force - except for CPs, it is difficult to produce a consistent material (particularly IPMC) - In aqueous systems the material sustains electrolysis at voltages >1.23V - To operate in air requires attention to the electrolyte - Low electromechanical coupling efficiency

Table G.2 EAP infrastructure (Cohen, 2005)

